ECONOMIC FEASIBILITY OF CAM-TYPE WAVE POWER GENERATORS.

Stephen Vincent Bisceglia

SECURITY CLASSIFICATION OF THIS PAGE (When Data Entered)

REPORT DOCUMENTATION PAGE

READ INSTRUCTIONS BEFORE COMPLETING FORM

1. REPORT NUMBER	2. GOVT ACCESSION NO.
3. RECIPIENT'S CATALOG NUMBER	
4. TITLE (and Subtitle) ECONOMIC FEASIBILITY OF CAM-TYPE WAVE POWER GENERATORS	5. TYPE OF REPORT & PERIOD COVERED THESIS
6. PERFORMING ORG. REPORT NUMBER	
7. AUTHOR(s) BISCEGLIA, STEPHEN VINCENT	8. CONTRACT OR GRANT NUMBER(s)
9. PERFORMING ORGANIZATION NAME AND ADDRESS MASS. INST. OF TECHNOLOGY	10. PROGRAM ELEMENT, PROJECT, TASK AREA & WORK UNIT NUMBERS
11. CONTROLLING OFFICE NAME AND ADDRESS SUPT, NAVPGSCOL (CODE 031) MONTEREY, CA 93940	12. REPORT DATE J N 78
	13. NUMBER OF PAGES 157
14. MONITORING AGENCY NAME & ADDRESS(if different from Controlling Office)	15. SECURITY CLASS. (of this report) UNCLASS
	15a. DECLASSIFICATION/DOWNGRADING SCHEDULE

16. DISTRIBUTION STATEMENT (of this Report)

APPROVED FOR PUBLIC RELEASE: DISTRIBUTION UNLIMITED

17. DISTRIBUTION STATEMENT (of the abstract entered in Block 20, if different from Report)

18. SUPPLEMENTARY NOTES

19. KEY WORDS (Continue on reverse side if necessary and identify by block number)

CAM-TYPE WAVE POWER GENERATOR

20. ABSTRACT (Continue on reverse side if necessary and identify by block number)

SEE REVERSE

DD FORM 1473 EDITION OF 1 NOV 65 IS OBSOLETE
S/N 0102-014-6601 | UNCLASS
(Page 1) SECURITY CLASSIFICATION OF THIS PAGE (When Data Entered)

ECONOMIC FEASIBILITY OF CAM-TYPE WAVE POWER GENERATORS

by

Stephen Vincent Bisceglia

B.S., United States Naval Academy
(1972)

Submitted in Partial Fulfillment
of the Requirements for the
Degree of

OCEAN ENGINEER

and the Degree of

MASTER OF SCIENCE IN MANAGEMENT

at the

MASSACHUSETTS INSTITUTE OF TECHNOLOGY

June, 1978

ECONOMIC FEASIBILITY OF CAM-TYPE WAVE POWER GENERATORS

by

Stephen Vincent Bisceglia

Submitted to the Department of Ocean Engineering and to the Alfred P. Sloan School of Management on May 12, 1978, in partial fulfillment of the requirements for the Degree of Ocean Engineer and the Degree of Master of Science in Management.

ABSTRACT

Model tests at M.I.T. have indicated that the cam-type wave power generator is capable of high efficiencies of energy extraction from ocean waves. This report presents a design methodology for determining costs of energy produced from wave power generators. Feasible designs were developed for ocean locations around the coast of the United States with the resulting breakeven costs with oil ranging from 14 to 30 $/BBL.

Thesis Supervisor: A. Douglas Carmichael
Title: Professor of Power Engineering

Thesis Advisor: Stephen C. Graves
Title: Assistant Professor of Management Science

ACKNOWLEDGEMENTS

I would like to express my gratitude to Professor A. Douglas Carmichael who first kindled my interest in the subject. His thoughtful advice was most appreciated.

Thanks also are due to Professor Stephen C. Graves, Mr. Jim Mays and Mr. Noel "Brye" Davis for their helpful suggestions, and to Mrs. Sandy Margeson who typed the manuscript.

TABLE OF CONTENTS

LIST OF SYMBOLS

A - wave amplitude

C_p - wave phase velocity

C_g - wave group velocity

C_o - deepwater group velocity

$H_{rms} = 2A$ - wave height

$H_s = \sqrt{2}\, H_{rms}$ - significant wave height

D - cam diameter

D_{max} - cam diameter at maximum power out

E - wave energy

g - gravitational constant

h - water depth

K - wave number

P - wave power

$\overline{P}$ - mean wave power

q - effective length multiplier with separation

T - wave period

$\overline{T}$ - mean wave period

d - separation distance

ρ - water density

λ - wavelength

ω - frequency

ξ - observed wave height/mean wave height

σ_T - standard deviation of wave period

σ_P - standard deviation of wave power

η - efficiency

CHAPTER 1

INTRODUCTION

Energy from renewable resources offers an alternative to conventional fuel-fired energy production systems. Escalating fuel prices, political/economic desires for energy independence and reduction in environmental pollution are all incentives for developing renewable resources. The cam-type wave power generator is one such resource, utilizing the energy in ocean waves.

The idea of extracting the energy in ocean waves by a cam-shaped nodding duck was first presented by Stephen Salter of the University of Edinburgh in 1974 (ref. 26). Since waves drive each other with high efficiency, Salter believed that an optimally shaped device would cause an incoming wave to react as though the device was just another wave.

In deepwater travelling waves each particle moves in a nearly circular orbit. At the surface the diameter of the orbiting particles equals the wave height. Below the surface the orbital diameters fall off exponentially with depth.

Salter's duck shape is displayed in figure 1-1. The wave side of the cam was designed to conform as nearly as possible to the diameters of the orbiting particles. The lee side of the cam was designed as a cylinder because this shape has constant displacement during the rocking of the cam and therefore transmits no energy.

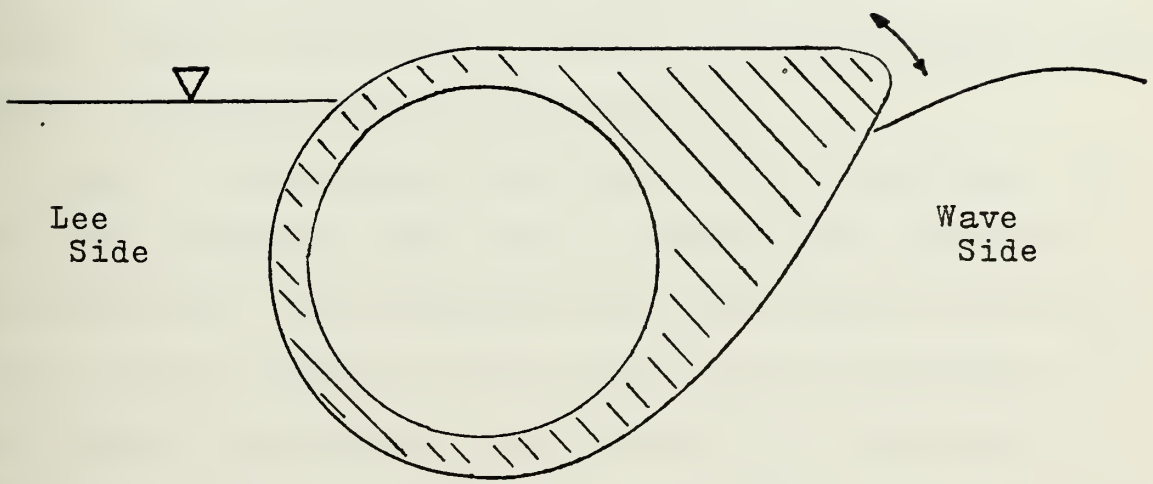

Figure 1-1: Profile of Salter Cam.

Salter tested a model of his device and found that it was capable of extracting nearly 90% of the wave energy incident on its length. Experiments conducted at M.I.T. with a similarly shaped cam also yielded high efficiencies.

Wave energy, like all other renewable resources, is characterized by low intensity and random flux. In order to predict the useful absorption of a wave energy device, data must be collected and analyzed for the desired ocean location. The following parameters adequately describe ocean waves for purposes of energy collection: distributions and mean values of wave height, wave period, variability of wave period, power density and variability of power density.

Before its economic feasibility may be determined, the Wave Power Generator (WPG) must be measured for performance in random seas. To accomplish this a model must be developed which is capable of dealing with environmental variables like wave height, wave period, period variability, power density and power density variability, and with design variables like cam diameter, energy storage, power rating and separation between WPG units.

Once performance is determined, subsystem components for structure, conversion, electrical generation, transmission and energy storage may be selected on the basis of feasibility, cost and efficiency.

The estimates of deliverable power and subsystem costs enable determination of the economic viability of the WPG with respect to conventional power sources.

This report deals with the four basic steps outlined above:

(1) Collection and analysis of ocean wave statistics;

(2) System performance modelling;

(3) Subsystem component selection;

(4) Analysis of investment opportunities.

CHAPTER 2

THEORETICAL AND EXPERIMENTAL BACKGROUND

Experiments on scale models of the cam have been conducted at M.I.T. and by Stephen Salter of Scotland. The basic characteristics of the M.I.T. cam are depicted in figure 2-1. This cam was tested at M.I.T. in both a 2-D mode and a 3-D mode: in the 2-D mode the cam's length filled the width of a narrow tow tank so that waves generated in the tank had a crest length equal to the cam's length; in the 3-D mode the cam was tested in a larger tow tank allowing separation between the ends of the cam and the tank's walls. In both cases the cam was rigidly fixed in space, being allowed only to roll about the axis of its length. This axis is parallel to wave crest.

The experiments at M.I.T. were conducted by N.B. Davis under the direction of Professor A.D. Carmichael and the results are documented in a thesis by Davis (ref. 7).

The efficiency of the cam as a wave power absorber is defined to be the percent of power in a wave of crest length equal to cam length which the cam absorbs. Davis tested the cam's efficiency as a function of non-dimensional frequency, $\omega\sqrt{a/g}$, for three levels of inertia: low = .060 Kgm^2, middle = .063 Kgm^2 and high = .081 Kgm^2. His resulting efficiency curves are graphed in figure 2-2. Also included in this

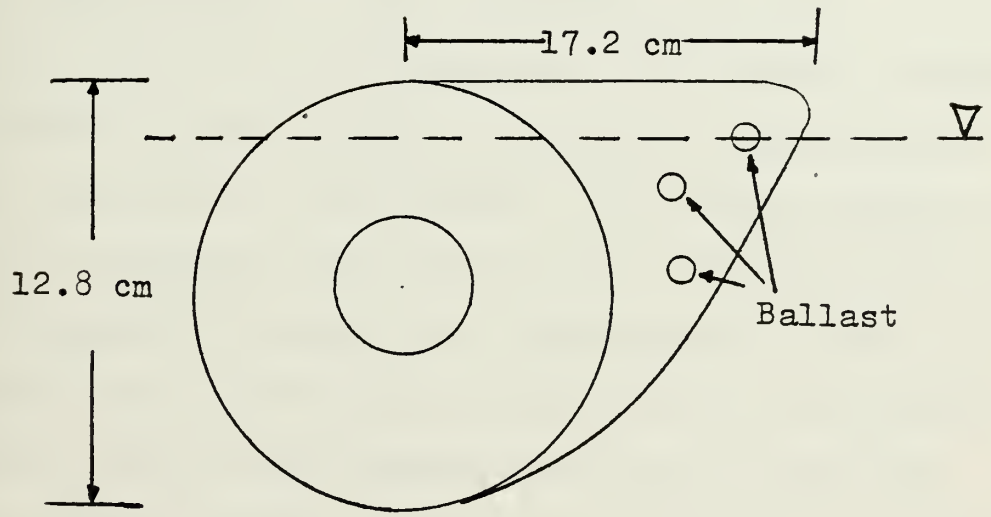

Cam Length = 35.5 cm

Figure 2-1: M.I.T. Cam Geometry

figure is the efficiency curve published by Stephen Salter. In each of these curves there is a fairly wide band of high efficiency levels. Increasing inertia appears to lower the frequency of optimal performance.

When the cam was tested in the 3-D mode, certain frequency waves produced very large increases in efficiency. This efficiency curve along with the associated 2-D curve for the cam with middle inertia is plotted in figure 2-3. Besides increasing the cam's efficiency, the 3-D mode displayed optimal efficiencies at lower frequencies than the 2-D mode.

Davis defined a non-dimensional cam response parameter, $\theta a/H$, where θ = peak-to-peak radian angular displacement, a = cam radius and H = wave height. He plotted response as a function of frequency for various levels of damping and this plot is included in figure 2-4. Superimposed on this plot are dashed lines of efficiency which show that the maximum efficiency occurs at the damping level which causes the response ($\theta a/H$) to have a value $\tilde{}$ 1.0. The level of damping was found to have no effect on the frequency of optimal performance.

In a paper by K. Budal (ref. 2) it is shown that the idealized Salter cam construction comprised of a linear row of closely spaced cams is capable of absorbing 100% of the power incident on its projected length. This helps to explain why the 2-D efficiencies in figure 2-2 are so high.

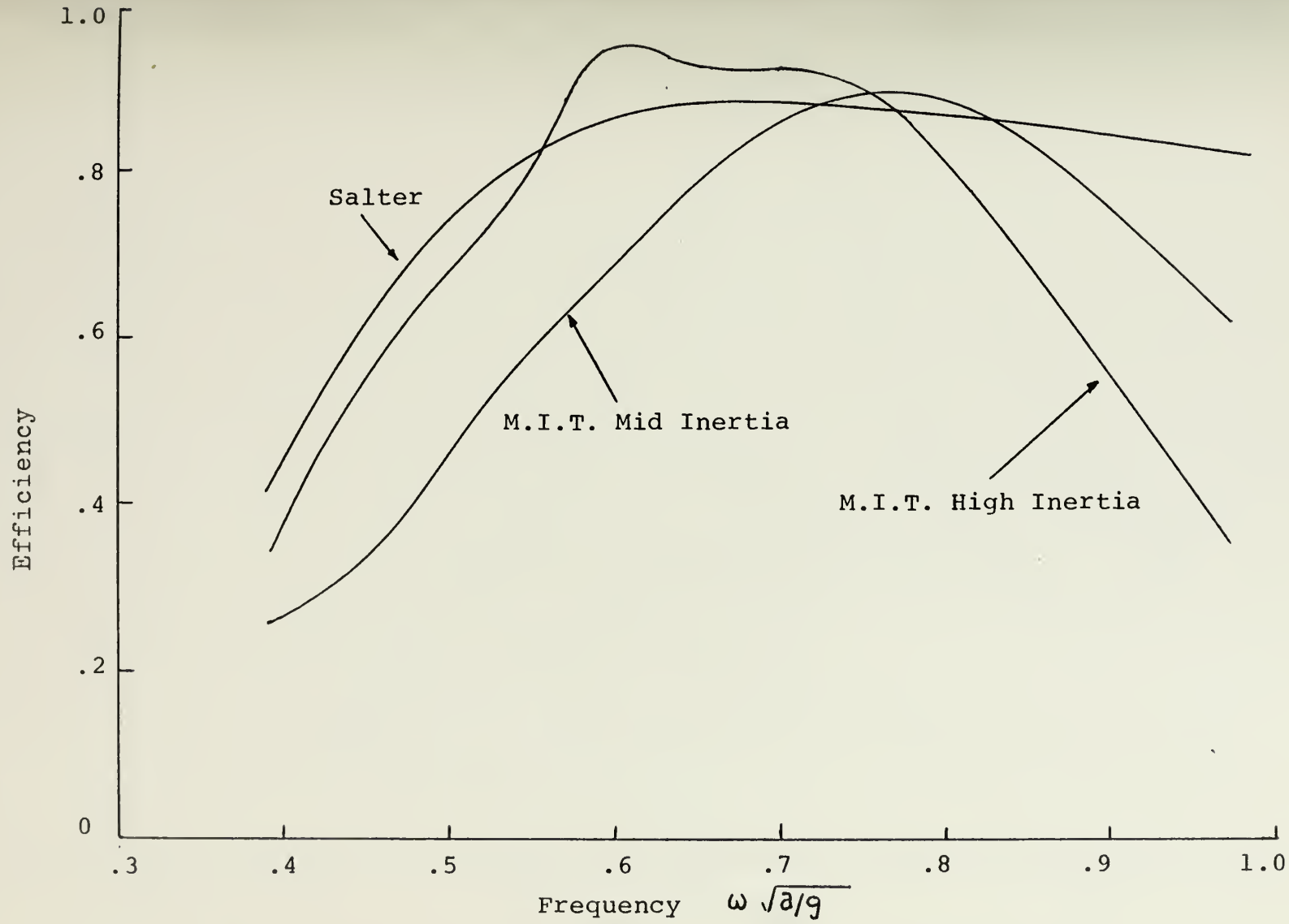

Figure 2-2: M.I.T. and Salter Optimum Performance Curves.

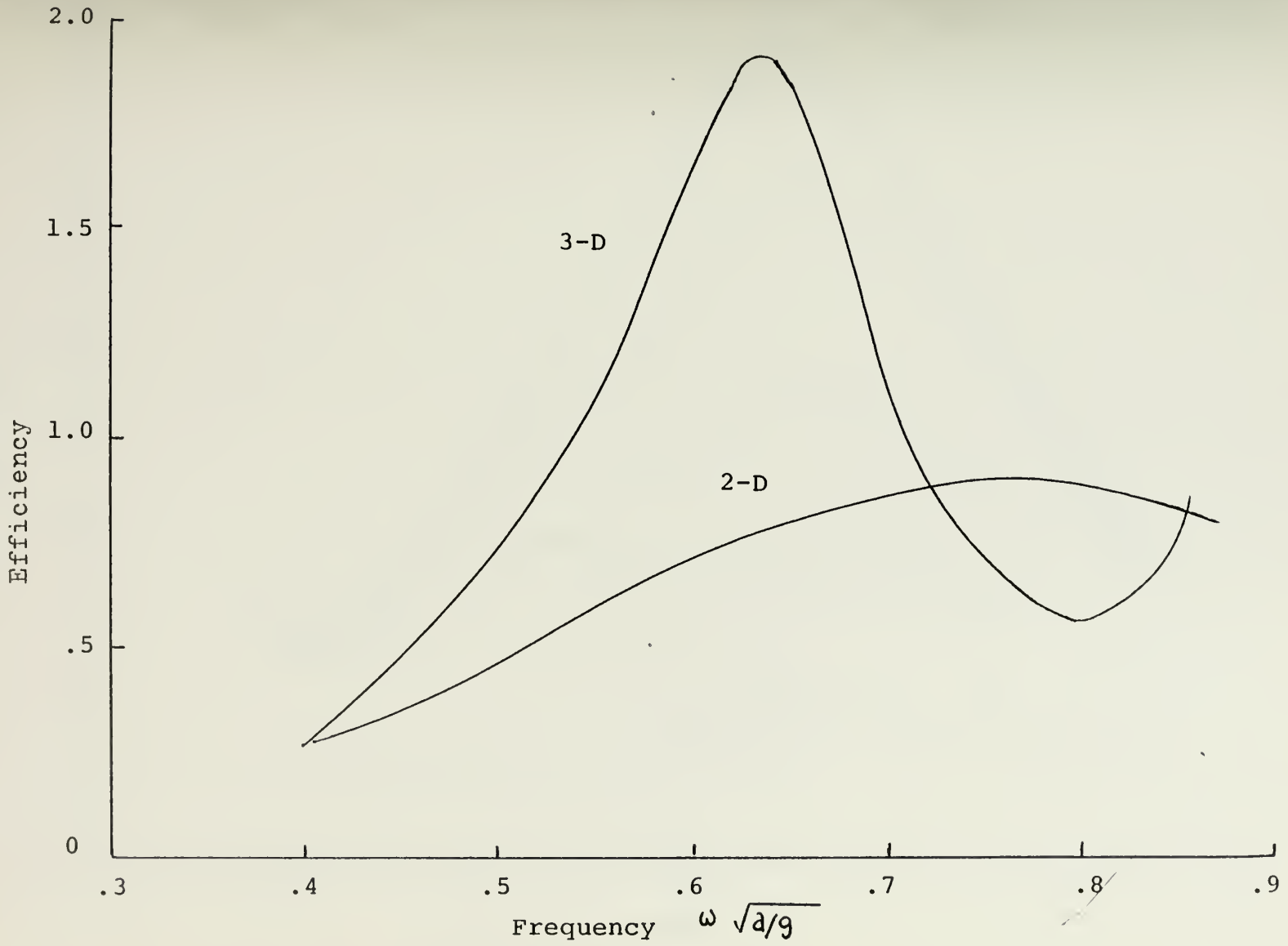

Figure 2-3: Optimal 3-D and 2-D Performance.

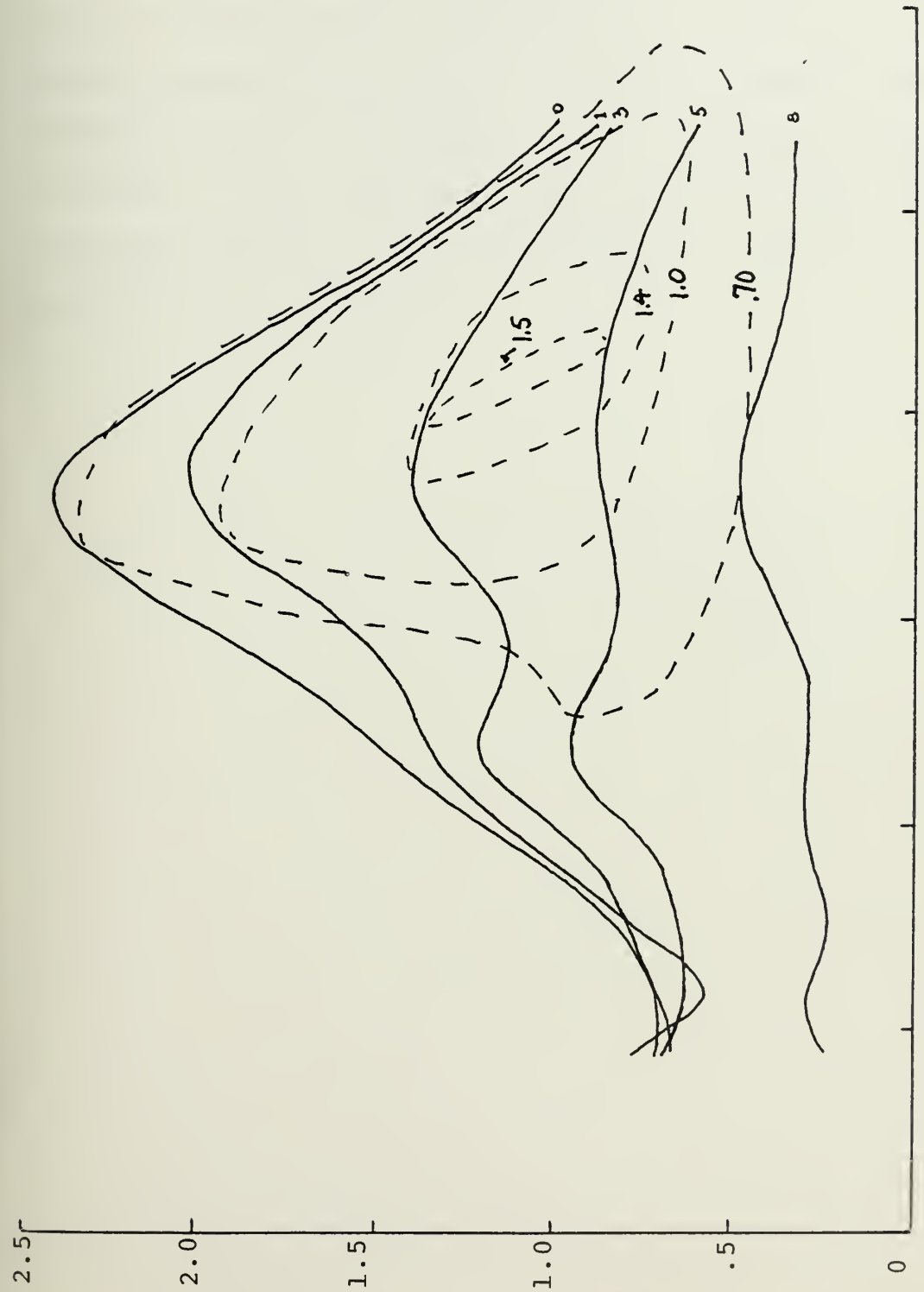

Figure 2-4: 3-D cam response and efficiency for 5 damping levels.

Budal also describes the possibility that a wave interaction effect on wave-absorbers separated by a distance of approximately one wavelength (which is large compared to the absorber's length) will cause dramatic increases in the efficiency of each absorber. This may explain why the M.I.T. experiments showed an increased efficiency when the cam was operating in the 3-D mode.

CHAPTER 3

ENERGY IN WAVES

3.1 Theoretical Derivation

The basic requirement of the wave power generator is to capture the energy that is transported across the surface of the water in the form of waves. Given a particular set of wave characteristics the level of power per unit length of free surface (kilowatts/meter) that exists in a train of waves may be determined.

Wave power is the product of the energy in a wave times the rate at which the energy is being transported. For plane progressive waves the average energy per unit length of free surface is

$$E = \frac{1}{2}\rho\ gA^2 \qquad (1)$$

The average rate of energy flux of a plane progressive wave across a vertical control surface is

$$\frac{dE}{dt} = \frac{1}{4}\rho\ g\omega A^2/K \qquad (2)$$

The rate at which the wave energy propagates is the mean energy flux rate (dE/dt) divided by the mean energy per unit length (E):

$$\frac{dE/dt}{E} = \frac{1}{2}\frac{\omega}{K} = C_g \tag{3}$$

Equation 3 shows that the energy in a wave propagates at the group velocity (C_g). Since the power in a wave is the product of energy times rate of energy propagation,

$$P = E\,C_g = \frac{1}{2}\rho g A^2 C_g$$

$$= \frac{1}{16}\rho g H_s^2\, C_g \tag{4}$$

For all depths of water,

$$C_g = C_p\left[\frac{1}{2} + \frac{Kh}{\sinh(2Kh)}\right] \tag{5}$$

But

$$C_p = \frac{gT}{2\pi} \tag{6}$$

Therefore,

$$P = \frac{1}{16}\rho g H_s^2\,\frac{gT}{2\pi}\left[\frac{1}{2} + \frac{Kh}{\sinh(2Kh)}\right]$$

$$= \frac{1}{32\pi}\rho g^2 H_s^2 T\left[\frac{1}{2} + \frac{Kh}{\sinh(2Kh)}\right] \tag{7}$$

The value of $[\frac{1}{2} + \frac{Kh}{\sinh(2Kh)}]$ may be graphed (figure 3-1) or tabulated (table 3-1).

Defining $P_* \equiv [\frac{1}{2} + \frac{Kh}{\sinh(2Kh)}]$,

$$P = \frac{1}{32\pi} \rho g^2 H_s^2 T P_* \qquad (8)$$

In British units,

$$P \simeq .028 H_s^2 T P_* \quad KW/Ft \qquad (9)$$

In metric units,

$$P \simeq H_s^2 T P_* \quad KW/M \qquad (10)$$

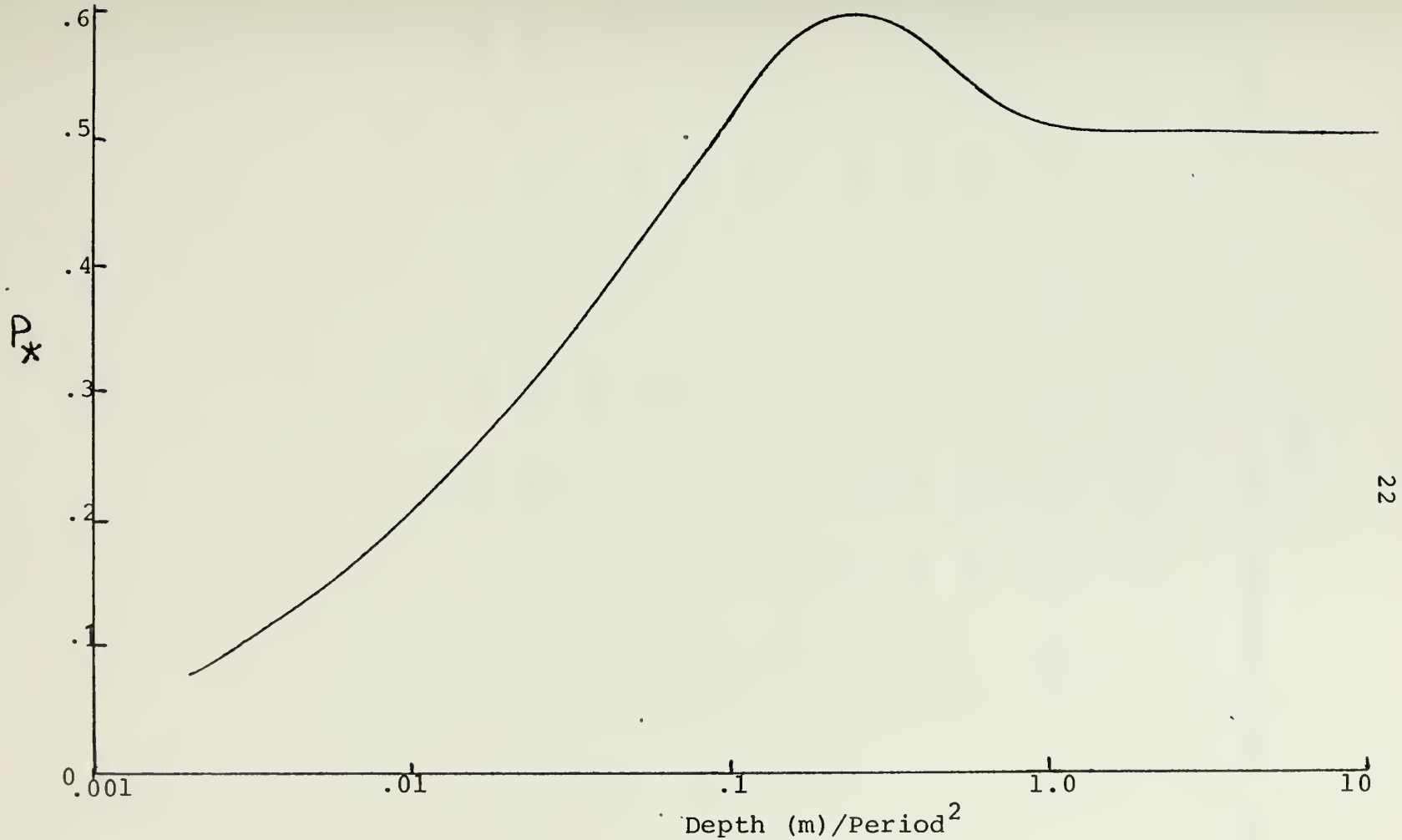

Figure 3-1: P_* as a Function of Depth/Period^2.

TABLE 3-1

VALUES OF P_* FOR VARIOUS WATER DEPTHS AND WAVE PERIODS

Wave Period (S) \ Water Depth (M)	3	6	9	15	20	30
1.5	.50	.50	.50	.50	.50	.50
3.5	.60	.54	.50	.50	.50	.50
5.5	.52	.59	.60	.54	.53	.50
7.5	.40	.53	.55	.60	.59	.54
9.5	.33	.46	.51	.56	.57	.58
11.5	.29	.40	.46	.53	.54	.60
13.5	.26	.34	.41	.49	.50	.56
15.5	.22	.31	.36	.44	.45	.53
17.5	.20	.28	.33	.41	.43	.51
19.5	.18	.25	.31	.37	.39	.49
21.5	.16	.23	.28	.33	.36	.47

3.2 Limitations on Wave Power

Before examining actual wave power statistics from various sites it will be worthwhile to survey some of the environmental phenomena which limit the development of power.

Wind speed is the most important factor in the development of waves. Darbyshire, Sverdrup-Munk and Neumann have all proposed spectra relating significant wave height to wind speed (U). These spectra show that H_s is proportional to U^2 or $U^{2.5}$ (ref. 15). This implies that the highest values of wave power will occur in regions or seasons with very high continuous wind speeds.

Fetch, the distance over water that the wind blows in an unobstructed manner, is another important element in wave power limitation. For a given wind speed significant wave height increases as fetch increases. Figure 3-2 displays the effect of fetch on H_s.

Related to fetch is sheltering. Harbors and other sheltered waterways cannot possibly experience the continuously high levels of power available in the open ocean.

In very shallow water locations wave energy may be dissipated in wave-breaking and bottom losses.

This very general survey should aid in predicting locations of the highest power densities. Since winds prevail from the west for the U.S. it is reasonable to expect

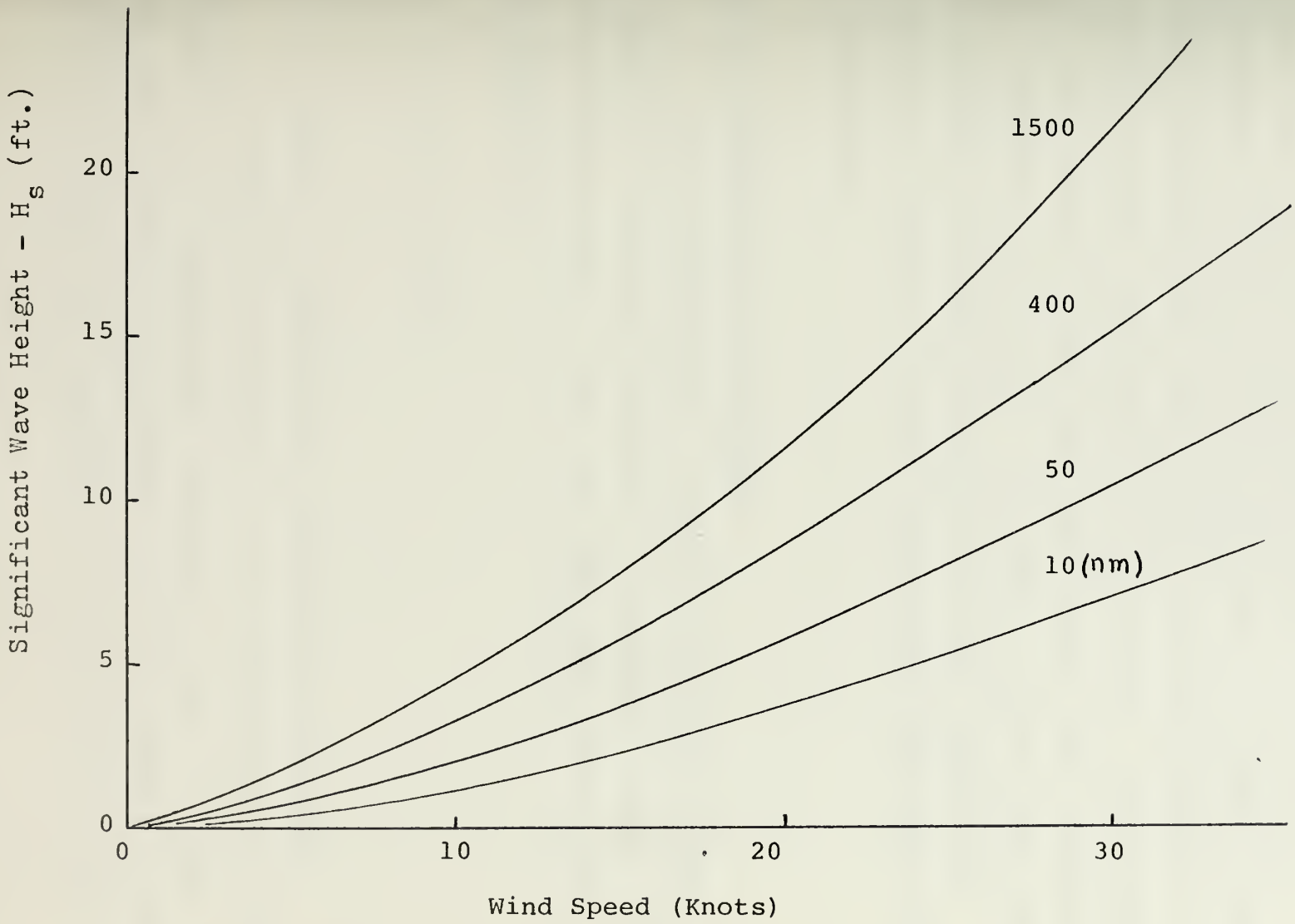

Figure 3-2: Effects of Fetch and Wind Speed on Significant Wave Height.

coastal power densities to be higher on the West Coast than on the East Coast, because of the effects of fetch and sheltering. Higher power densities are anticipated at deep ocean locations rather than coastal locations because of the effects of fetch, sheltering and dissipation. Since winds are more severe in the winter months higher power densities are expected during winter. The actual values of wave power at different locations and during different seasons are detailed in Chapter 4 and they substantiate these very general observations.

3.3 Probability Distributions

3.3.1 Wave height. In spectral analysis of wave records the Rayleigh distribution is generally assumed for wave heights (refs. 4, 15). The simplified form of this distribution is

$$P(\xi) = \xi e^{-\xi^2/2} \tag{11}$$

where ξ = observed wave height/mean wave height.

A statistical analysis of this distribution was performed on 1963 samples from statistics in ref. 12. The Rayleigh expression was inverted using the computer library program MIT-SNAP and a regression line was fitted to the

inverted distribution. The regression yielded $r^2 = .88$, with small and evenly distributed residuals. Although the r^2 is not particularly high, the regression does indicate that the Rayleigh assumption is a reasonable approximation to the observed data.

3.3.2 Wave period. If little is known about the wave period at a particular location then a good approximation (ref. 10) to the distribution can be achieved by using

$$P\left(\frac{T}{\bar{T}}\right) = 1 - e^{-.675\left(\frac{T}{\bar{T}}\right)^4} \tag{12}$$

This equation yields a distribution which is symmetric about its mean.

The statistics used in estimating power in this report all assume that periods are normally distributed with a standard deviation σ_T. A regression line was fitted to the inverted normal distribution for the same 1963 samples used in the wave height analysis. The value of r^2 was .96 and the residuals were small and uniformly distributed.

3.3.3 Independence of height and period. Wave heights and periods are generally assumed to be independent (refs. 20, 32). A statistical test for correlation between height and period was performed using 1000 observations from joint

height-period tables scattered over all seasons at Nags Head, North Carolina (data from ref. 32). Mean wave periods for each of ten wave height groups were tabulated and a hypothesis test for correlation was conducted using a 5% risk of type I error. Since the data was reduced to only ten wave height groups the test was performed using manual methods and the t=distribution.

$$H_0 : \rho = 0$$

$$H_1 : \rho \neq 0$$

Test for $t = r\sqrt{\frac{n-2}{1-r^2}}$

where $r^2 = \frac{\text{explained variance}}{\text{total variance}} = \left|1 - \frac{S^2(T/H)}{S_T^2}\right|$

n = number of observations

The assumed form of the regression equation is

$$E(T/H) = \hat{\alpha} + \hat{\beta}H$$

$$S^2(T/H) = \frac{1}{n}(\Sigma T^2 - \hat{\alpha}\,\Sigma T - \hat{\beta}\Sigma TH)$$

$$S_T^2 = \frac{1}{n}(\Sigma T^2 - \bar{T}\Sigma T)$$

$$\begin{pmatrix} \hat{\alpha} \\ \hat{\beta} \end{pmatrix} = \begin{pmatrix} \Sigma T \\ \Sigma TH \end{pmatrix} \times \begin{pmatrix} n & \Sigma H \\ \Sigma H & \Sigma H^2 \end{pmatrix}^{-1}$$

i	H_i	T_i	H_i^2	H_iT_i	T_i^2
1	1	9.6	1	9.6	92.16
2	2	9.2	4	18.4	84.64
3	3	8.5	9	25.5	72.25
4	4	8.2	16	32.8	67.24
5	5	8.3	25	41.5	68.89
6	6	8.8	36	52.8	77.44
7	7	9.8	49	68.6	96.04
8	8	9.0	64	72.0	81.0
9	9	10.6	81	95.4	112.36
10	10	8.4	100	84.0	70.56
Σ	55	90.4	385	500.6	822.58

$$\bar{T} = 9.04$$

$$\begin{pmatrix} \hat{\alpha} \\ \hat{\beta} \end{pmatrix} = \begin{pmatrix} 90.4 \\ 500.6 \end{pmatrix} \times \begin{pmatrix} 10 & 55 \\ 55 & 385 \end{pmatrix} = \begin{pmatrix} 8.81 \\ .041 \end{pmatrix}$$

$$S^2(T/H) = \frac{1}{10}(822.58 - 8.81\ (90.4) - .041\ (500.6))$$

$$= .563$$

$$S_T^2 = \frac{1}{10}(822.58 - 9.04\ (90.4)) = .536$$

$$r^2 = \left|1 - \frac{.563}{.536}\right| = .05$$

$$r = .224$$

$$t = .224\sqrt{\frac{10-2}{1-.05}} = .65$$

For a 5% risk of Type I error, t = 2.3. Therefore, accept hypothesis $H_0 : \rho = 0$, that there is no correlation between H and T.

3.3.4 Wave power. Nath (ref. 20) derived the probability distribution for wave power under the assumptions that Power (P) ~ H^2T, which has already been shown to be valid, that height can be represented by the Rayleigh distribution and that T^2 can be represented by the Rayleigh distribution. This last assumption for T^2 is the same distribution presented in section 3.3.2 for use when wave period standard deviation is unknown, that is,

$$P\left(\frac{T}{\bar{T}}\right) = 1 - e^{-.675\left(\frac{T}{\bar{T}}\right)^4}$$

Let $y = H^2T$ = power

$\bar{y}$ = mean power

Using the above assumptions, Nath derived the following distribution:

$$P_y(y) = \frac{1}{\bar{y}} e^{-y/\bar{y}}$$

$\bar{y}$ = standard deviation

A statistical test of this distribution was performed using the same 1963 samples that were used in the height and period tests. The distribution was inverted and a regression line was fitted to the inversion with $r^2 = .99$. The regression strongly suggests validity of this exponential distribution.

A further test was conducted on standard deviations of wave power arrivals. The exponential distribution yields an expected value of $\sigma_P/P = 1.0$. Data from Pierson (ref. 22) was utilized with 12 monthly summaries at 20 different locations. A regression line was fitted on the observed standard deviation of power (σ_P) vs. the theoretical standard deviation ($\bar{P}$). The regression line was

$$\sigma_P = 2.83 + 1.03 \bar{P}$$

with $r^2 = .86$.

With values of σ_P ranging up to 350 KW/M in the data, the regression constant (2.83) is negligible. The slope of 1.03 compares favorably with the expected slope of 1.0. These results further validate the use of the exponential power arrival distribution.

It is important to note that the time between observations of wave power may play a significant role in the shape of the distribution. Most of the records which were used in this report are based on monthly summaries of observations taken every 12 hours. The distribution of power over any given 12 hour interval is clearly not as severe as the exponential distribution, largely because of the persistent nature of weather patterns.

It is beyond the scope of this report to attempt to determine the shape of the power distribution over a 12-hour interval, but a confidence interval about the expected value of σ_P/P can easily be established. Using 150 sets of data from the Marine Environmental Service, Canada (ref. 38), with each data set containing 5 observations of wave energy in a given 12-hour interval, a mean and standard deviation of energy were computed.

$n = 150$

$\bar{x}$ = sample mean = $\sigma_E/E = .156$

S = sample standard deviation = .132

$$\sigma_{\bar{x}} = \frac{S}{\sqrt{n-1}} = \frac{.132}{\sqrt{149}} = .0108$$

For a 95% confidence interval,

$$\bar{x} \pm 1.96\ \sigma_{\bar{x}} = .156 \pm 1.96\ (.0108)$$

$$= .156 \pm .021$$

Range: .135 → .177

In other words over any given 12 hour interval the standard deviation of wave energy is expected to be 15.6% ± 2.1% of the mean wave energy. This is obviously much less than the expected 100% using the exponential distribution.

CHAPTER 4

WAVE CLIMATOLOGY

The problem of defining ocean waves statistically is not new, yet, it is only within the past decade that acceptable techniques for recording data have been developed. The U.S. Army Corps of Engineers Civil Engineering Research Center (CERC) has compiled the most accurate data available by its system of wave gauges around the coast of the U.S. (ref. 32). Unfortunately, all of the wave gauges are located within one mile of the coast and are, therefore, not very useful in predicting open-ocean power densities. The manual Ocean Wave Statistics (ref. 12) provides an acceptable compilation of joint wave height and period distributions for very large open-ocean areas around the world. These two sources and references 22 and 38 provided the data for analysis of ocean waves around the U.S.

Since this report deals with a feasibility study, the statistics of ocean waves will be most useful if they present a very broad picture. Raw data from 17 coastal locations and 29 open-ocean locations was analyzed and summarized to present as broad a picture as possible, but still to retain enough identity to perform calculations necessary for the study. Tables 4-1 to 4-5 contain the following variables:

Region - North, Middle and South Atlantic and
North, Middle and South Pacific off the coast
of the U.S.

Ocean location - Coastal waters (within 1 mile)
Open-ocean (about 100 miles off shore)

Seasons - Dec-Feb; Mar-May; Jun-Aug; Sep-Nov

Wave Height - H in meters

Wave Period - T in seconds

Wave power density - P in KW/M

Non-dimensional power variability - σ_P/P

Non-dimensional period variability - σ_T/T

It is worthwhile to point out some of the strengths and limitations of these tables. Hundreds of thousands of observations from over 300 records were summarized to create these tables; therefore, the tables should not be applied to any specific location. Data for coastal regions is more accurate than data for deep ocean locations. Calculations of power density were performed by the methods outlined in Chapter 3. The values of wave period (T) in the deep-ocean sections for Atlantic regions are probably not very accurate, as these observations are based on shipborne wave-recorders. For this reason and since wave period remains essentially unchanged with depth (ref. 32) only one value of σ_T/T was calculated for each region, based on coastal readings.

The graphs in fig. 4-1 show the variation of the mean power level over the seasons for the East and West coasts.

TABLE 4-1

WAVE CLIMATOLOGY: DECEMBER TO FEBRUARY

	COASTAL				DEEP OCEAN				
	$\bar{H}$	$\bar{T}$	$\bar{P}$	$\sigma_P/\bar{P}$	$\bar{H}$	$\bar{T}$	$\bar{P}$	$\sigma_P/\bar{P}$	$\sigma_T/\bar{T}$
North Atlantic	1.2	8.5	8.7	.92	3.6	6.7	54.6	.90	.33
Mid Atlantic	1.0	8.3	5.2	1.02	2.9	6.2	31.1	1.02	.31
South Atlantic	.9	7.7	4.0	.80	2.5	6.3	28.0	.94	.38
North Pacific	--	--	--	--	5.2	10.0	150	.98	.30
Mid Pacific	1.1	10.8	6.1	.80	3.3	10.9	90	1.02	.25
South Pacific	.9	11.9	6.2	.70	2.4	11.9	33	.90	.25

TABLE 4-2

WAVE CLIMATOLOGY: MARCH TO MAY

	COASTAL				DEEP OCEAN				
	$\bar{H}$	$\bar{T}$	$\bar{P}$	$\sigma_P/\bar{P}$	$\bar{H}$	$\bar{T}$	$\bar{P}$	$\sigma_P/\bar{P}$	$\sigma_T/\bar{T}$
North Atlantic	1.1	8.2	5.6	.90	3.1	6.3	38.8	.97	.28
Mid Atlantic	.9	8.1	3.3	.88	2.6	6.0	24.9	1.10	.27
South Atlantic	.8	7.6	2.6	1.10	2.3	6.0	21.5	1.01	.36
North Pacific	--	--	--	--	2.7	9.8	45	.88	.34
Mid Pacific	1.0	10.4	6.9	.71	2.4	9.7	27	.91	.33
South Pacific	.9	13.3	6.6	.65	2.1	11.8	22	.83	.29

TABLE 4-3

WAVE CLIMATOLOGY: JUNE TO AUGUST

	COASTAL				DEEP OCEAN				
	$\bar{H}$	$\bar{T}$	$\bar{P}$	$\sigma_P/\bar{P}$	$\bar{H}$	$\bar{T}$	$\bar{P}$	$\sigma_P/\bar{P}$	$\sigma_T/\bar{T}$
North Atlantic	.8	7.4	2.9	.86	2.4	5.7	21.2	1.10	.20
Mid Atlantic	.6	8.0	1.9	1.05	2.2	5.6	16.9	1.15	.19
South Atlantic	.5	6.7	1.5	1.06	2.0	5.6	14.6	1.06	.31
North Pacific	--	--	--	--	1.7	11.2	17	1.07	.29
Mid Pacific	.9	11.6	6.7	.70	1.5	10.6	13	1.09	.27
South Pacific	.8	14.0	6.2	.55	1.5	13.5	12	.86	.24

TABLE 4-4

WAVE CLIMATOLOGY: SEPTEMBER TO NOVEMBER

	COASTAL				DEEP OCEAN				
	$\bar{H}$	$\bar{T}$	$\bar{P}$	$\sigma_P/\bar{P}$	$\bar{H}$	$\bar{T}$	$\bar{P}$	$\sigma_P/\bar{P}$	$\sigma_T/\bar{T}$
North Atlantic	1.1	8.7	5.4	1.0	3.0	6.4	37.1	.93	.31
Mid Atlantic	.9	8.5	3.7	.97	2.6	6.0	25.0	1.05	.27
South Atlantic	.8	7.0	2.6	1.15	2.3	6.1	21.6	.97	.36
North Pacific	--	--	--	--	3.9	11.9	110	.93	.25
Mid Pacific	.9	11.8	7.2	.55	3.3	10.4	80	1.04	.28
South Pacific	.7	14.4	5.4	.60	2.2	14.3	35	1.15	.21

TABLE 4-5

WAVE CLIMATOLOGY: ALL SEASONS

	COASTAL				DEEP OCEAN				
	$\bar{H}$	$\bar{T}$	$\bar{P}$	$\sigma_P/\bar{P}$	$\bar{H}$	$\bar{T}$	$\bar{P}$	$\sigma_P/\bar{P}$	$\sigma_T/\bar{T}$
North Atlantic	1.0	8.5	5.2	.98	3.2	6.3	37.1	.98	.31
Mid Atlantic	.8	7.9	3.1	1.03	2.7	5.9	25.6	1.08	.34
South Atlantic	.7	6.7	2.5	1.08	2.4	6.0	22.1	.99	.34
North Pacific	--	--	--	--	3.4	11.0	81	.97	.28
Mid Pacific	1.0	10.4	5.7	.70	2.6	10.3	52	1.01	.29
South Pacific	.9	13.2	4.9	.65	2.1	13.2	25	.94	.23

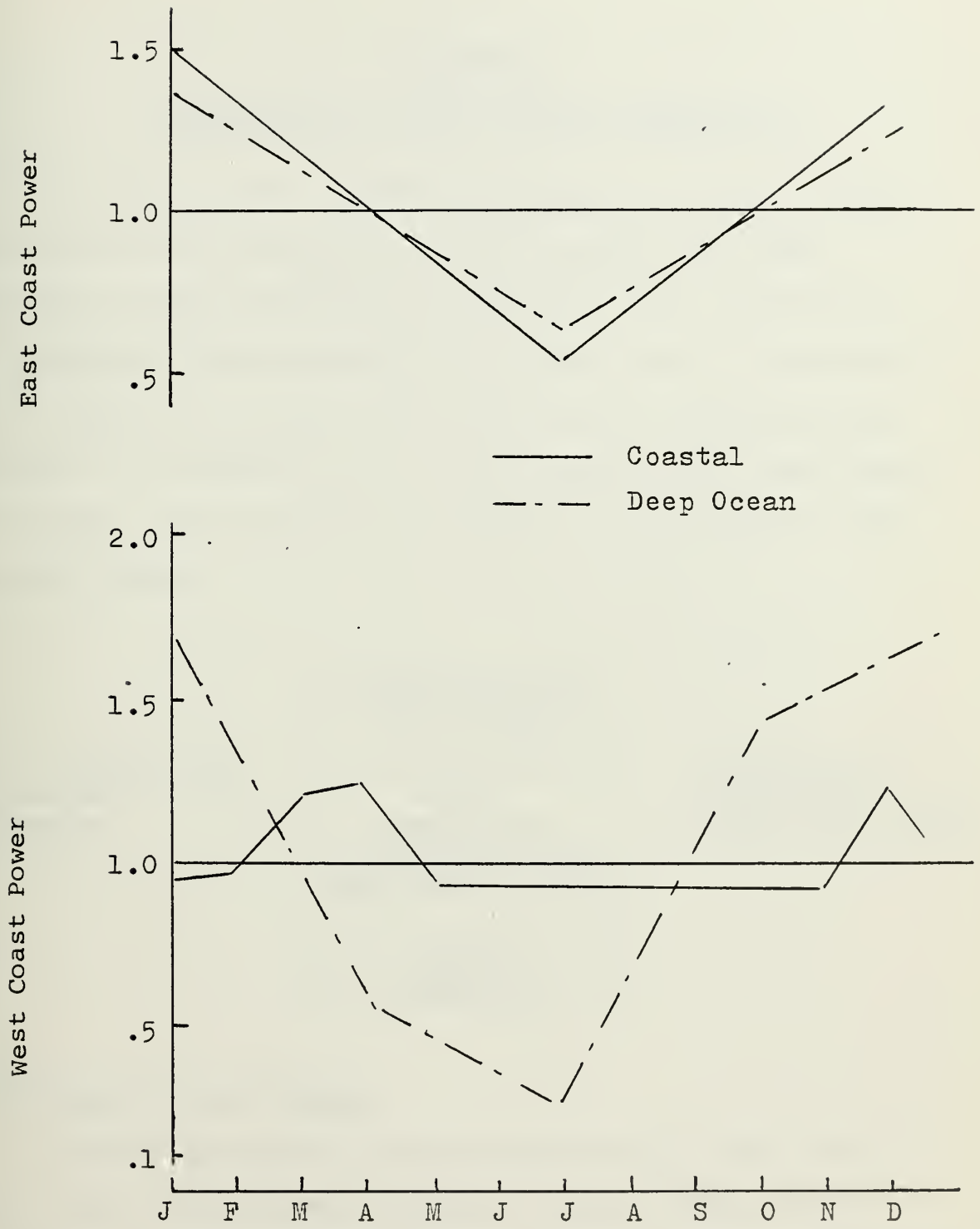

Figure 4-1: Variation over year of mean power non-dimensionalized to mean monthly average.

CHAPTER 5

FORMULATION OF MODEL FOR WPG EVALUATION

In the previous chapters experimental evidence which substantiates the viability of the cam-type wave power absorber and the environmental phenomena which affect the cam's operation were presented. The next step in the feasibility study is to analyze the cam with all its associated parameters to determine how it might operate in a real-world environment. This task may be viewed in the pattern of the flowchart below:

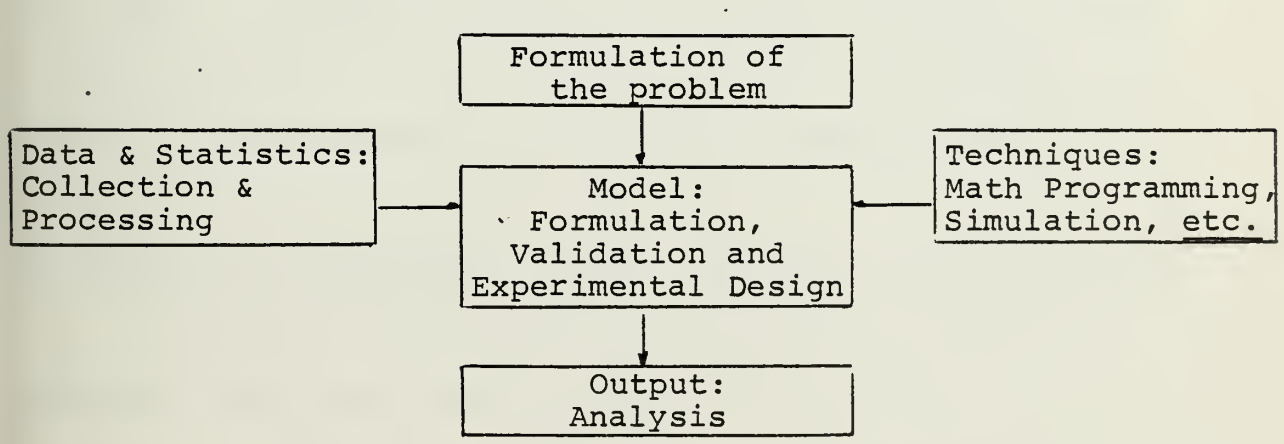

Formulation of the Problem

The cam system may be characterized by length, diameter, separation between elements, natural frequency of oscillation, motion damping, energy storage, a scheme of conversion to energy in a useful form and the users' demand for that energy.

The cam's environment (the ocean) is essentially characterized at any location by distributions of wave height, period or frequency of waves, power or energy in waves, water depth and distance from land.

The coupling between the cam and its environment is characterized by sets of efficiency curves which are functions of cam design and the environment.

The basic problem is the same for all energy-related systems: that is, to optimally design the parameters of the cam (at the feasibility-study level of detail) and to locate the system so that it delivers the least expensive energy to the users. The model must deal with the stochastic nature of the environment and be flexible enough to determine the effect on performance of variations in system design.

Collection and processing of real world data and statistics

Cam efficiency characteristics and environmental variables have been presented in previous chapters.

Formulation of the model

There is no necessity to deal with both performance and costs simultaneously. Performance will be analyzed first.

The model must be capable of handling discrete-time random inputs, a large number of variables and parameters, mathematically intractable efficiency distributions,

comparisons of alternative systems or operating conditions, reproducible experiments, and output statistics in the form of summaries with frequency distributions.

The obvious model type selection for handling the above conditions is simulation. The simulation language GPSS was chosen for the following reasons: (1) the author's familiarity with its use; (2) discrete-time capabilities; (3) ability to deal with complicated distributions; (4) many commands for assembling statistics; (5) debugging capabilities; (6) transaction flow tracking capabilities; and (7) repeatability of experiments. The model description is included in Appendix A and the program listing in Appendix B.

Model Validation

Several experiments were performed on the model to check its logical and statistical validity. From the table POAVA the distribution of power available was plotted to check its correlation with the input exponential distribution. Several efficiency curves were reproduced by simulating non-random seas and extracting data from the table EFFIC (efficiency). Statistics from the table PEROD (period) were correlated with several different input period distributions. Individual model segments were checked for proper operation using the block count table (a standard output with GPSS) to verify that transactions (wave power arrivals) proceeded in a logical sequence when the model was constrained to force operation of each segment.

Experiments were designed and performed to test the effects of changing environmental conditions and system parameters on system output. These experiments with the analyses will be discussed in Chapter 6.

CHAPTER 6

SIMULATION RESULTS AND ANALYSIS

The simulation model was run with a large number of different configurations in order to develop design lanes or determine the effects on the system of variable cam diameters, hydrodynamic efficiency, wave period variability, wave power variability, energy storage, power demand, power rating, power availability and cam separation.

6.1 Cam diameter - no separation

Iterations were performed with the model to determine the diameter of maximum power output for a range of wave period variances. The maximum output diameter is independent of wave period variance but is different for each of three levels of inertia tested at M.I.T. The results are listed in Table 6-1.

TABLE 6-1

CHARACTERISTICS OF MAXIMUM POWER OUTPUT DIAMETER

Inertia	$\omega\sqrt{a/g}$	λ/D	η/η_{max}
Low	.66	7.3	.83
Middle	.76	5.4	.93
High	.64	7.7	1.0

Note that the maximum power output occurs near the apex of efficiency curves from the M.I.T. experiments for each level of inertia. The high inertia design delivers more power with a smaller cam diameter (smaller $\omega\sqrt{a/g}$) and therefore is the optimal choice of the three. The efficiency listed in table 6-1 is non-dimensionalized to the efficiency of the high inertia value. The actual number value of the efficiency is a function of the variability of wave period about its mean: this will be discussed in section 6.3.

The question next arises as to whether or not this single cam diameter indeed delivers the most power from the waves since wave periods are varying about the mean and optimal cam diameter is a function of wave period. The model was tested to see if varying the cam diameter about its optimal mean would produce any increase in system efficiency. An arbitrary entity was devised representing the standard deviation of cam diameters about the mean value obtained from table 6-1. This entity is defined σ_D. Figure 6-1 shows the simulated results of power out and standard deviation of power out vs. σ_D/σ_T. The results indicate that the maximum power output diameter for a system of cams in a given random sea is a point design, in other words, all cams in the system should have the same diameter, since the mean power decreases and the spread of power increases as diameters are increasingly varied about the point mean.

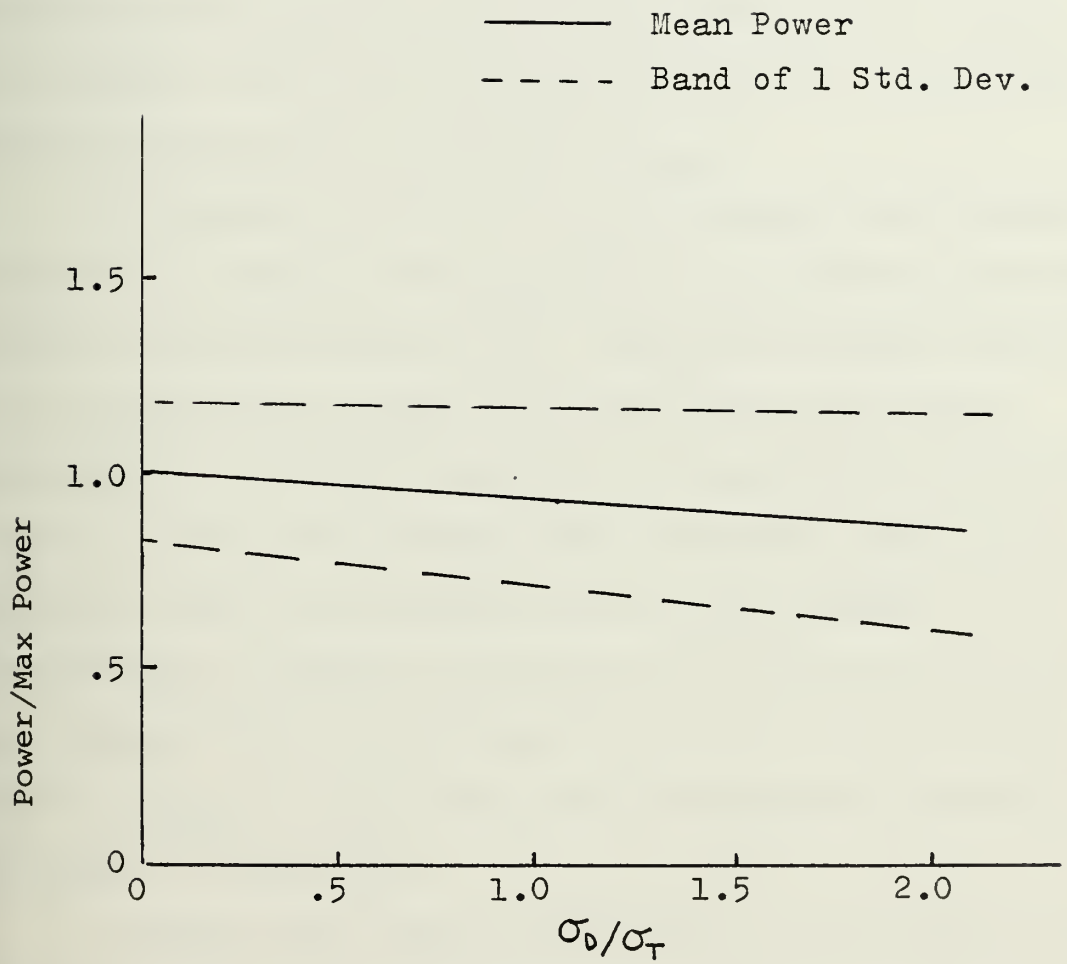

Figure 6-1: Effect of Varying Cam Diameters about Point Maximum.

Since it is possible that the minimum cost/KW system will have a smaller diameter than the maximum output system, off-design performance was analyzed with the model. The performance is depicted in figure 6-2, where power (P) is non-dimensionalized with the maximum power output (P_{max}), and diameter (D) is non-dimensionalized with the diameter at which maximum power is delivered (D_{max}).

The spread of power delivered changes considerably as diameter is reduced from D_{max} due to the filtering characteristics of the efficiency curve. Because of this, figure 6-2 must be adjusted to ensure that all points have equal availability. The availability, or the percent of time that power is equal to or greater than a specific power level, was extracted from the simulation model output tables. The availability of power at each point of the curve in figure 6-2 was compared with the availability of the maximum output power ($P/P_{max} = 1.0$). The curve of adjustment factors is included in figure 6-3.

Assuming that the marginal value of increased availability is equal to the marginal cost of increased power, the adjustment factor curve may be multiplied point by point with the off-design power curve to yield the adjusted curve of figure 6-4. This adjusted curve is used when cost estimates are applied to find the minimum cost diameter.

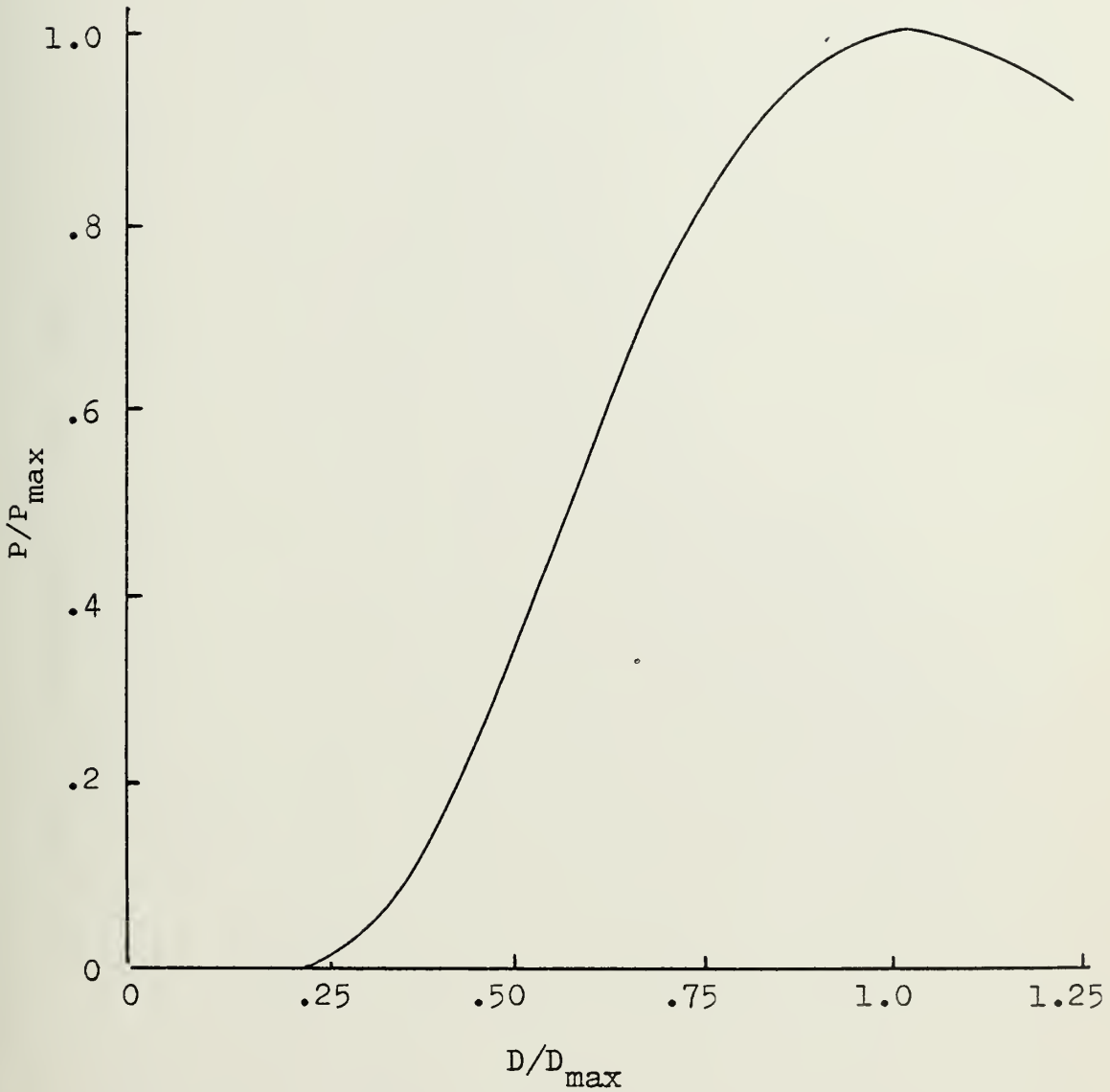

Figure 6-2: Delivered Power vs Cam Diameter - No Separation

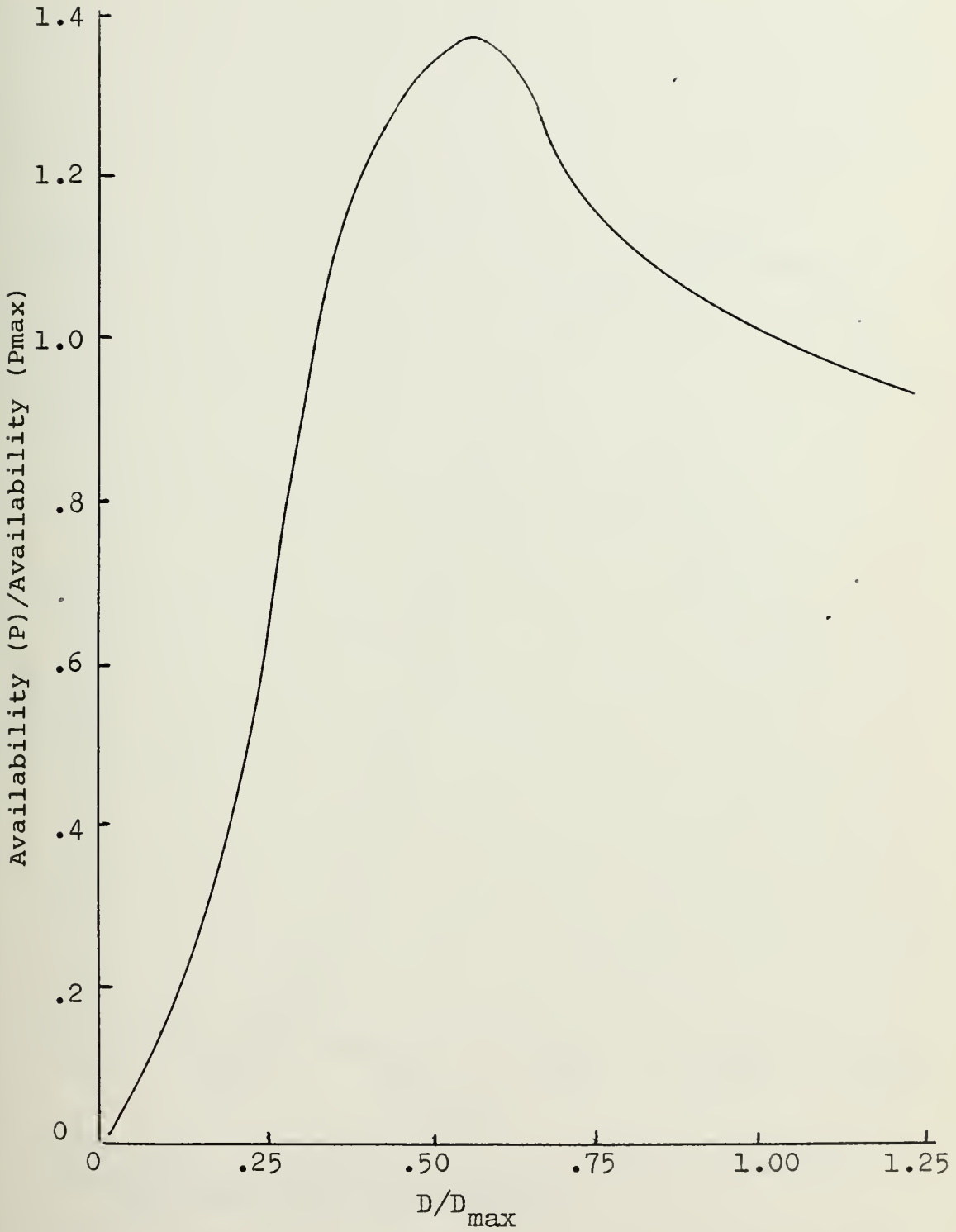

Figure 6-3: Availability Adjustment Factor For Off-Design Diameters - No Separation

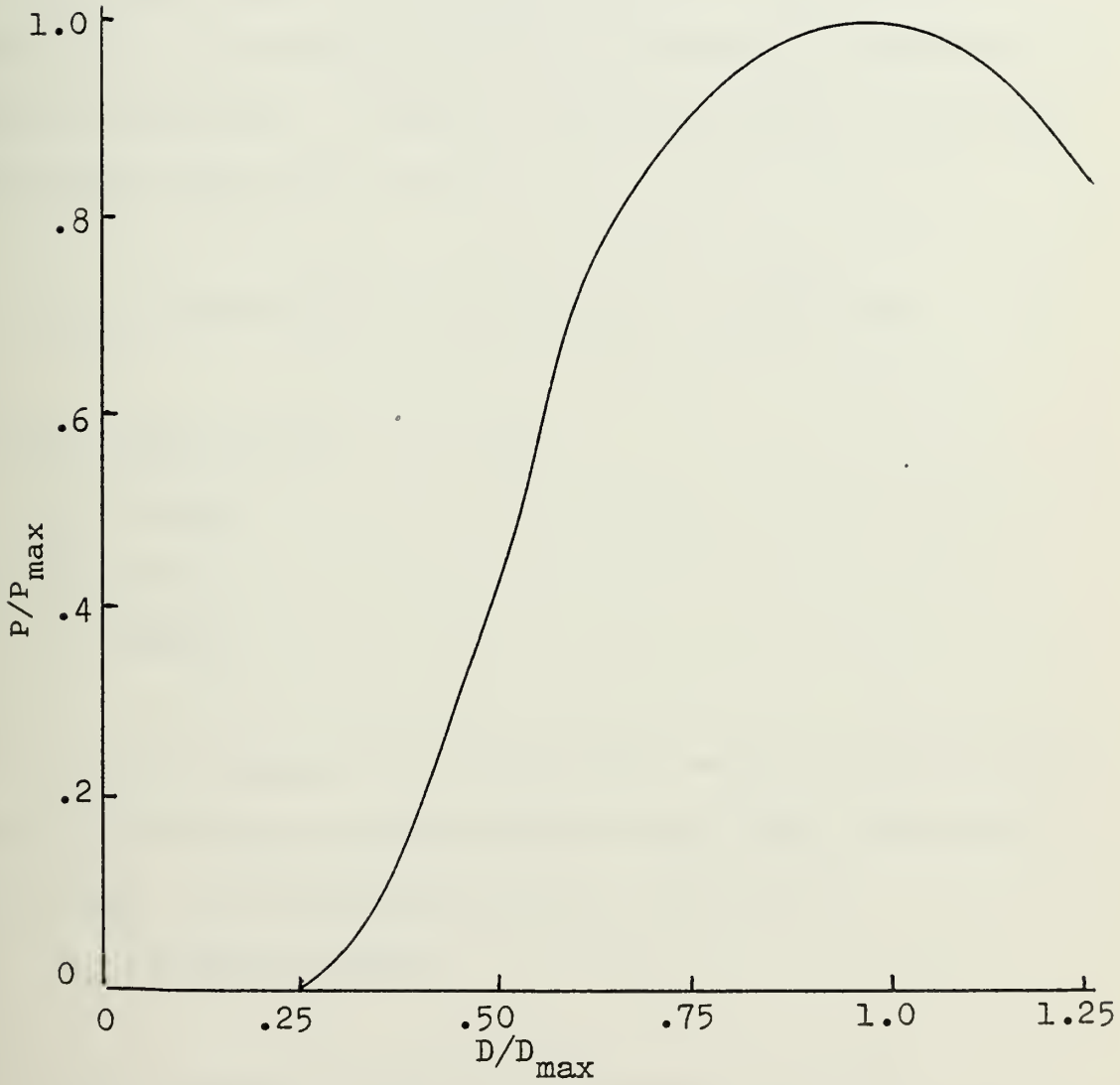

Figure 6-4: Delivered Power vs Diameter Adjusted For Equivalent Availability.

6.2 Minimum cost/KW diameter selection - no separation

With the off-design performance of the cam known, all that is needed is the corresponding cost curve to find the minimum cost/KW design diameter. The basic trade-off involves only structural costs and delivered power. According to Kyrkos (ref. 17) structural costs are directly related to the weight of structure. A useful structural weight estimating relationship (from ref. 25) is

$$W_1 = 1.68341\ CN^2 + 167.1721\ CN - 23.283 \text{ tons} \qquad (1)$$

where $CN = LBZ \times 10^{-5}$

L = length

B = beam

Z = depth

With the Salter cam, structural weight is essentially embodied in the circular cylindrical main body. Therefore, beam = depth = cam diameter and $CN = LD^2 \times 10^{-5}$.

For constant length,

$$W_1 \sim 1.68341 \times 10^{-10}\ D^4 + 1.671721 \times 10^{-3}\ D^2$$

$$\sim D^2$$

Therefore, off-design cam costs are proportional to D^2. The resulting cost curve, non-dimensionalized to the cost of the cam at D_{max} is drawn in figure 6-5 along with the off-design power curve. Dividing the $\$/\$_{max}$ curve point-by-point by the P/P_{max} curve yields $\frac{\$/\$_{max}}{P/P_{max}}$ or non-dimensional \$/KW.

From the figure, \$/KW is minimized at $D/D_{max} = .60$. In other words, the minimum cost/KW system will have a diameter which is 60% of the diameter at maximum power output, where the cam delivers 68% of the power of D_{max} at 36% of the cost of D_{max}.

6.3 Variability of wave period

The non-dimensional parameter chosen to describe the variability of wave period is σ_T/T. A given cam design will deliver less power as the value of σ_T/T increases, since the cam will be caused to operate outside its region of maximum efficiency more often with higher σ_T/T. The simulation model was run with various values of σ_T and various values of T yielding the curves in figures 6-6, 6-7, and 6-8. Figure 6-8 represents the efficiency curve adjusted for equivalent availability.

Typical values of σ_T/T (from the tables in Chapter 4) are displayed in figure 6-8 with the resulting 2-D cam efficiencies between 60-70%.

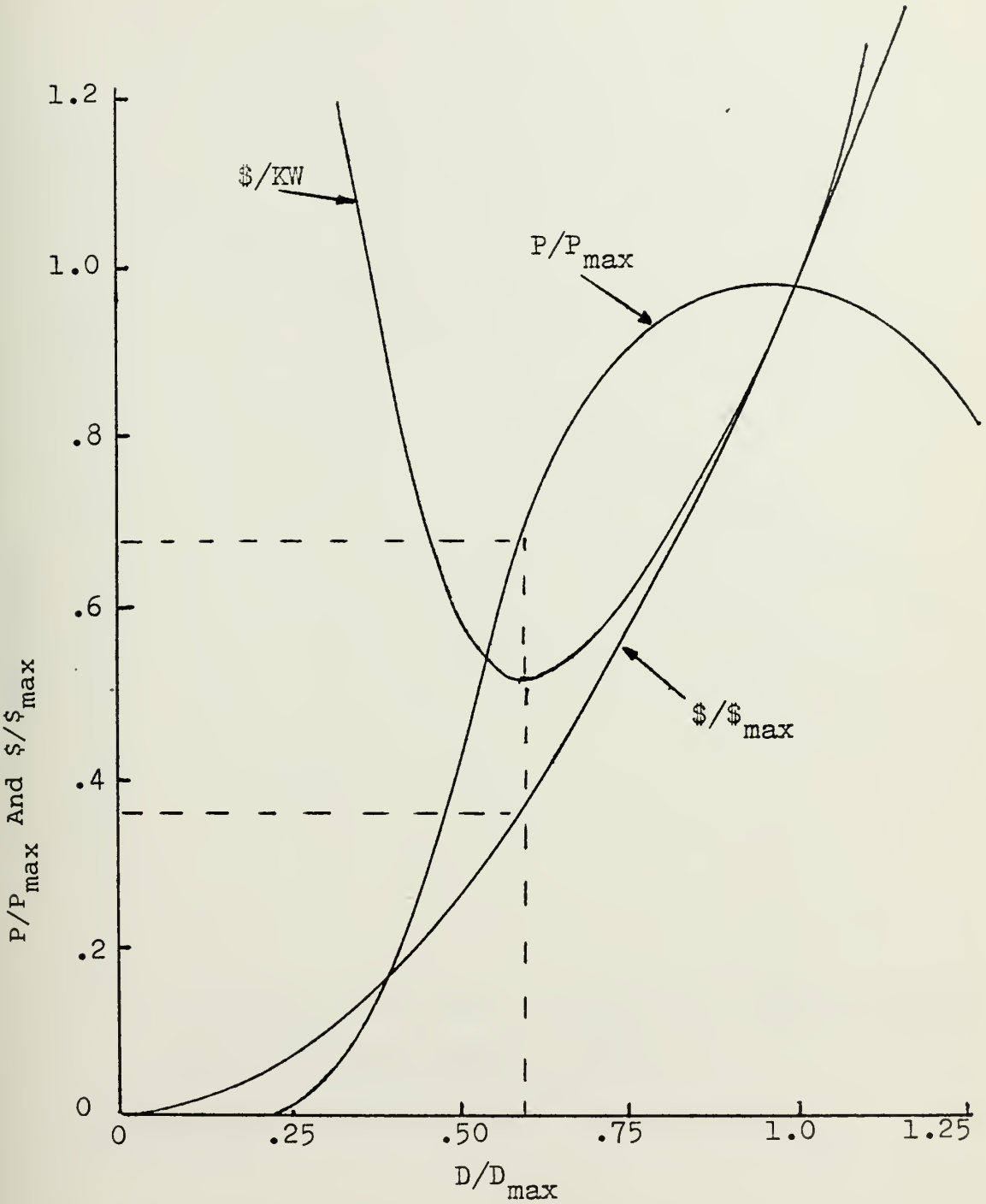

Figure 6-5: Minimum Cost Diameter Selection - No Separation.

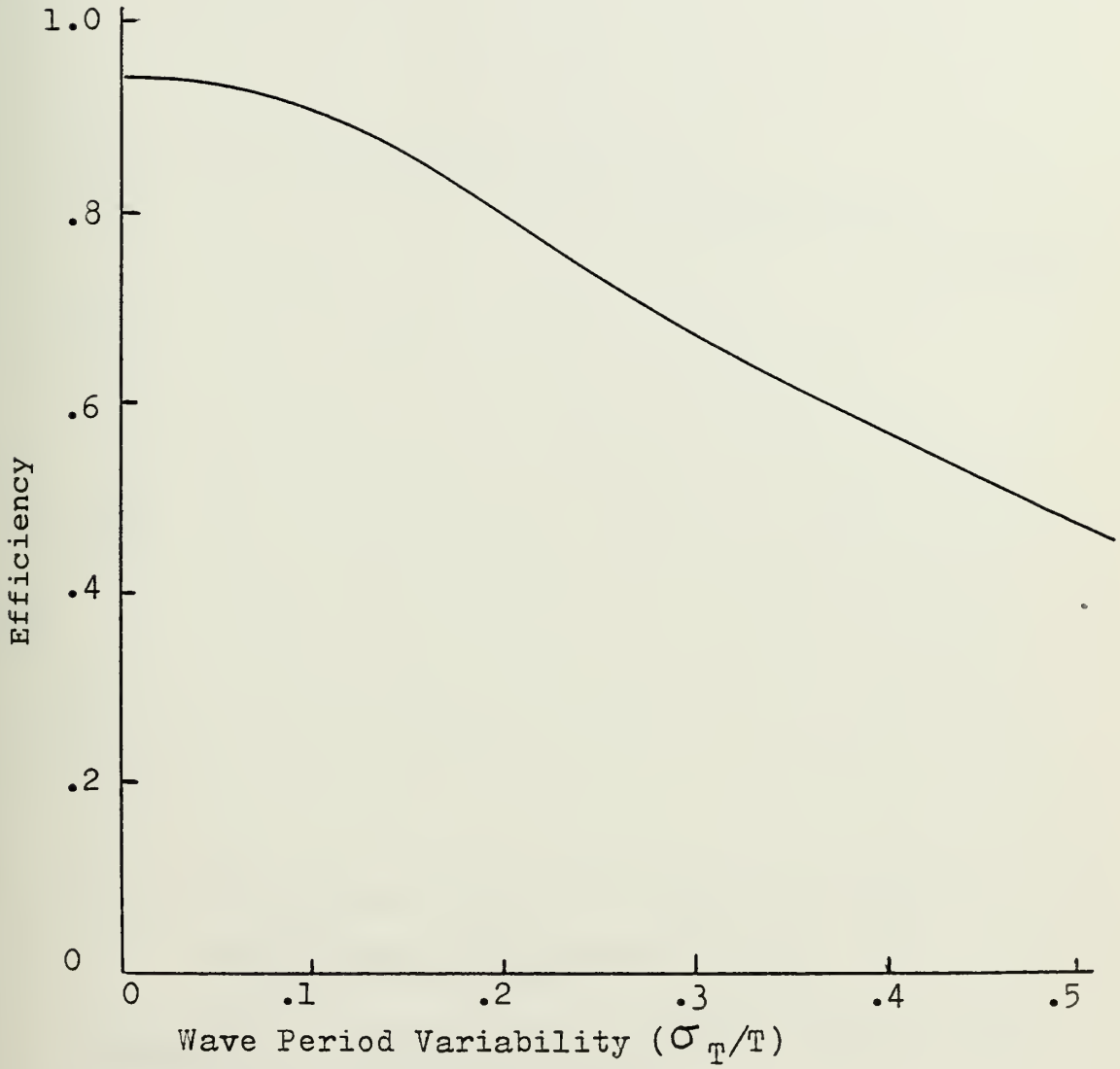

Figure 6-6: Cam Efficiency - No Separation.

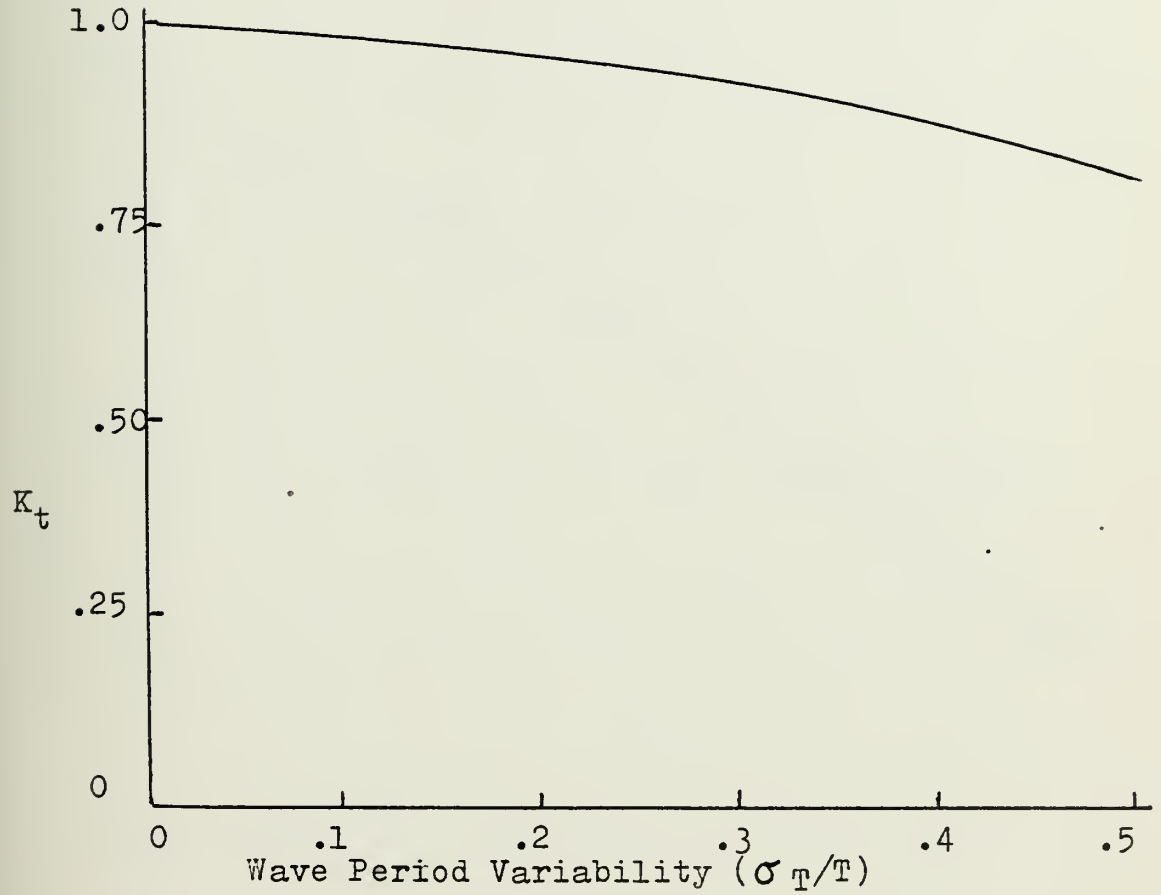

Figure 6-7: Availability Adjustment Factor Curve For Cam Efficiency Curve.

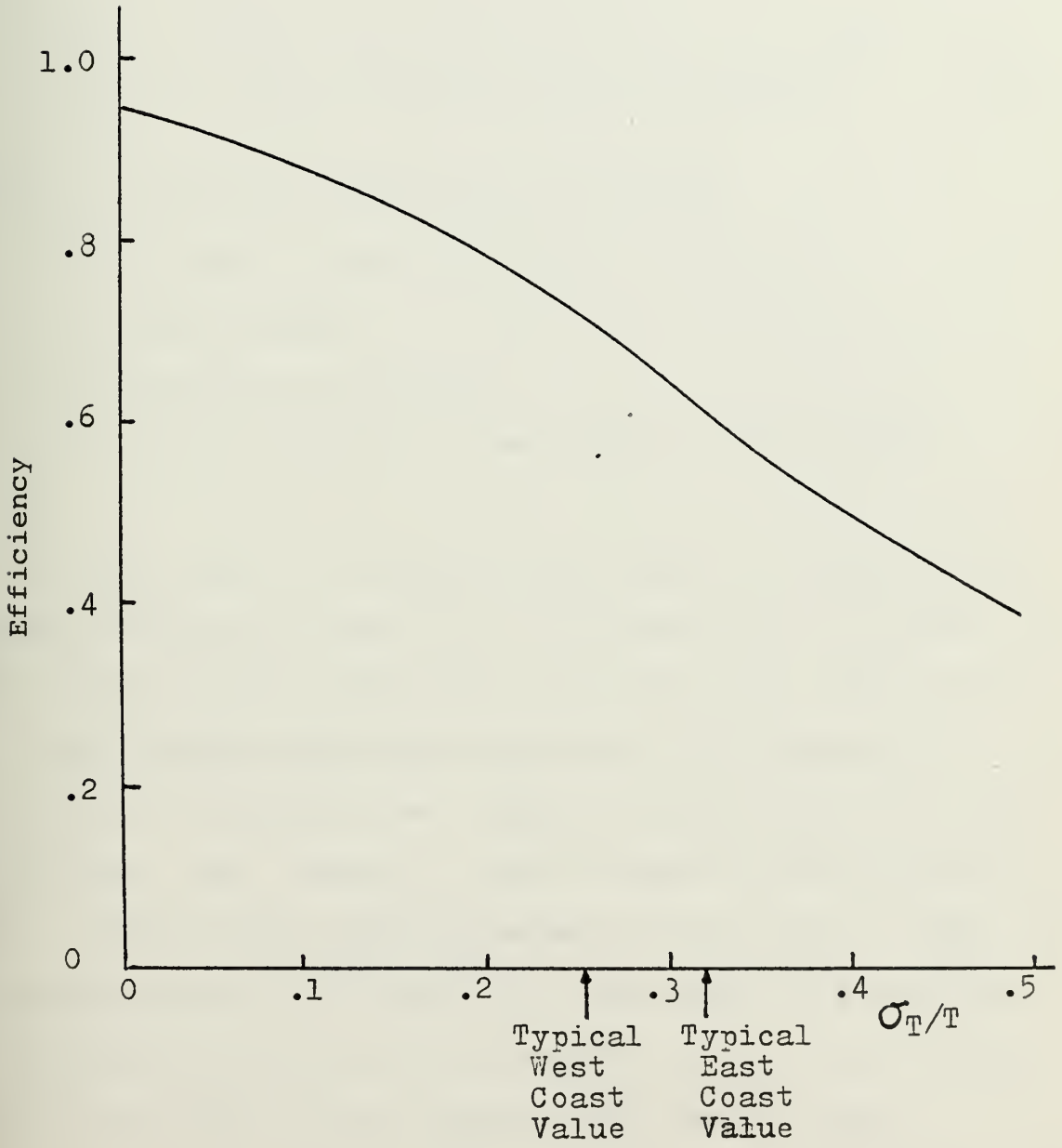

Figure 6-8: Efficiency Curve Adjusted For Equivalent Availability - No Separation.

6.4 Cam separation

Budal (ref. 2) has shown that separation may effectively increase the efficiency of a wave power absorber by wave interaction. He defines a factor, q, where

$$q = \left[1 + \frac{2}{N} \sum_{n=1}^{N} (N-n)\cos(nKd \sin\gamma)\, J_o(nKd)\right]^{-1} \qquad (2)$$

where q = effective efficiency multiplier

N = number of power absorbers

K = wave number

d = separation distance

γ = angle between cam and normal to wave crest

Davis (ref. 7) displayed the effect of separation by drawing efficiency curves for a 2-D mode and a 3-D mode. In the 2-D mode maximum efficiency was about 95%, while in the 3-D mode maximum efficiency was about 175% (figure 2-3). Since the 3-D mode data was taken in an open tank, the cam effectively "saw" images of itself caused by the two tank's walls. Davis' data was reexpressed to the form $q = \frac{\eta_{3-D}}{\eta_{2-D}}$, and plotted against Kd in figure 6-9. The separation distance, d, was taken to be twice the distance from the cam's center to the tank wall, or the distance from cam to image.

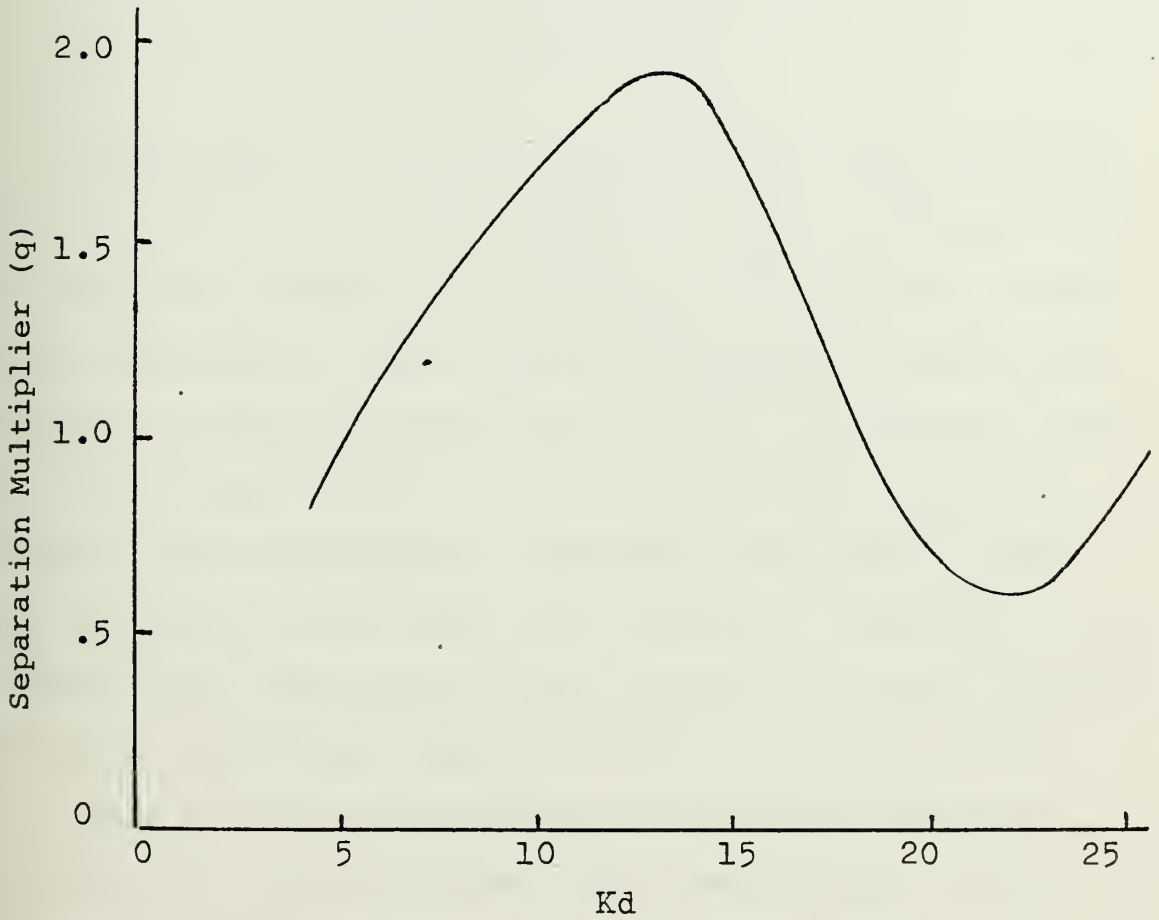

Figure 6-9: Effect of Separation Using MIT Experimental Data.

There appears to be a discrepancy between the observed "q" and the "q" expected from Budal's analysis. Assuming $N = 3$ and $\gamma = 0$, Budal's equation yields,

$$q = [1 + \frac{2}{3}(2\ J_o(Kd) + J_o(2Kd))]^{-1} \qquad (3)$$

This equation is plotted as the solid line in figure 6-10. For the observed data plotted in the same figure, the value of Kd was divided by 3 to achieve the visible correlation between the observed data and Budal's equation. This is the discrepancy referred to previously, and it is also the reason that the horizontal axis in that figure is left unmarked. Because of the discrepancy, conclusions about the optimal value of Kd may not be drawn with certainty. However, it may be stated that there exists some value of separation distance which will yield appreciable increases in cam efficiency.

With the 2-D cam, efficiency was shown to decrease as the value of σ_T/T increases. This same effect occurs with the 3-D cam. Figure 6-11 shows the cam efficiency as a function of σ_T/T based on a cam of middle inertia designed at the maximum power output, that is, at $\omega\sqrt{a/g} = .63$.

Figure 6-10: Separation Effect Comparison Between MIT Observations And Budal Equation.

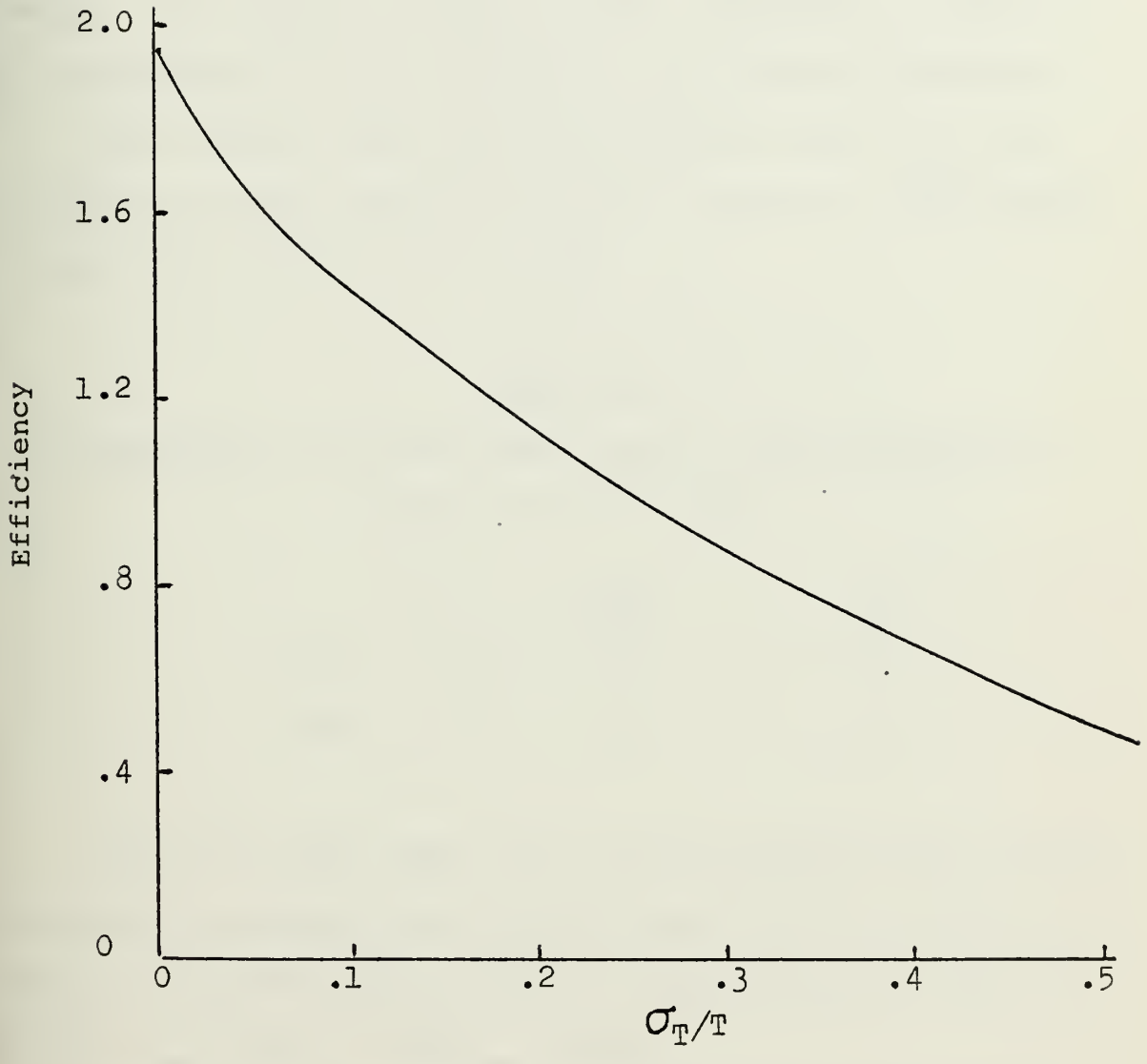

Figure 6-11: Cam Efficiency Curve With Separation At Optimal Separation Distance Adjusted For Equivalent Availability.

6.5 Minimum cost/KW diameter selection - with separation

It was shown in section 6.2 that the optimum (minimum cost/KW) diameter is not the same as the maximum output diameter. An analysis similar to that performed on the 2-D cam was performed on the 3-D cam for off-design diameters.

Davis showed that the maximum power output for the 3-D cam with middle inertia occurs at a value of $\omega\sqrt{a/g}$ which is lower than that for the 2-D cam:

TABLE 6-2

COMPARISON OF MAXIMUM POWER OUTPUT CHARACTERISTICS FOR THE 2-D AND 3-D CAMS

	$\omega\sqrt{a/g}$	λ/D
2-D	.76	5.4
3-D	.63	7.9

Table 6-2 shows that for a given frequency wave optimal cam diameter is smaller for the 3-D cam than the 2-D cam. The diameter at maximum power output is 32% smaller for the 3-D cam, or, D_{max} (3-D) = .68 D_{max} (2-D).

Figure 6-12 shows the off-design 3-D performance; figure 6-13 shows the availability adjustment factor; figure 6-14 shows the adjusted off-design performance curve and figure 6-15 shows the minimum $/KW diameter. The analysis is similar to that performed in section 6.2.

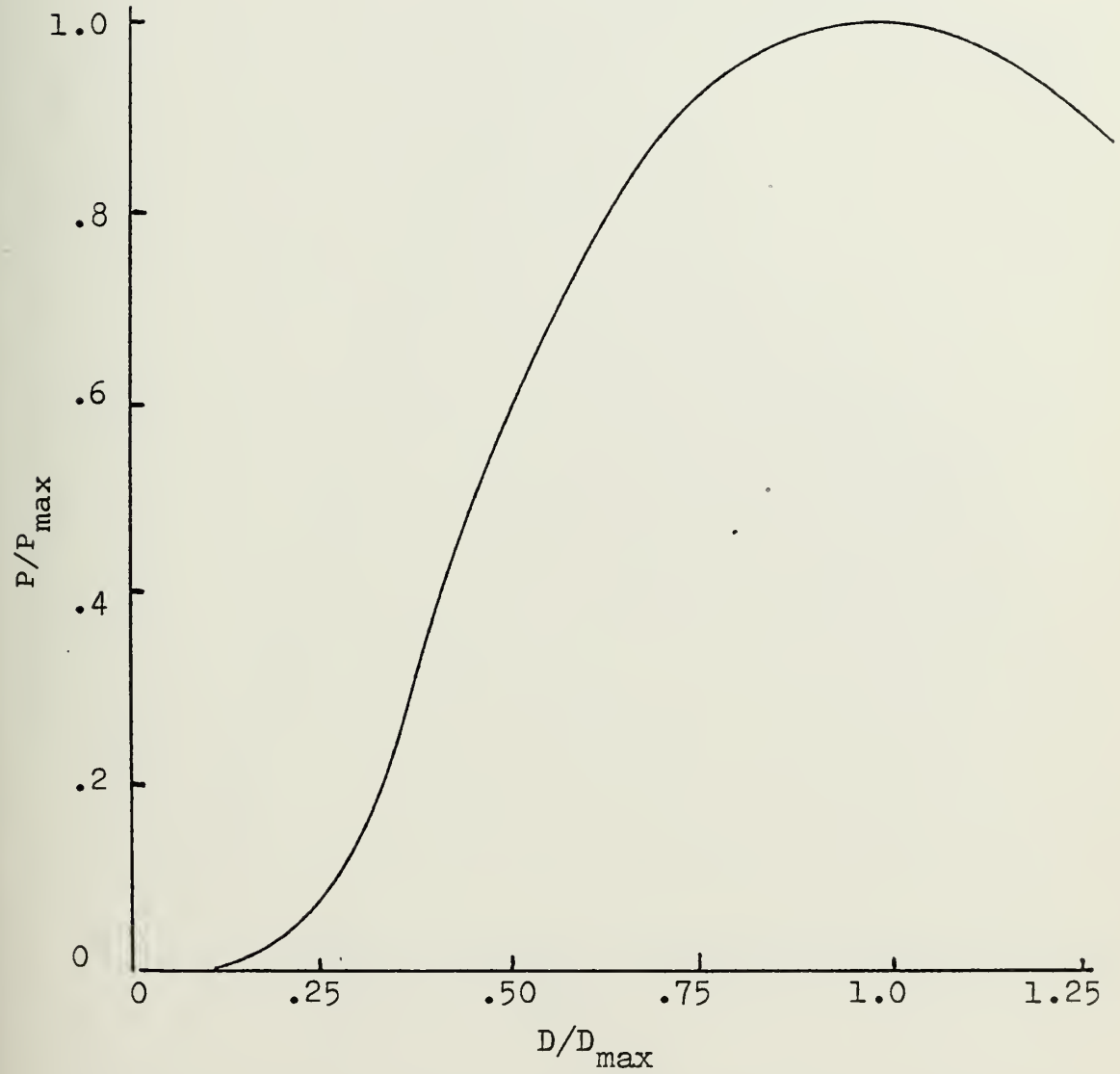

Figure 6-12: Delivered Power vs Cam Diameter - With Separation.

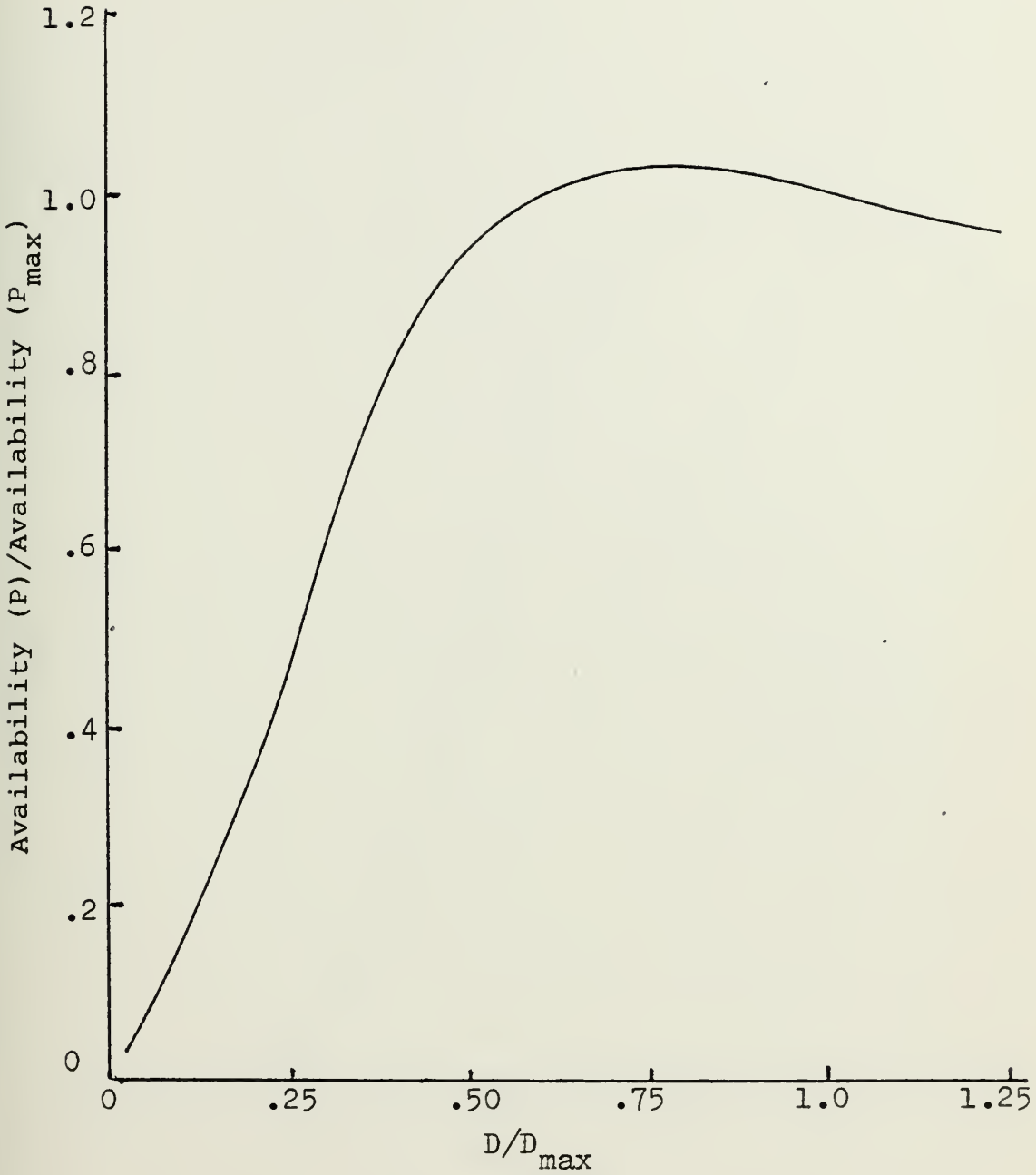

Figure 6-13: Availability Adjustment Factor For Off-Design Diameters - With Separation.

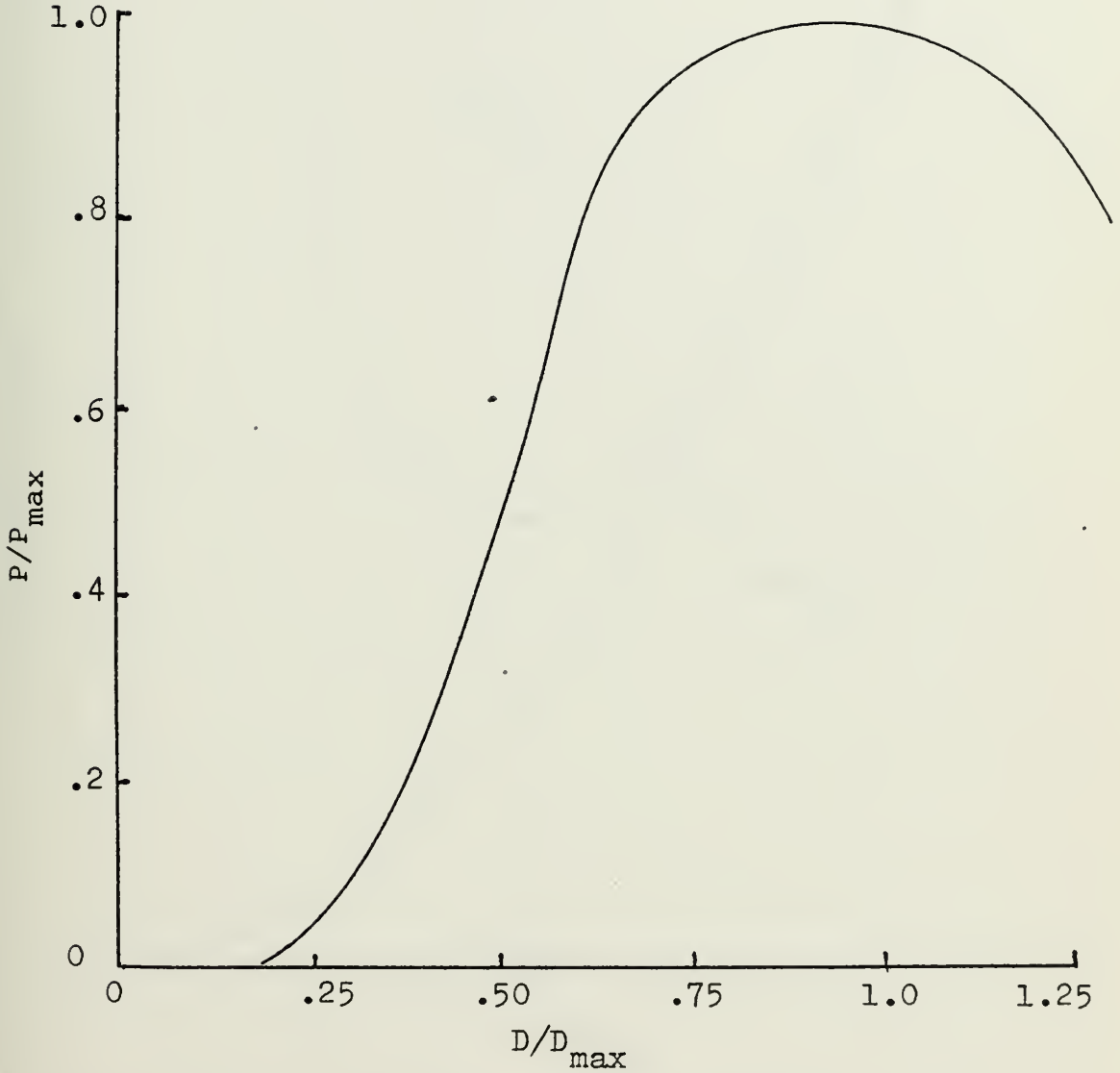

Figure 6-14: Delivered Power vs Diameter Adjusted For Equivalent Availability - With Separation.

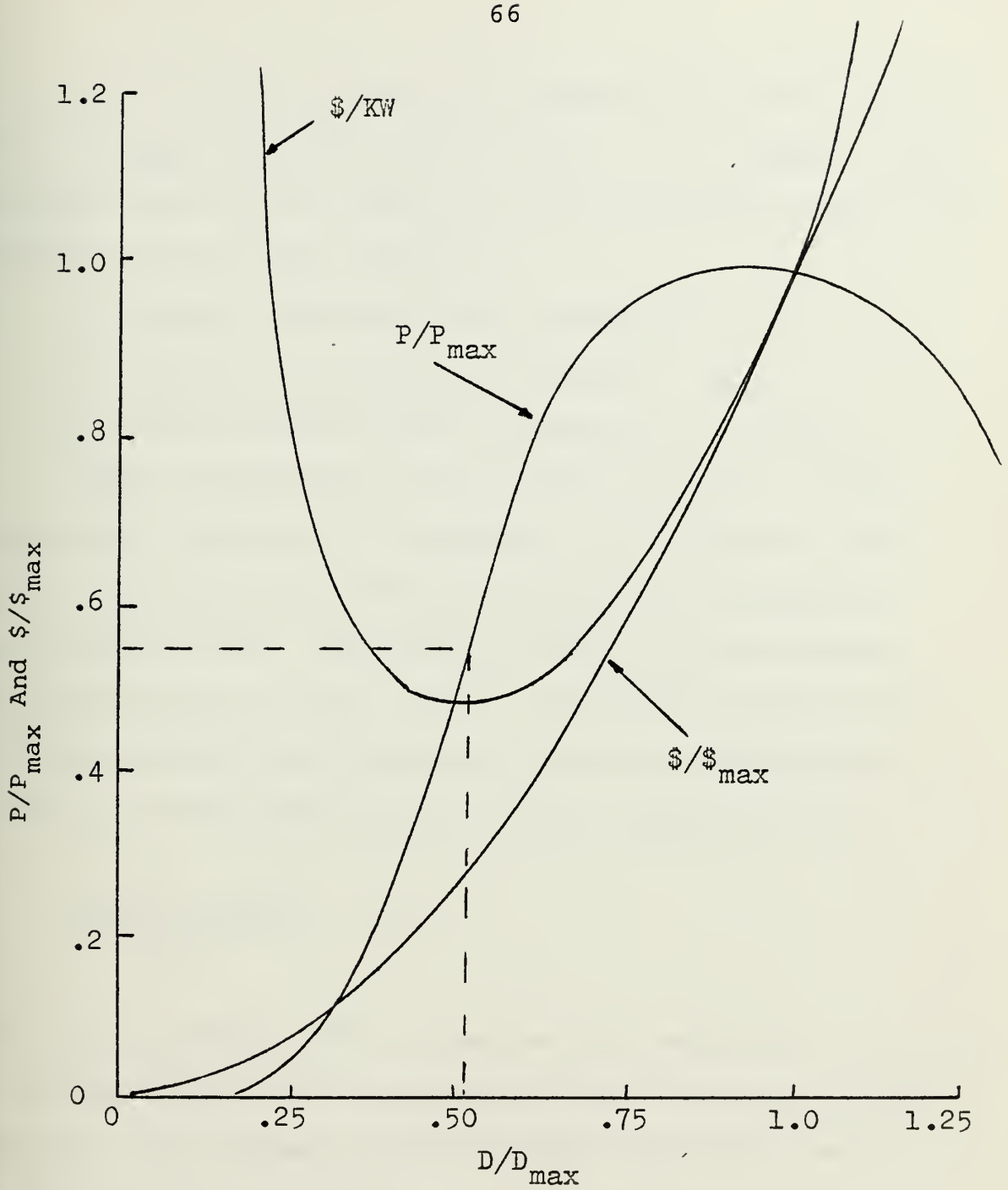

Figure 6-15: Minimum Cost Diameter Selection - With Separation.

Note that the minimum cost diameter for the 3-D cam is about .52 D_{max}, while for the 2-D cam it is .60 D_{max}. Separation then will play an important role in reducing costs of the system for these three reasons:

1. Higher efficiency for a given σ_T/T
2. Smaller maximum output diameter (D_{max})
3. Smaller minimum cost diameter ratio (D/D_{max})

These observations may be used to provide a rough estimate for the value of separation. At a typical value of $\sigma_T/T = .30$, the factor reduction in diameter of maximum power output is .68. The factor reduction in the minimum cost diameter is .52/.60 = .867. Using these three factors and again assuming that structural costs are proportional to D^2, the structural \$/KW of the cam with separation is

$$\frac{(.68)^2\ (.867)^2}{1.4} \approx .25$$

times the structural \$/KW of the cam with separation, assuming no additional costs for separation. This remarkable savings indicates that further research should concentrate heavily in the area of cam separation.

6.6 Energy storage, power rating and availability

A very definite trade-off exists between demand (assumed to equal power rating for this analysis) and availability (% of time that power is equal to or greater than demand), for any given level of energy storage. A family of curves of demand vs. availability may be drawn for any level of energy storage using results from simulation model runs. As the example in figure 6-16 displays, there is a very sharp "knee" in each curve of demand vs. availability. Assuming the marginal value of increased availability equals the marginal cost of incremental power, an optimal curve may be drawn which is tangent to these "knees".

The example in figure 6-16 is for an energy storage of 30 hours, that is, the storage system is capable of delivering power at rated capacity for 30 hours. Figure 6-17 displays a system of these curves for various levels of energy storage.

6.7 Optimal level of energy storage

The curves in figure 6-17 were reexpressed to plot demand as a function of energy storage with lines of constant availability in figure 6-18. The line of maximum value of energy storage represents the highest output per unit of storage possible for any availability/demand combination. The graph shows that for most levels of availability the maximum power output per unit cost of energy storage ranges from 3 to 7 hours of storage.

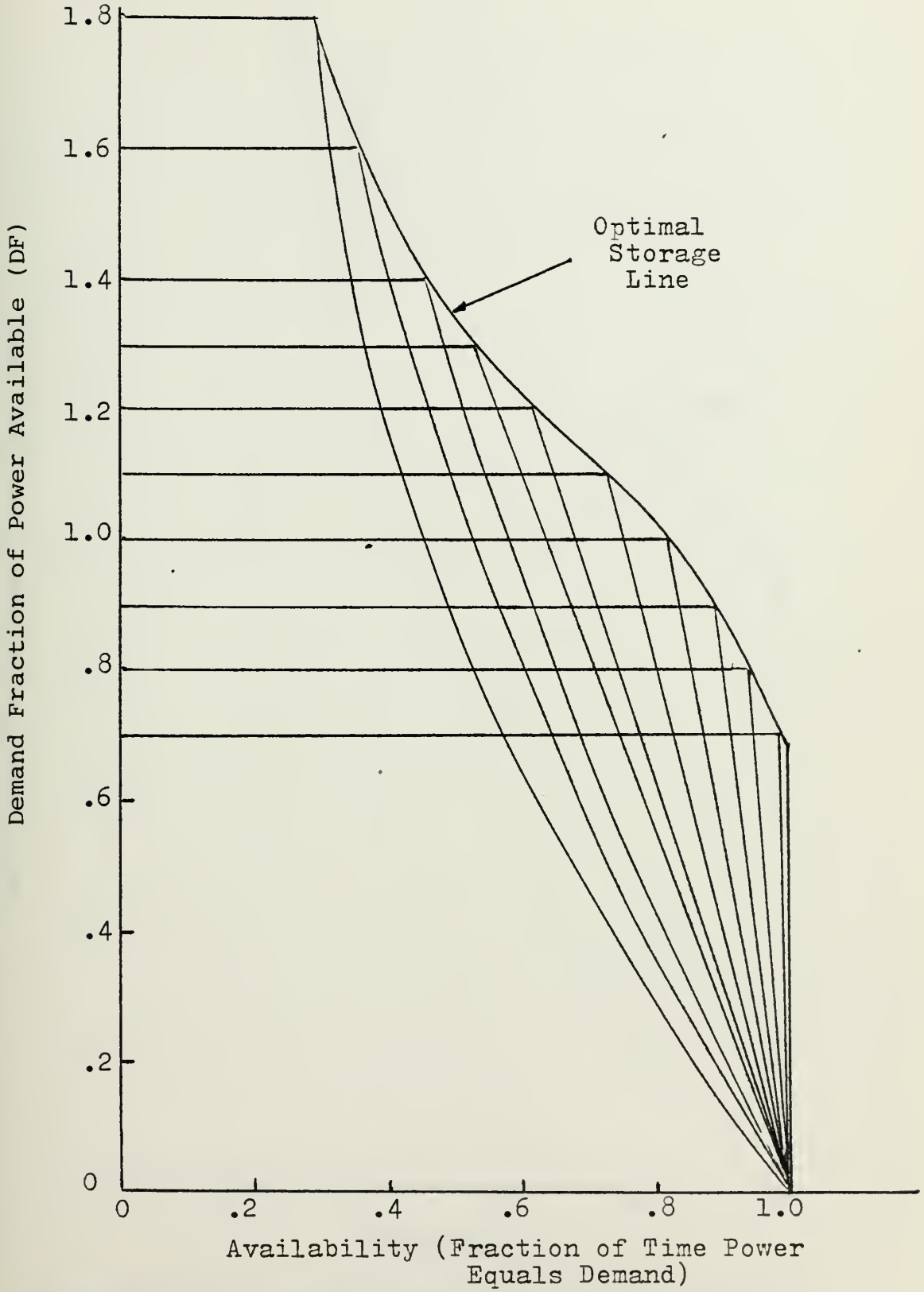

Figure 6-16: Sample Storage Curve Construction.

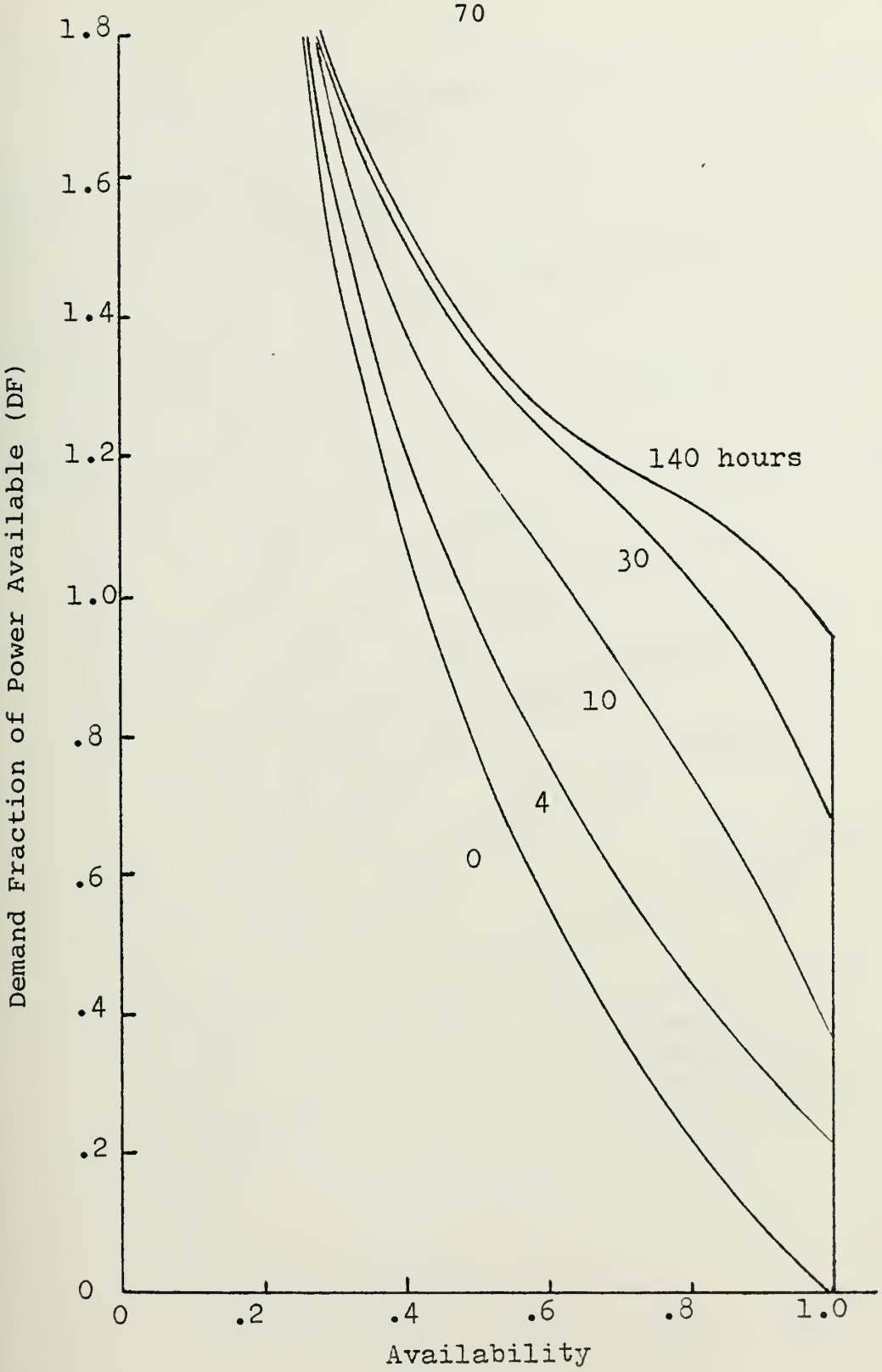

Figure 6-17: Design Lanes For Storage Capacity (Hours of Storage Required For Given Level of Demand).

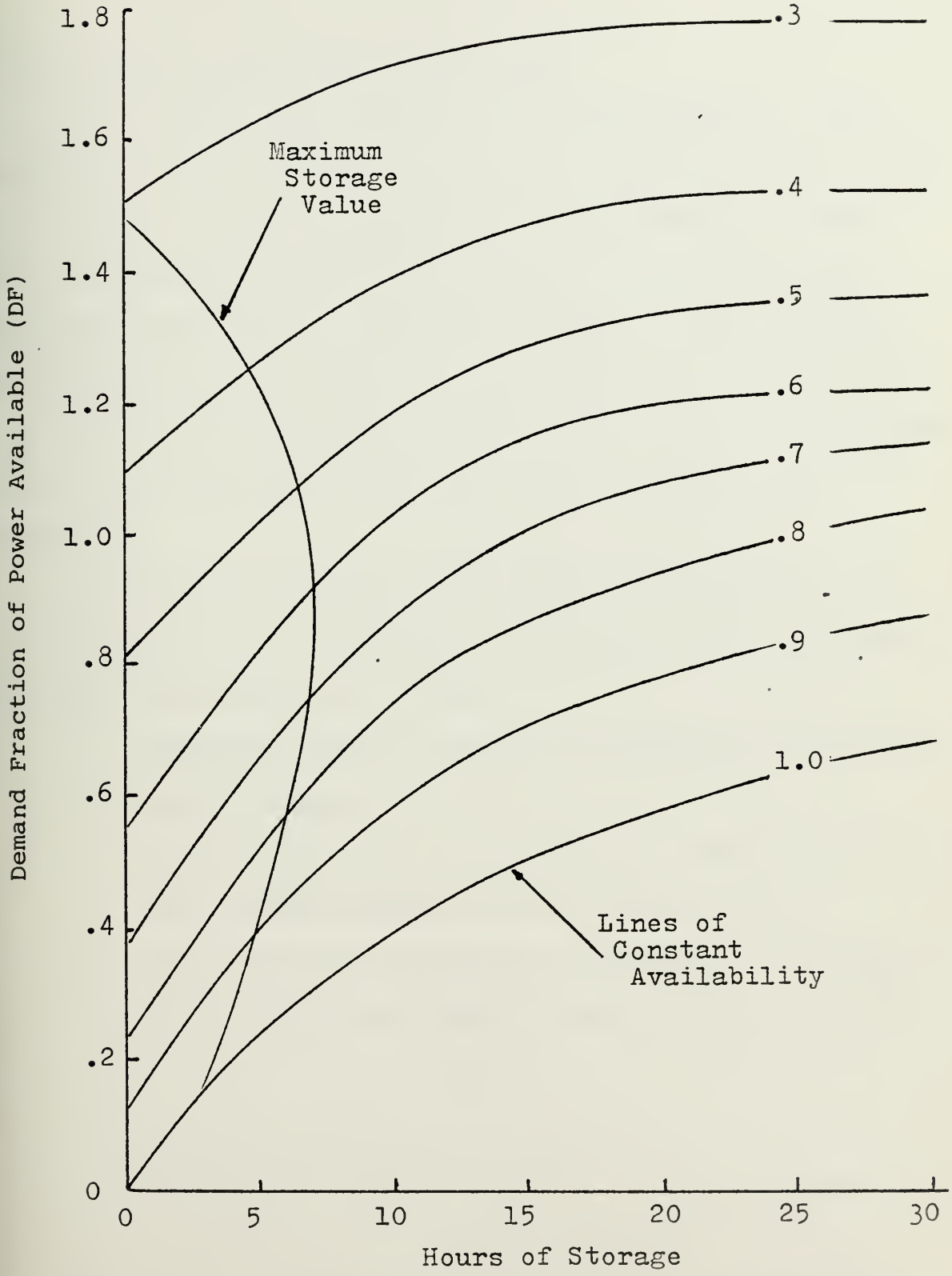

Figure 6-18: Demand Fraction and Availability Tradeoff Lanes.

6.8 Variability of wave power ($\sigma_p/\bar{P}$)

The design lanes are based on the exponential power function, whose standard deviation (σ_p) equals the mean power ($\bar{P}$), or $\sigma_p/\bar{P} = 1.0$. The tables cited in Chapter 4 on wave power availability indicate that $\sigma_p/\bar{P} \approx 1.0$ for most deep ocean and some coastal locations. However, there are some locations where the value of this parameter may be less than 1.0. For this reason an adjustment factor needs to be applied to the design lanes to account for this change in power variability.

Using the simulation model the adjustment factor (K_s) was determined and it is graphed in figure 6-19. The procedure for using the curve is as follows:

1. Determine energy storage requirements from previous design lanes;
2. Enter figure 6-19 with the actual value of $\sigma_p/\bar{P}$ for the desired location and retrieve K_s; and
3. Multiply K_s by the energy storage from the design lanes to find the actual energy storage required.

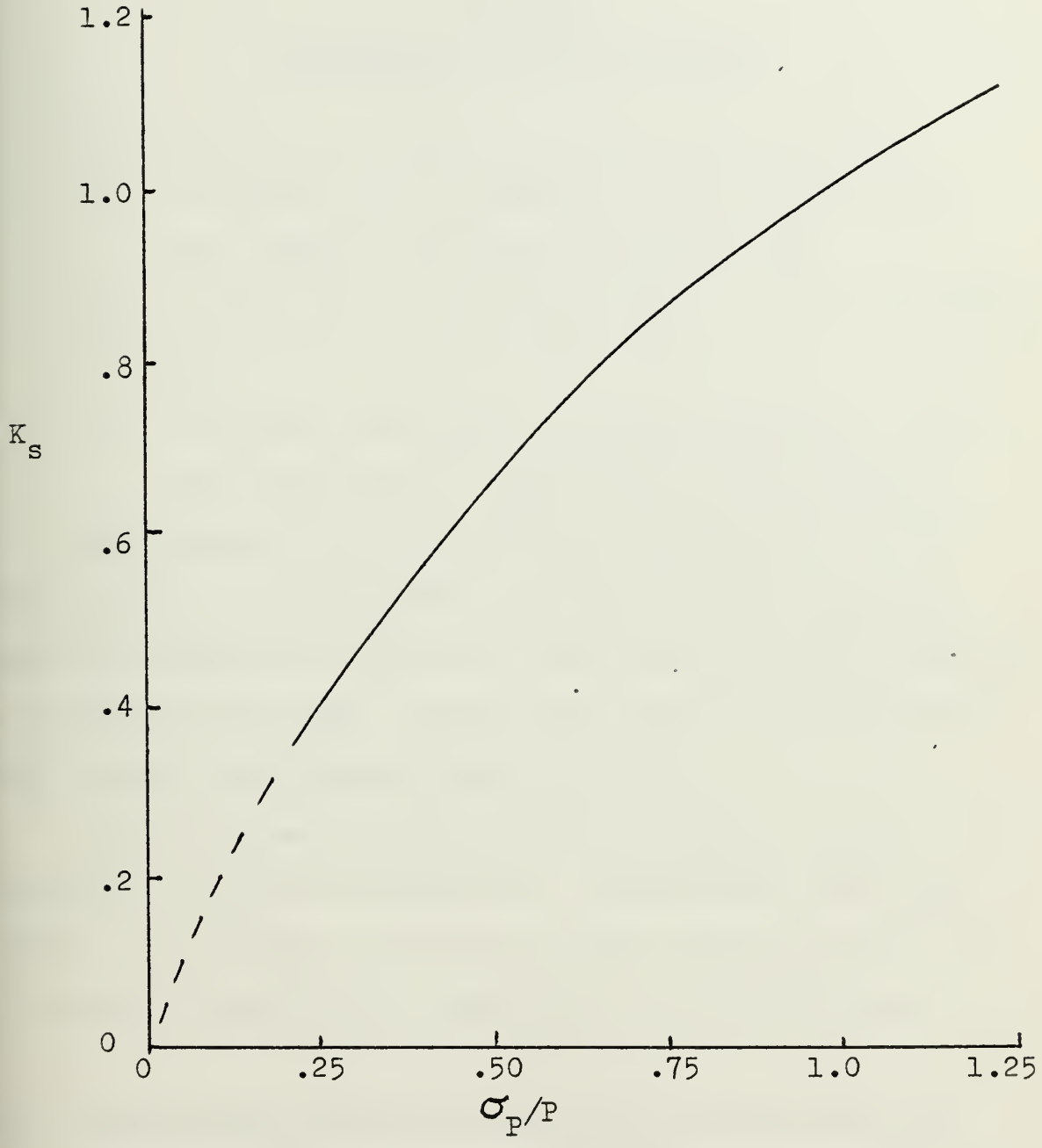

Figure 6-19: Storage Reduction Factor (K_s) vs Variability of Wave Power.

CHAPTER 7

FEASIBILITY TRADEOFF STUDIES

The objectives of any feasibility study include:

1. To define a set of feasible alternatives which meet initial performance requirements;
2. To determine cost-effectiveness of the alternatives; and
3. To assume definition of the alternatives to the level required for first order cost estimates.

The feasibility design should be balanced. It is inappropriate at the feasibility level to select specific subsystem components unless the user specifies such a selection as a design requirement. Subsystems should be identified by their general performance characteristics.

The subsystems analyzed in this chapter include structure, conversion, generation, transmission and energy storage. The effect of seasons on mean power available and a process for power rating selection are also discussed.

7.1 Seasonality effect on selection of mean power level

The design lanes in Chapter 6 are all based on a mean power level ($\bar{P}$). This mean changes from season to season. Using figure 4-1 and assigning $\bar{P}_{annual} = 1.0$, a typical seasonal breakdown may be described as follows:

Season	$\bar{P}_{season}$
Summer	.60 $\bar{P}_{annual}$
Winter	1.40 $\bar{P}_{annual}$
Fall/Spring	1.00 $\bar{P}_{annual}$

The question arises concerning selection of the design $\bar{P}$, that is, should the system be designed for the minimum $\bar{P}$ (summer), the maximum $\bar{P}$ (winter), or the mean $\bar{P}$ (fall/spring)? Designing for the maximum $\bar{P}$ yields the most power delivered, but designing for the minimum $\bar{P}$ costs the least.

The lowest $/KW system depends on the tradeoff between delivered power and conversion/generation/transmission (CGT) costs. The tradeoff is independent of structural costs because maximum power output diameter selection is independent of seasons. Energy storage costs are assumed to be constant over the seasons.

The mean power delivered varies with season. If the system is designed for the minimum $\bar{P}$, then during summer months it is rated at 100% of the power available, during spring and fall it is rated at 60% of the power available, and during winter it is rated at 43% of the power available. The components of this system will have a higher utilization than the components of a system designed for the maximum $\bar{P}$ (winter).

Besides this variation in mean deliverable power, the availability of the power delivered changes with season for a given design. For example, if the system is designed for the minimum $\bar{P}$ and a value of X is assigned to the availability of the rated power during summer, then during winter months the availability of the rated power will be greater than X because the mean power level in the ocean is higher.

Assuming that the marginal value of availability equals the marginal cost of power, then the equivalent power delivered for each of three designs (min $\bar{P}$, mean $\bar{P}$, and max $\bar{P}$) may be adjusted for availability by using figure 6-18 and holding energy storage constant.

Table 7-1 lists the power rating, the deliverable power, the availability adjustment factor and the equivalent power delivered for each of the three designs (min $\bar{P}$, mean $\bar{P}$, and max $\bar{P}$) over all seasons, non-dimensionalized to the mean $\bar{P}$ design.

TABLE 7-1

RELATIVE POWER DELIVERED FROM SEASONAL DESIGNS

Design	Power Rating	Delivered Power	Availability Correction	Equivalent Delivered Power
Max $\bar{P}$	1.40	1.11	.93	1.03
Mean $\bar{P}$	1.00	1.00	1.00	1.00
Min $\bar{P}$	.60	.67	1.25	.83

If conversion/generation/transmission (CGT) costs represent 0% of the total system cost then the max $\bar{P}$ design is optimal since it delivers the highest equivalent power. If CGT costs are 100% of the total system cost then the min $\bar{P}$ design is optimal since it has the least cost.

Using data in table 7-1, the costs of power for CGT costs representing varying percentages of total cost were calculated and displayed in table 7-2. The minimum cost/KW designs are circled in the table. Since CGT costs are expected to lie between 10% and 40% of total system cost the selection of the annual mean power level for design considerations is the optimal selection.

TABLE 7-2

RELATIVE $/KW FOR COMPETING DESIGNS

	CGT costs as % of total cost					
Design	0	10	20	30	40	50
Max $\bar{P}$	.97	1.02	1.06	1.09	1.13	1.17
Mean $\bar{P}$	1.00	1.00	1.00	1.00	1.00	1.00
Min $\bar{P}$	1.20	1.16	1.11	1.07	1.02	.97

7.2 Structure

The most critical structural design element for the WPG will be longitudinal bending moments. The Load Line Regulations (ref. 4) assert that good design practice requires that values of length/depth lie between 10 - 13.5 for ocean-going vessels. For vessels operating in the Great Lakes regions where wave heights are limited, the Regulations require L/D less than 13.5 for vessels less than 325 feet in length and L/D less than 19 for vessels with lengths greater than 600 feet. One of the reasons for these requirements is that insufficient depth lacks the necessary moment of inertia to give proper longitudinal stiffness.

The strength of the cam lies in its circular cylindrical backbone. Ocean-going vessels midship cross-sections are more nearly approximated by box shapes than circles, implying that for similarly sized structures the cam will have a lower midship section moment of inertia than the ocean-going vessel. With this in mind it would therefore be prudent to restrict the cam's maximum value of L/D to 10. If interconnections between cams are deemed feasible then the total L/D rather than the individual cam's L/D must be less than 10. If cam interconnections are flexible then the L/D requirement may be relaxed since the flexible link will not carry a load.

Structural costs are frequently based on structural weight (W). A set of cost relationships based on Maritime Administration data (ref. 17) for ocean-going tanker design in 1977 follows:

Material Cost	M1 = 530W
Direct Labor Cost	M4 = 384W
Indirect Material Cost	M5 = 31.8W
Indirect Labor Cost	M6 = 69.12W
Material Engineering Cost	M7 = 10.6W
Overhead Cost	M9 = 45.31W
Total Cost	TC = 1070.83W

Structural weight (W) is estimated from the following equation:

$$W = YCF^{.65} Z^{.65} L(1008) \frac{(1.108-.016\ L/D)(1.12-.0163\ L/D)}{(35.8-L/D)(14+L/D)}$$

where $Y = 3.8 - 1.1(L/D) + .1(L/D)^2$

$C = 1.0 + 1.32/\sqrt{L}$

$F = 3.8 + 2.1\ L/1000$

$Z = 5.95\ L^2 D(C_b+.7) \times 10^{-8}$

(L is in feet)

For the cam design, C_b = .785. Holding L/D constant at 10, the equation reduces to

$$W = 1.075 \times 10^{-4} \left(1+\frac{1.32}{\sqrt{L}}\right)\left(3.8 + \frac{2.1\ L}{1000}\right)\cdot 65\,(L^2D)\cdot 65\,(L)$$

(L & D in feet)

This equation was computed for a range of diameters from 1 - 50 meters with the resulting weight/length a function of D^2:

$$\frac{\text{Weight (tons)}}{\text{Length (m)}} = .1865\ D^2 \qquad \text{(D in meters)}$$

The proportionality constant, .1865, represents the average of the constants calculated for the various diameters. The standard deviation of the constants calculated was ±3% of the mean, verifying the proportionality of structural weight with D^2 for the cam.

The total cost/length for the cam structure is,

$$TC = \$1070.83\ W$$
$$= \$1070.83\ (.1865\ D^2)$$
$$= \$199.71\ D^2 \text{ per meter of length}$$

7.3 Conversion

The characteristics of the conversion system are governed by the following design requirements:

(1) the cam's rocking motion must be converted to rotational motion at speeds compatible with generator requirements;

(2) damping characterized by variable damping coefficients must be utilized to achieve high efficiencies;

(3) the system must operate with variable speed inputs characterized by $\theta a/H \cong 1.0$ for maximum efficiency;

(4) the system must control power surges; and

(5) the system must operate in an ocean environment.

Only one conversion method, hydraulic/pneumatic satisfies all these requirements.

In order to fulfill requirement (1), variable speed radial piston, axial piston or vane pumps may be used. The slow speed input implies that piston pumps will be best suited to the conversion.

The pump power takeoff will require a fixed reference which may be fulfilled by floating an object behind the cam or submerging a ballast weight beneath the cam. In either case the fixed reference will be attached to the ends of the cam and through seals and bearings the cam will rotate about the reference.

Hydrostatic drives are best suited to applications requiring wide ranges of speeds and torques. The basic elements of the hydrostatic drive are a pump, a motor and a pump driver. Mechanical energy from the cam driver is converted to fluid energy by the pump and reconverted to mechanical energy by the motor for use by the electrical generator. Since it is possible to provide infinitely variable pump and motor displacements, speed ratios may be stepless.

There are four basic pump/motor configurations:

(1) Constant capacity pump, constant capacity motor:

This configuration provides a fixed ratio drive speed which is proportional to the displacements of the pump and motor. If the two units have equal displacement then the drive ratio is one and output speed equals input speed. Speed variation may be accomplished by using bypass flow in which case power is diverted away from the motor and wasted in the form of heat.

(2) Variable capacity pump, constant capacity motor:

This configuration provides clutching, constant torque and variable speed. With the pump at zero displacement, the system is clutched and motor speed is zero. An increase in pump displacement increases motor speed, up to the design limit, with approximately constant torque.

(3) Constant capacity pump, variable capacity motor:

This system delivers constant power over the design speed range. Reduction in motor displacement results in increased speed but reduced torque.

(4) Variable capacity pump, variable capacity motor:

This arrangement is particularly well-suited for designs requiring a wide range of speeds and torques. It combines the constant power characteristics of system (3) and the constant torque characteristics of system (2).

Of these configurations system (4) is best suited to the WPG. The variable pump allows selection of the optimum damping ratio and the variable motor allows operation over a wide range of input speeds without wasting power. Use of this system implies coupling with a variable speed generator.

For the constant speed generator application system (2) appears best suited. The variable pump could be controlled to select optimum damping. A valving mechanism for wasting excess energy, or an energy storage link, would be necessary because of the constant motor speed requirement.

In any configuration gearing is possible between the fluid motor and the electrical generator.

Table 7-3 lists the characteristics of hydrostatic conversion.

Direct mechanical conversion will not be feasible because the cam's velocity reaches zero twice with each passing wave. In a purely mechanical system the rocking motion could be converted to rotational motion with an arrangement of ratchet/pawl and worm/crown gear mechanisms. Mechanical, infinitely variable speed transmissions, like the Voight unit utilized in wind power, are capable of applying damping when coupled with field modulated electrical generators. But with zero velocity twice each cycle a clutch would be needed between the drive and the generator to account for inertia effects. Since the transmission must be non-slip in order to apply appropriate damping, the clutch requirement causes the purely mechanical conversion system to be infeasible.

7.4 Electrical Generation

Acceptable schemes for generation compatible with power grids may be generally classified as constant speed constant frequency (CSCF) and variable speed constant frequency (VSCF).

7.4.1 CSCF Systems. Synchronous and induction generators belong to this category. The constant speed requirement dictates the use of energy storage between the cam's rocking motion and the generator shaft or a valving mechanism which wastes excess energy. Suitable control systems are required for sensing and reacting to input speed variations.

7.4.2 VSCF Systems. There are several types of variable speed machines in existence today, all of which are more costly than the CSCF machines.

(1) AC-DC-AC. The AC-DC-AC conversion system is an AC generator with DC field excitation. The variable frequency DC output is rectified and converted to AC through the use of an inverter or a motor/generator set. The system rapidly reaches stability with the variable speed input. AC-DC-AC may be attractive in deep-ocean installations where DC transmission to shore is most economical.

(2) Double Output Induction Generator. This machine makes use of an induction generator with rotor energy regeneration. Both rotor and stator supply power to the electrical grid. Power from the stator which is generated at grid frequency is directly fed to the grid. Power from the rotor which is generated at slip frequencies is first converted to DC, then inverted to AC before being fed to the grid. Efficiencies greater than 80% can be achieved with input speed variations from 20% to 100% of rated speed.

(3) Pole-changing Generator. This generator electromagnetically alters the field pole pattern according to shaft speed. The electrical output is constant in frequency. There are no restrictions on input speeds.

(4) Field-modulated Generating Systems. These units are generally excited by an AC power source fixing the output frequency and modulated by rotational frequency. High shaft speeds are required. Output efficiencies are comparable to synchronous machines and constant over input speed ratios of 5:1.

Comparisons of off-speed efficiencies for several generators are displayed in figure 7-1.

Table 7-4 compares costs and efficiencies for a number of generation units.

7.5 Optimal Power Rating

It was shown in section 7.1 that the WPG will deliver the most power over all seasons if the design is based on the mean annual power level. But the selected design power level may be more narrowly defined than this.

Power rating can be optimized. If the power rating selected is a small fraction of the mean annual power available ($\bar{P}$) then the WPG will deliver very little power. If the power rating is selected as several times $\bar{P}$ then the system will deliver more power but at a higher cost. For the analysis that follows the $/KW of the conversion/generation/transmission (CGT) subsystem is assumed to be constant.

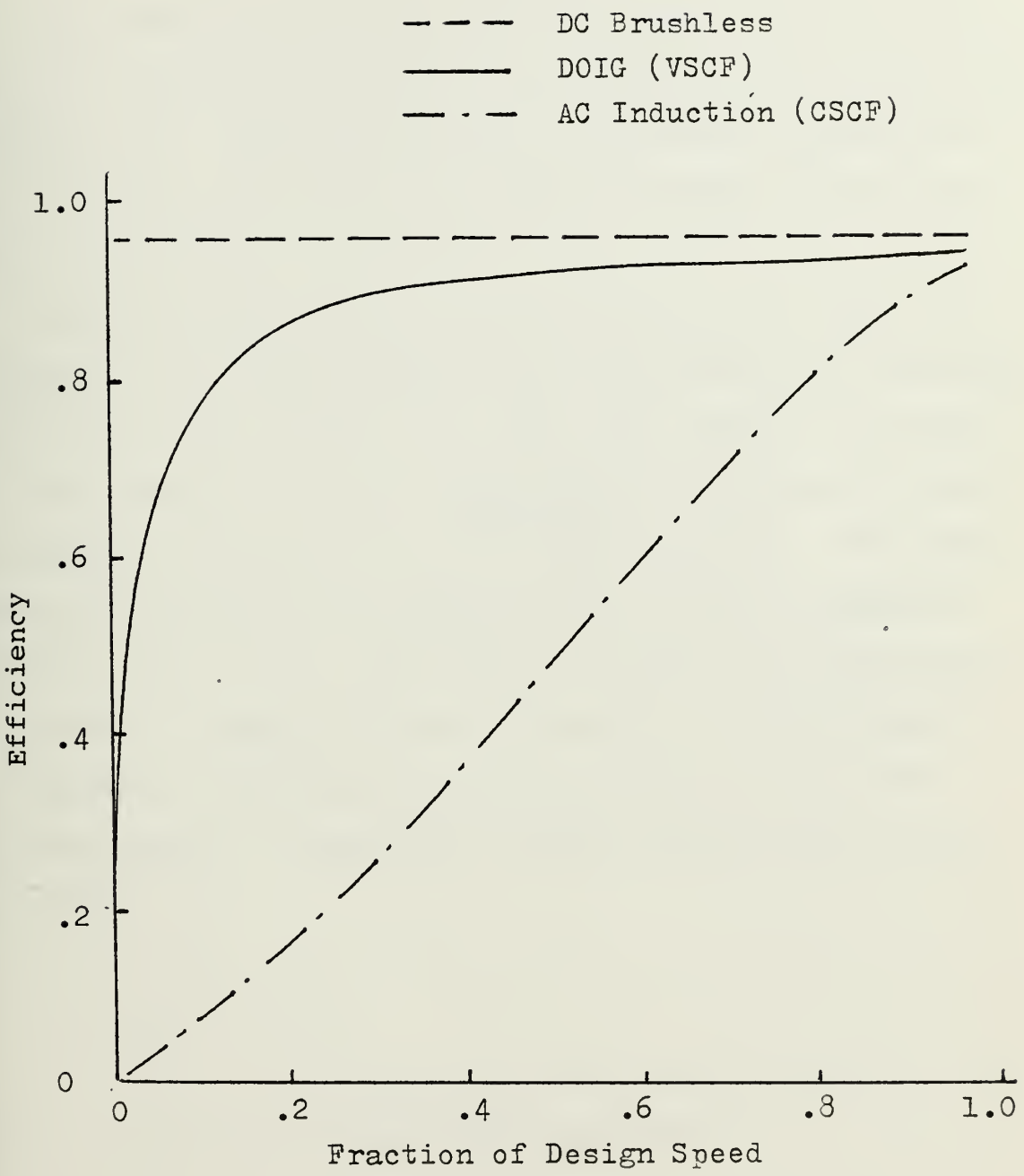

Figure 7-1: Off-Design Performance of Several Electrical Generators.

The fraction of total power delivered up to any given level of $\bar{P}$ may be derived from the simulated zero storage line in figure 6-17. Expressing power rating as PR = fraction of power available, the resulting curve is plotted as the solid line in figure 7-2.

The two dashed lines in this figure are included for comparison of simulated results with the theoretically derived exponential power distribution. The upper dashed line represents the fraction of all wave arrivals for any given PR from the equation, Fraction = $1 - e^{-PR}$ (see Chapter 3). The lower dashed line represents the theoretical fraction of power in those waves for any PR. The solid line which also represents the fraction of power in waves lies above the lower dashed line because of the filtering characteristics of the WPG efficiency curve. An empirical formula for the solid line was derived:

$$Y = K\,(1 - e^{-PR}),$$

where Y = fraction of total power available

$K = .90$

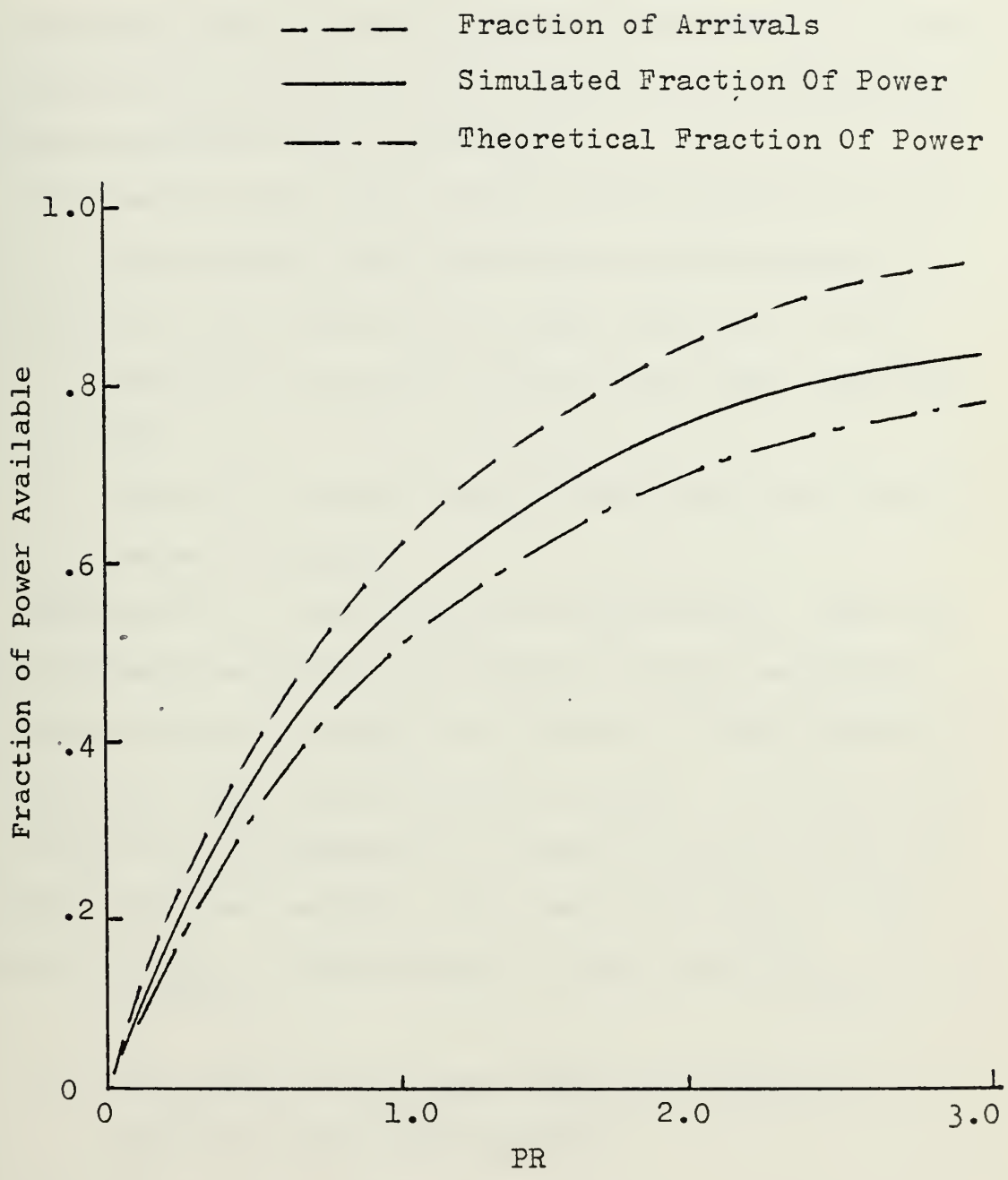

Figure 7-2: Fraction of Power Available in Waves up to a Certain Level of Power Rating (PR).

Once the power rating is selected the fraction of total power captured may be calculated. The following assumptions make the calculations more tractable:

(1) the CGT subsystem delivers all the power in waves having power levels less than rated capacity;

(2) for waves having power levels above the rated capacity, the system delivers the rated capacity; and

(3) there is a maximum power level above which the cam ceases to operate.

Assumption (3) requires some clarification. The WPG has not yet been tested for operation in severe sea states, but it is reasonable to expect that there is some maximum sea condition above which the cam cannot operate. In this situation the cam may be submerged or allowed to float with power generation apparatus secured. This maximum condition may be expressed as PR_{max}. The fraction of power above PR_{max} is lost.

Let Y = fraction of total power available which is captured by the CGT subsystem

PR = design power rating

PR_{max} = maximum power rating

Y = (1) all of the power up to rated capacity +

+ (2) some fraction of the power between rated capacity and maximum capacity +

+ (3) none of the power above the maximum capacity.

Term (1) above = $K(1 - e^{-PR})$

Term (3) = 0

Term (2) was derived in its general form. Referring to figure 7-3, term (2) graphically is the ratio of Area A/Area (A+B). In numerical form, term (2) is

$$\frac{K(PR)\,[e^{-PR} - e^{-PR_{max}}]^2}{(1 - e^{-PR_{max}})(1 + PR_{max}) + PR - PR_{max} - (1-e^{-PR})(1+PR)}$$

Therefore,

$$Y = K(1-e^{-PR}) + \frac{K(PR)\,[e^{-PR} - e^{-PR_{max}}]^2}{(1-e^{-PR_{max}})(1+PR_{max}) + PR - PR_{max} - (1-e^{-PR})(1+PR)} \qquad (1)$$

Although the value of PR_{max} is not known, $PR_{max} = 3$ is a reasonable assumption. Referring to figure 7-2, $PR_{max} = 3$ corresponds to 95% of all waves and 84% of all power. In other words the assumption of $PR_{max} = 3$ implies that the system will be completely shut down for 5% of the time due to excessive sea conditions and 16% of the total power available will be lost.

Equation 1 was calculated for $PR_{max} = 3$ and plotted in figure 7-4. The dashed line in this figure represents $Y = K(1-e^{-PR})$, which corresponds to a system which is shut down when power levels exceed PR.

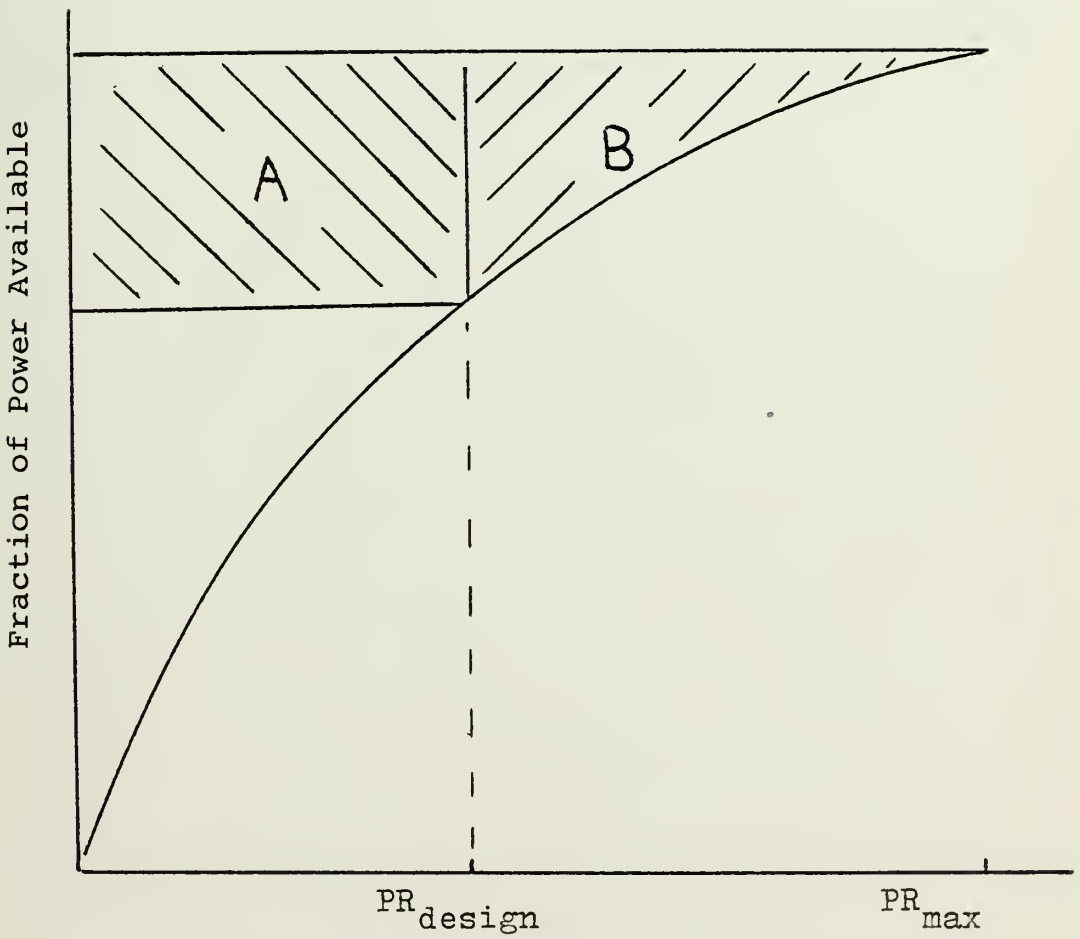

Figure 7-3: Graphical Representation of Fraction of Power Between Rated and Maximum Capacity.

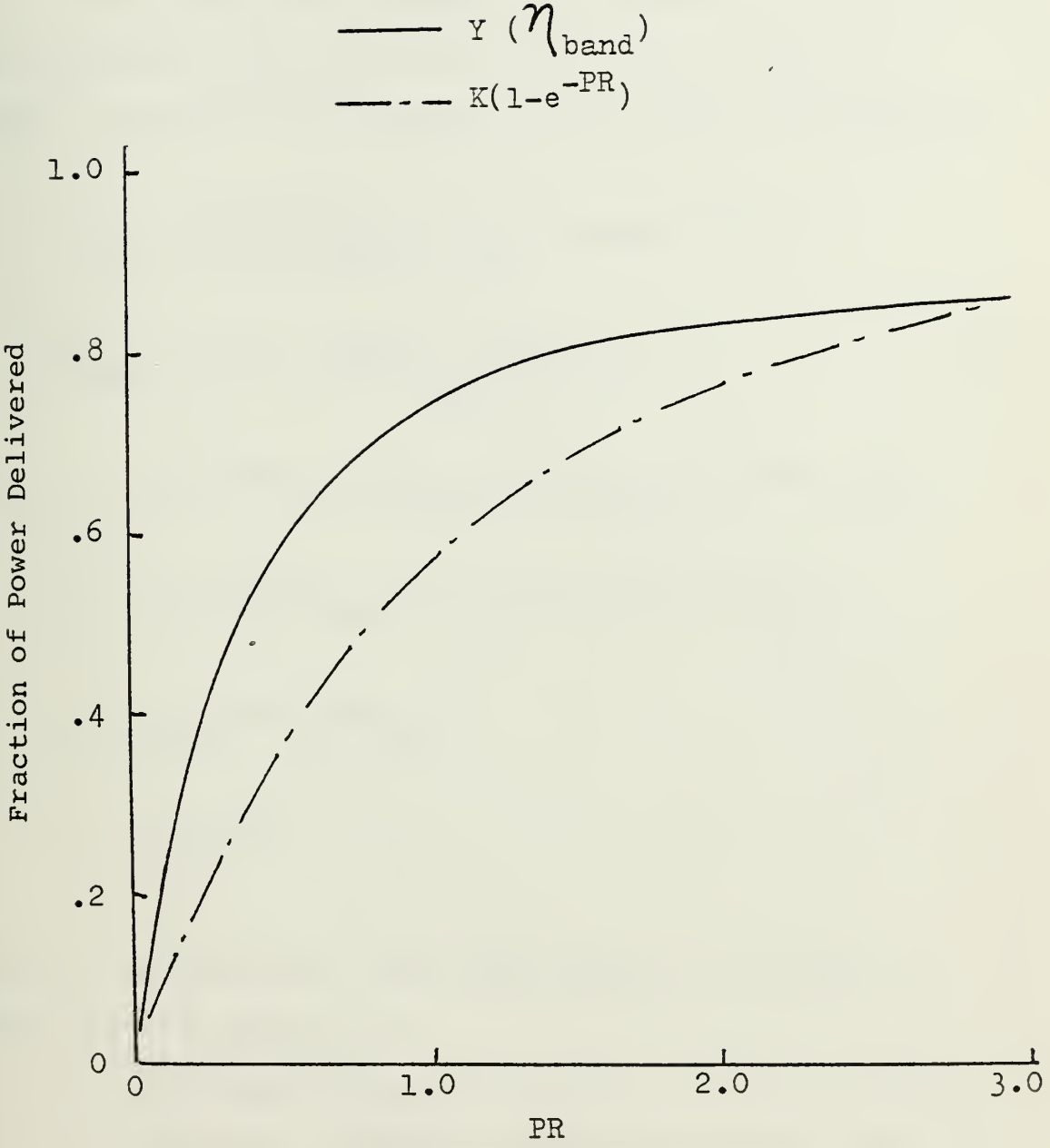

Figure 7-4: Fraction of Power Delivered With Power Rating = PR and PR_{max} = 3.0 .

Since costs are assumed to be linear with size for the CGT subsystem, the slope of the "Y" line in figure 7-4, dY/dPR, is actually the marginal cost of the CGT subsystem,

$$MF_{cgt} \equiv \frac{\$/KW\ cgt}{\$/KW\ system - cgt} = dY/dPR$$

$$\frac{dY}{dPR} = Ke^{-PR} + \frac{[A][B] - [C][D]}{[A]^2} \qquad (2)$$

where $A = (1-e^{-PR_{max}})(1+PR_{max})+PR-PR_{max}-(1-e^{-PR})(1+PR)$

$$B = K(e^{-PR}-e^{-PR_{max}})^2-2KPRe^{-PR}(e^{-PR}-e^{-PR_{max}})$$

$$C = KPR(e^{-PR}-e^{-PR_{max}})^2$$

$$D = -PRe^{-PR}$$

Values of dY/dPR (eq.2) have been plotted in figure 7-5.
Example use of figure 7-5:

(1) Calculate MF_{cgt}.

(2) With MF_{cgt} enter the vertical axis and mark the corresponding point on the MF_{cgt} line.

(3) Read down to horizontal axis for the design power rating, which is just PR x $\bar{P}$.

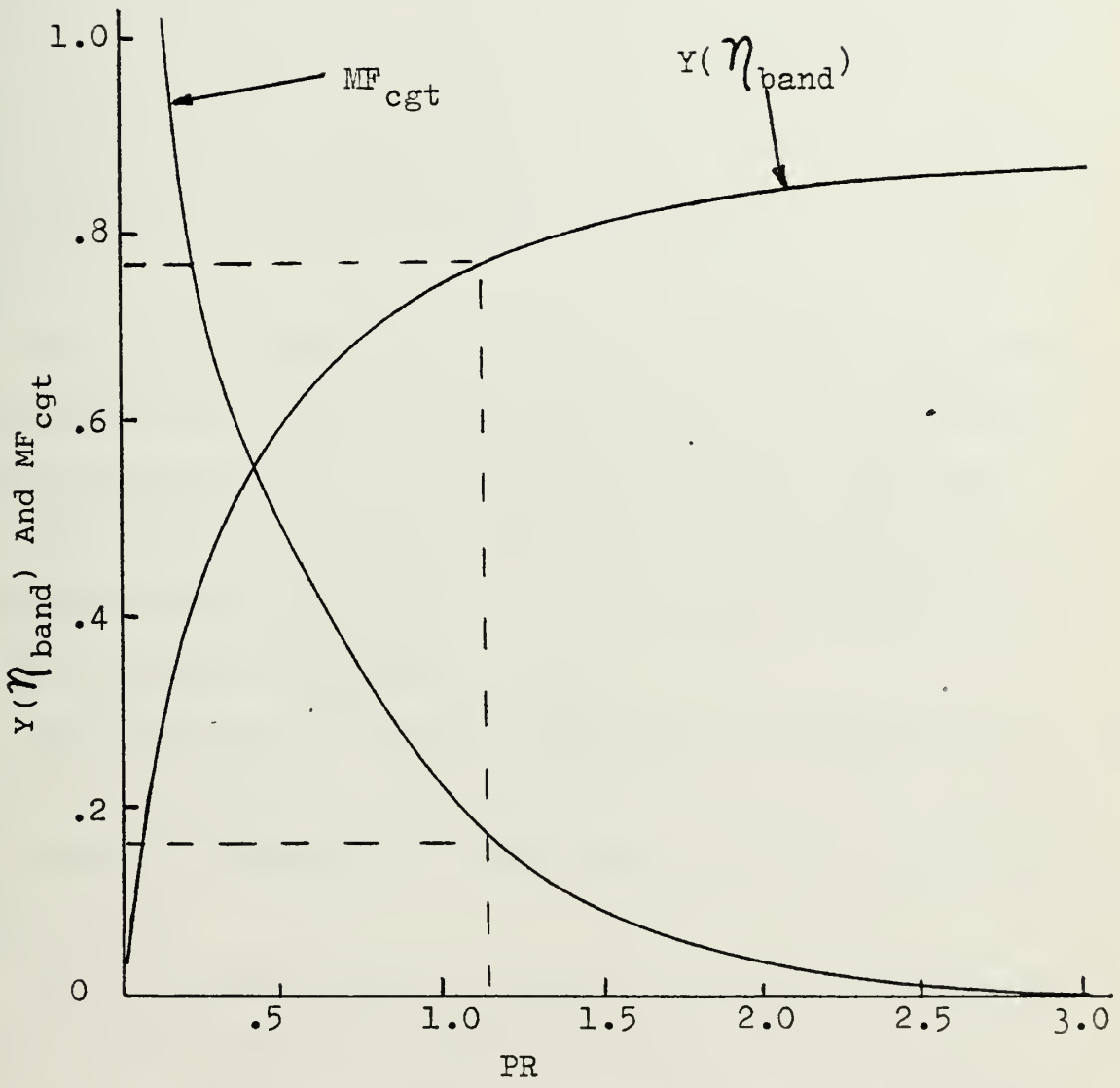

Figure 7-5: Design Lane For Selecting Optimal Power Rating And Bandwidth Efficiency Given Marginal Cost of CGT Subsystem.

(4) Mark the point on the "Y" line which is vertically above or below the point on the MF_{cgt} line and read across to the value of Y.

Numerical example:

$MF_{cgt} = .16$

Design power rating = $1.18\ \bar{P}$

Fraction of power collected (Y) = .77

The design power rating is optimal for the assumptions stated previously. This number multiplied by the cost/KW of the CGT subsystem yields the actual cost of the subsystem.

The fraction of power collected, Y, may be regarded as a subsystem efficiency, and it will be referred to in Chapter 8 as the bandwidth efficiency, η_{band}.

Efficiencies of specific generation, conversion and transmission equipments are assumed to be 1.0 in this analysis and they must, therefore, be taken into account in the final design process.

The preceding analysis may be utilized to show that variable speed generators should be used in the WPG system. A constant speed generator will operate between a cut-in and a cut-out wave power level. Below the cut-in level no power is delivered. Between the cut-in and cut-out levels the generator produces constant power equaling the cut-in power level.

Numerically, the amount of delivered power for the constant speed generator without energy storage is

$$Y - K(1 - e^{-PR}) =$$

$$\frac{K(PR)(e^{-PR}-e^{-PR_{max}})^2}{(1-e^{-PR_{max}})(1+PR_{max})+PR-PR_{max}-(1-e^{-PR})(1+PR)}$$

Graphically, the constant speed generator's delivered power corresponds to the difference between the "Y" line and the "$K(1-e^{-PR})$" line in figure 7-4. Figure 7-6 compares the plots of the variable speed generator (Y) with the constant speed generator ($Y - K(1-e^{-PR})$). Clearly, the constant speed generator without energy storage cannot compete with the variable speed generator. In addition, the spilled power with the constant speed generator must be dissipated as heat in the hydraulic conversion system which increases conversion costs.

It was pointed out in section 7.3 that energy storage for the constant speed generator must include a hydraulic link. But hydraulic energy storage is prohibitive in cost (see table 7-6). If the hydraulic conversion link is coupled with kinetic energy storage, like a flywheel, then the flywheel must physically be located in the cam. The input rotational speeds of about 1 RPM from the cam to the hydraulic link would have to be increased to about 20,000 RPM for efficient flywheel operation. This is infeasible.

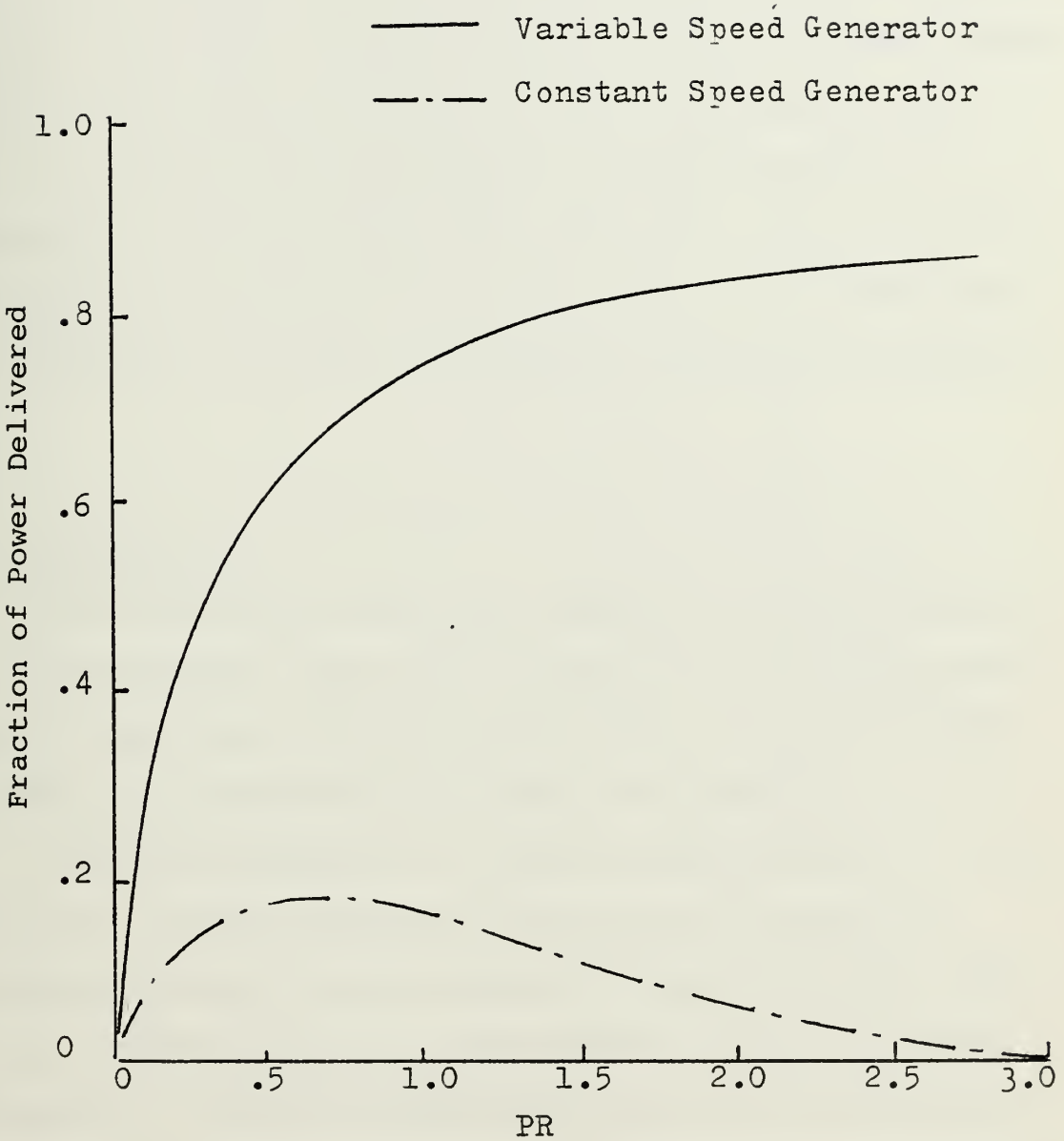

Figure 7-6: Comparison of Power Delivered by Variable Speed and Constant Speed Generators.

With variable speed generators the flywheel, or any other energy storage device, could be located ashore and many WPG units could feed a single storage device. Flywheel speeds could be controlled electrically rather than mechanically.

For these reasons the variable speed generator is preferrable to the constant speed generator. From table 7-4 the brushless DC generator with processing for inversion to grid AC appears to be the most feasible generation subsystem.

7.6 Transmission

The transmission subsystem depends on system configuration. For distances less than 20 miles, AC electrical transmission is the most cost effective method. Beyond 20 miles from shore, DC transmission is most cost effective.

It is not necessary to require transmission of electricity. Power generated at the cam may be used in hydrolysis of water for production of gaseous hydrogen (GH_2) or liquid hydrogen (LH_2) or even some derivative of hydrogen like ammonia. GH_2 may be feasibly piped over long distances and LH_2 may be transported by barge. The hydrogen produced may be sold commercially or used to run a fuel cell for electrical generation.

Characteristics of the various transmission schemes are displayed in table 7-5.

7.7 Energy Storage

Since the power in ocean waves varies so considerably with time, some form of energy storage may be required in the system. As previously mentioned the CSCF design with hydraulic pressure energy storage is infeasible. In VSCF systems energy storage may be accomplished by means of flywheels, batteries or containerized hydrogen (GH_2 or LH_2).

Comparisons of various energy storage methods are outlined in table 7-6.

For GH_2 storage additional costs are incurred in electrolysis and reconversion to electricity. For LH_2 storage additional costs are incurred in electrolysis, liquefaction and reconversion. These added costs are outlined in table 7-5.

From table 7-6 the three most likely forms of energy storage are lead-acid batteries, modern flywheels and LH_2. LH_2 is included here because it may become the optimal storage medium if the WPG is sited at great distances from shore.

The technology of lead-acid batteries is well known. The only major limitation imposed by the use of these batteries is the slow charging rates (in hours for the costs associated with batteries in table 7-6). Lead-acid batteries with charging rates on the order of minutes do exist, but the costs are several times the cost listed in table 7-6. Slow

charge batteries may be feasible if electrical inputs come from a large number of sources scattered over a large geographic area, which may tend to smooth out the power delivery.

A considerable amount of interest has been generated in the past few years over the use of high energy density flywheels. Energy densities have been dramatically increased through the use of composites like fused silica and protection costs have been reduced because at failure stresses the composites shatter in millions of small pieces instead of large steel chunks like flywheels of the past. Run down times for composite flywheels in vacuum chambers have been shown to be on the order of months. The limitations on flywheel energy storage are:

(1) very high rotational speeds (20,000-25,000 RPM);

(2) vacuum chamber sealing; and

(3) inherent rotational inertia.

The high rotational speeds can be achieved electrically by using a multipole generator to drive a permanent magnet motor in the flywheel. The high generator/motor pole ratio achieves the desired high rotational speeds. The interface is electrical, reducing the vacuum chamber sealing complexity. During charge the flywheel acts as a motor, and during discharge it acts as a generator. The use of the multipole

generator is an added cost to cost of flywheel storage. The rotational inertia limitation can be eliminated by using counter-rotating flywheels or by rigidly securing the unit to the earth.

Taking into consideration all capabilities, limitations, costs and efficiencies for the various energy storage schemes, the modern flywheel appears to be the most viable system for the WPG.

7.8 Other subsystems

Mooring and direction-keeping subsystems cannot be analyzed until free-floating tests are conducted on the cam. In Ocean Thermal Energy Conversion (OTEC) systems, mooring costs typically run about 10% of structural costs; this cost will be assumed for the WPG.

There will undoubtedly be a reduction in the effective mean power density at a particular site due to the inability of the cam to maintain itself parallel to wave crests and its inability to maintain a perfect fixed reference, assuming the fixed reference is not a structure fixed to the ocean floor. These effects, however, will not appreciably distort the overall design. If the power density is effectively reduced then all system components, except structure, will be down-sized accordingly.

TABLE 7-3

CONVERSION SYSTEMS (no storage)

	$/KW	Efficiency
Pneumatic	75	.55
Oil hydraulic	64	.65

TABLE 7-4

ELECTRICAL GENERATION SYSTEMS

	$/KW	Efficiency
Synchronous	60	.94
Induction	39	.93
FMGS	172	.80
Pole changing	900	.60
DC/AC	133	.86
Multipole	86	.95
Rectifier	30	.92

TABLE 7-5

TRANSMISSION (100 MW nominal sizing)

	$/KW 1 mile	$/KW 100 miles	Efficiency
DC electric cable	11	101	.95
GH_2 pipeline	30	131	.98
LH_2 barge	--	114	.95
Fuel cells	--	179	.70
Electrolyzer	--	89	.84
Liquefaction	--	234	.80

Factor increase in cost for designs other than 100 MW:

1 MW: 4.3

50 MW: 1.4

500 MW: .7

TABLE 7-6

ENERGY STORAGE

	$/KW	lb/KWh	Ft^3/KWh	Efficiency
Lead-acid battery	37	67	2.0	.60
Modern flywheel	80	20	.67	.95
LH_2	82	.06	.01	.35
Oil hydraulic	490	125	11.1	.60
Compressed air	674	143	15.1	.50
GH_2	735	2.9	.08	.40

CHAPTER 8

COST ANALYSIS

8.1 Costs

Capital costs include costs for structure, conversion, generation, transmission and storage. Annual costs may be expressed as a % of capital costs. Data was assimilated from various sources for ocean-based power generating systems to produce the following annual costs:

	% of Capital Cost
Taxes	2.5
Insurance	2.0
Operating and Maintenance	5.5
Depreciation and Overhead	2.0
Return	11.0
	23.0

The annual fixed charge rate of 23% must be adjusted, or annuitized, for the life cycle of the investment. The annuitized fixed charge rate (AFCR) =

$$\frac{r}{1 - \frac{1}{(1+r)^n}}$$

where r = fixed charge rate

n = investment life (years)

The investment life for the WPG is assumed to be 20 years which yields AFCR = .2337.

8.2 Power Analysis

The WPG may be analyzed by two methods: (1) fuel saver credit - a conventional plant is shut down with the resulting savings in fuel; and (2) baseload capacity credit - a conventional plant is physically replaced by the WPG.

8.2.1 Fuel saver credit analysis. The simplest application of the WPG is fuel saving. Power from the WPG is fed directly into the utility grid and depending on the grid load, conventional fuel-fired plants are backed off with a savings in fuel resulting. The value of the fuel savings to the utility network requires knowledge of the Incremental Heat Rate (IHR: BTU/KWh). The IHR represents the number of BTU's of fuel saved with the reduction of one KWh of conventional generation. IHR varies constantly. It is currently about 9500 BTU/KWh for off-peak power, 11000 BTU/KWh mean power and 12300 BTU/KWh for peak power.

The value of any fuel-less power generator as a fuel saver is

$$\text{Fuel Saver Value } (¢/KWh) = [(\text{Fuel Cost } (¢/10^6 \text{ BTU})] \times \times \frac{\text{IHR(BTU/KWh)}}{10^6} \quad (1)$$

Figure 8-1 shows this relationship between fuel costs and fuel saver values for various IHR's.

The busbar cost equation is the basic formula for all power cost analyses:

$$\text{Power Cost } (¢/KWh) = \frac{[\text{Capital Cost } (\$/KW) \times \text{AFCR(Fraction/yr)}] \times 100¢/\$}{[\text{Availability (Fraction)}] \times 8760 \text{ hrs/yr}} \quad (2)$$

To simplify the use of the equation, the following abbreviations will be used:

FSV = Fuel saver value (¢/KWh)

BLEC = Baseload energy cost (¢/KWh)

AV = Availability (fraction)

CC = Capital cost ($/KW)

AFCR = Annuitized fixed charge rate (fraction/yr)

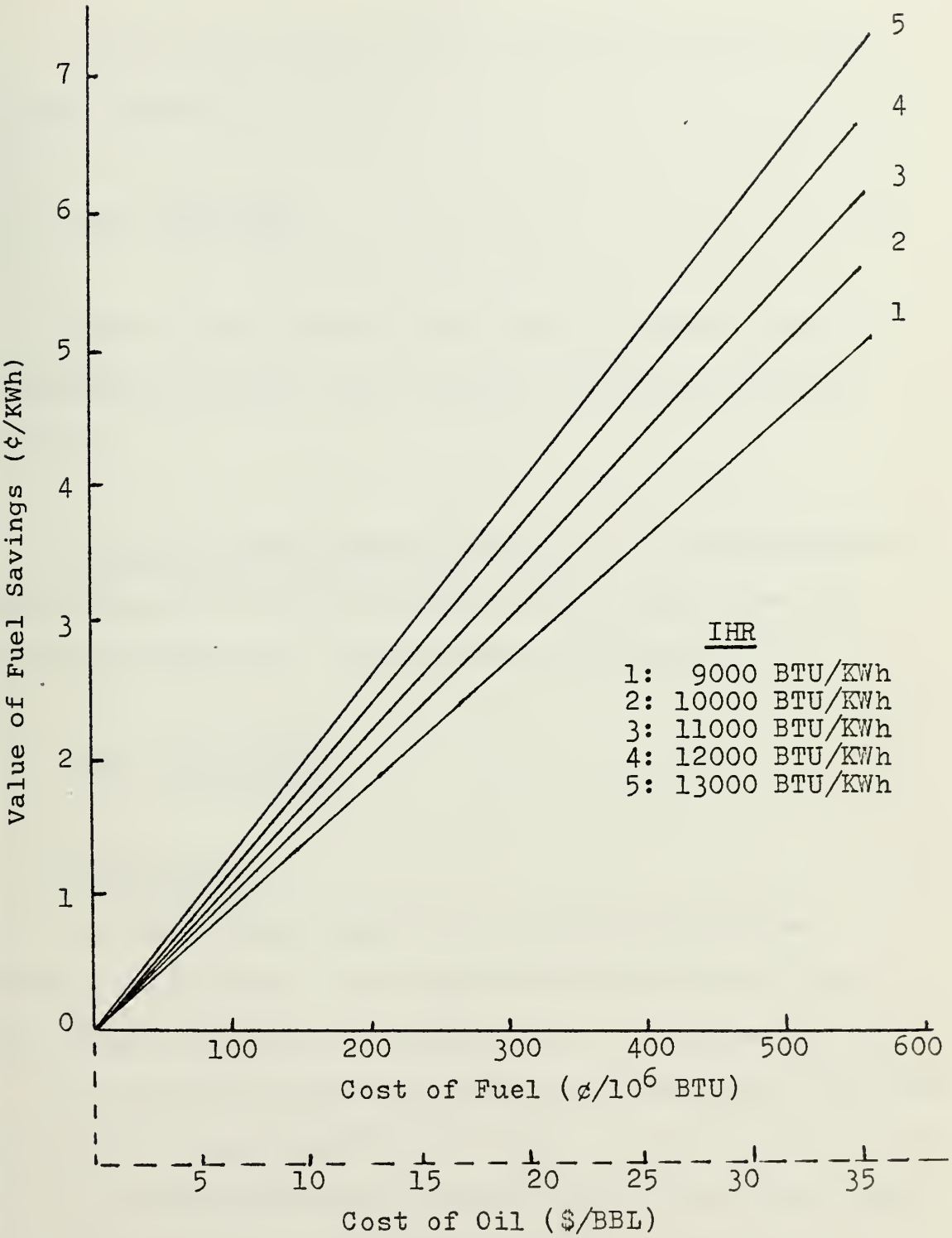

Figure 8-1: System Incremental Heat Rate

In fuel saver analysis the following variation of the busbar equation applies:

$$FSV = \frac{CC\ (AFCR)}{87.6\ (AV)} \qquad (3)$$

Once the fuel saver value (FSV) is known, the corresponding breakeven fuel cost may be determined from figure 8-1.

8.2.2 Baseload capacity credit. If the availability of power from the WPG is sufficiently high then base load credit may be applied. The pertinent equation is,

$$BLEC = \frac{CC\ (AFCR)}{87.6\ (AV)} \qquad (4)$$

8.3 Availability

At first glance there is no difference between equations (3) and (4). The actual difference lies in the rather complex notion of availability as it applies to the WPG. In fuel saver analysis it does not matter when the power from the WPG is introduced to the grid: as power arrives from the WPG, conventional plants are shut down. For this reason the availability of the mean power level in the ocean is equal to 1.0 for the fuel saver analysis (neglecting adjustment factors).

Therefore, $AV_{fs} = 1.0$.

In the baseload analysis the concept of availability for the WPG changes: it is the level of power which the WPG can be relied upon to deliver for a certain fraction of the year. The level of demand achievable and the energy storage required for a given value of availability may be extracted from figure 6-18.

It was mentioned in section 7.1 that the mean power level changes with seasons. For this reason baseload credit may only be applied to the lowest seasonal value, that is, to .60 $\bar{P}$, the level in summer months. Remaining power may be assigned fuel saver credit. The amount applied to baseload is .60 (A)(DF), where A = availability from figure 6-18 and DF = demand fraction from figure 6-18. The amount applied to fuel savings is (1-AFCR)(1-.60(A)(DF)), where (1-AFCR) adjusts for the difference between fuel savings and baseload value. The availability in the baseload analysis then is, AV_{bl} = .60(A)(DF)+(1-AFCR)(1-.60(A)(DF)).

There are two adjustment factors which must be applied to both definitions of availability:

(1) A certain fraction of the year must be set aside for equipment maintenance and down-time. Conventional plants which are mechanically more complex than the WPG assign AV = .75. Ocean Thermal Energy Conversion plants which are

less complex mechanically than the WPG assume AV = .95. It seems reasonable to set aside a mechanical availability of .85 for the WPG.

(2) In Chapter 7 a method was introduced for optimizing power rating (figure 7-5). The bandwidth efficiency, η_{band}, is an adjustment factor which must be applied to availability.

The two adjustment factors may now be applied to AV_{fs} and AV_{bl} (the bars over $\overline{AV}_{fs}$ and $\overline{AV}_{bl}$ in the following equations imply adjusted versions).

$$\overline{AV}_{fs} = .85 \quad \eta_{band} \tag{5}$$

$$\overline{AV}_{bl} = .85 \quad \eta_{band} \quad (.60(A)(DF)+(1-AFCR)(1-.60(A)(DF)) \tag{6}$$

The value of (A) in equation (6) for use in figure 6-18 is .75, since baseload analysis of the WPG should be conducted with respect to conventional plants which assume AV = .75.

Substituting equations (5) and (6) into equations (3) and (4) yields the relationships for WPG cost analysis:

$$FSV = \frac{CC\ (AFCR)}{87.6\ (\overline{AV}_{fs})} \tag{7}$$

$$BLEC = \frac{CC\ (AFCR)}{87.6\ (\overline{AV}_{bl})}$$

8.4 System Design

8.4.1 Site selection. The first step in the system design process is to select the site for operation of the WPG from the tables in Chapter 4. Data should be extracted from the "All Seasons" table since the WPG delivers the most power when designed to mean annual power levels.

8.4.2 Diameter selection - without separation effect. In Chapter 6 it was shown that D_{max} occurs at $\omega\sqrt{a/g} = .64$. Utilizing the dispersion relation, $D_{max} = .2034\ T^2$. The minimum cost diameter was shown to be 60% of D_{max} delivering 68% of the power of D_{max} (figure 6-5). Therefore, design diameter = $.122\ T^2$ and the power available = 68% of the maximum power. This delivered power may be termed a system design efficiency and will be defined η_{design}. Therefore, $\eta_{design} = .68$.

Structural cost = $\$199.71\ D^2$. Applying the factor increase for mooring cost, structural cost = $1.1(199.71) \times (.122\ T^2)^2 = 3.27\ T^4/P_{del}$, where P_{del} = power delivered to user.

The cam efficiency is extracted from figure 6-8 using the site selection parameter σ_T/T.

8.4.3 Diameter selection - with separation effect. With separation, D_{max} (3-D) = .68 D_{max} (2-D), and the minimum cost diameter occurs at .52 D_{max}, delivering 56% of the power at D_{max}. Therefore D_{max} (3-D) = .68 (.2034 T^2) = .1383 T^2, and the design diameter = .52 (.1383 T^2) = .072 T^2.

Structural cost with separation = 1.1 (199.71)*
*(.072 T^2)^2 = 1.139 T^4/P_{del}

The cam's efficiency is extracted from figure 6-11 using the site selection parameter σ_T/T.

8.4.4 Conversion. The hydrostatic drive is the selected conversion system with a cost of 64 $/KW and efficiency of .65.

8.4.5 Generation. The DC/AC generation scheme is the selected method of electrical generation with a cost of 133 $/KW and an efficiency of .86.

8.4.6 Power rating selection. Power rating (PR) is obtained from figure 7-5. The bandwidth of useable power (η_{band}) is also determined from figure 7-5.

8.4.7 Transmission. DC Cable transmission is the selected method having a cost of 101 $/KW with an efficiency of .95.

8.4.8 Storage. The flywheel storage system is the most feasible choice for the WPG. Storage is not necessary for the fuel saver analysis, but it may be necessary (or desireable) in the baseload analysis. The cost of storage is 80 $/KWh with an efficiency of .95. The actual storage quantity in hours is determined by multiplying the number of hours determined from figure 6-18 by the storage reduction factor (K_s) in figure 6-19 using the site selection parameter σ_p/P. The flywheel input/output device is the multipole m/g set having a cost of 86 $/KW with an efficiency of .95.

8.5 Design Method for Fuel Saver Analysis

8.5.1 With separation effect.

$$\eta_{design} = .56$$

$$\eta_{conv} = .65$$

$$\eta_{gen} = .86$$

$$\eta_{trans} = .95$$

η_{cam} : from figure 6-11

$$\eta_{overall} = \eta_{design}\ \eta_{cam}\ \eta_{conv}\ \eta_{gen}\ \eta_{trans}$$

$$= .30\ \eta_{cam}$$

$$P_{del} = \eta_{overall}\ \bar{P}$$

$$\$_{structure} = \frac{1.139\ \bar{T}^4}{P_{del}}$$

$$\$_{CGT} = \left(\frac{\$_{trans}}{\eta_{trans}} + \frac{\$_{gen}}{\eta_{trans}\ \eta_{gen}} + \frac{\$_{conv}}{\eta_{trans}\ \eta_{gen}\ \eta_{conv}}\right)(PR)$$

$$\$_{CGT} = 389(PR)$$

Use figure 7-5 to determine PR and η_{band}:

$$MF_{CGT} = \frac{389(PR)}{\$_{structure}};$$

perform iteration with values of MF_{CGT} and PR to make this equation valid.

$$CC(\$/KW) = \frac{1.139\ T^4}{P_{del}} + 389(PR)$$

$$\overline{AV}_{fs} = .85\ \eta_{band}$$

$$FSV = \frac{CC(AFCR)}{87.6(\overline{AV}_{fs})}$$

8.5.2 Without separation effect. The following changes are made to the analysis of section 8.5.1:

$\eta_{design} = .68$

$\eta_{overall} = .36\ \eta_{cam}$

η_{cam} : from figure 6-8

$$CC = \frac{3.27\ T^4}{P_{del}} + 389(PR)$$

8.5.3 Example fuel saver calculation. North Atlantic, all seasons, with separation.

$$\bar{T} = 8.5 \text{ sec}$$

$$\bar{P} = 37.1 \text{ KW/M}$$

$$\sigma_T/T = .31$$

From figure 6-11, for $\sigma_T/T = .31$, $\eta_{cam} = .83$

$$\eta_0 = .30 \quad \eta_{cam} = .25$$

$$P_{del} = \eta_0 \bar{P} = 9.24 \text{ KW/M}$$

$$\$_{structure} = \frac{1.139(\bar{T})^4}{P_{del}} = 643 \text{ \$/KW}$$

$$MF_{CGT} = \frac{389}{643} (PR)$$

Performing iteration in figure 7-5 yields PR = .68, $\eta_{band} = .64$.

$$CC = \$_{structure} + \$_{CGT} = 643 + 389(PR) = 908 \ \$/KW$$

$$\overline{AV}_{fs} = .85\ \eta_{band} = (.85)(.64) = .54$$

$$FSV = \frac{CC(AFCR)}{87.6(\overline{AV}_{fs})} = \frac{(908)(.2337)}{87.6(.54)} = 4.49 \ ¢/KWh$$

FSV = 4.49 ¢/KWh

The corresponding breakeven fuel cost for fuel savings = 4.49 ¢/KWh may be determined from figure 8-1. For IHR = 11000 BTU/KWh the breakeven fuel cost is 4.05 $/10^6 BTU, or 26 $/BBL of oil.

8.6 Design Method for Baseload Analysis

This method is the same as that for the fuel saver except that $\overline{AV}_{bl}$ must be calculated using equation 6. Costs must be calculated for zero storage and for the highest return storage (figure 6-18). The lower cost design should be selected.

8.6.1 Example baseload calculation. North Atlantic, all seasons, with separation:

(1) No storage

$\bar{T}$ = 8.5 sec

$\bar{P}$ = 37.1 KW/M

σ_T/T = .31

σ_P/P = .98

η_0 = .25

P_{del} = 9.24 KW/M

η_{band} = .64

CC = 908 $/KW

$\overline{AV}_{bl} = .85\ \eta_{band}\ (.60(A)(DF)+(1-AFCR)(1-.60(A)(DF))$

from figure 6-18, for A = .75 and zero storage,

DF = .31

$\overline{AV}_{bl}$ = .43

$$BLEC = \frac{CC(AFCR)}{87.6(\overline{AV}_{bl})}$$

= 5.63 ¢/KWh

(2) With storage

From figure 6-18 the storage quantity yielding maximum return is 5.26 hours, at A = .75 and DF = .67. From figure 6-19 with σ_P/P = .98, K_s = .982. Actual storage required = $K_s(5.26)$ = 5.16 hours.

Storage cost = 80 $/KWh

$\eta_{storage} = .95$

Storage I/O cost = 86 $/KW

$\eta_{I/O} = .95$

60% of power is diverted to storage:

$$\$_{storage} = \frac{(.6)(86)}{(.95)^2(.95)} + (.4)(86) = 95 \text{ \$/KW}$$

$$\overline{AV}_{bl} = .85\ \eta_{band}\ [.60(A)(DF)+(1-AFCR)(1-.60(A)(DF)]=.46$$

$$\eta_0 = .6(.30)\ \eta_{cam}\ \eta_{storage}\ \eta_{I/O}^2 + .4(.30)\ \eta_{cam}$$

$$= .23$$

$$P_{del} = \eta_0\ \bar{P} = 8.71 \text{ KW/M}$$

$$CC = 908\ (\frac{.25}{.23}) + 426 + 95 = 1514 \quad \$/KW$$

$$BLEC = \frac{CC(AFCR)}{87.6(\overline{AV}_{bl})} = 8.78 \quad ¢/KWh$$

The cost of baseload energy is lower for the system without energy storage than for the system with energy storage implying that even the best energy storage scheme, the flywheel, is still too costly for economical use. It is worth

noting, however, that the demand fraction (DF) without energy storage is .31, while DF with energy storage is .67. This means that in order to achieve a certain level of baseload credit, more than twice as many no-storage WPG's would have to be assigned to the baseload as would be required with storage-configured WPG's.

8.7 Hypothetical Ocean Energy Farm Cost Calculation

The energy farm electrolyzes water to produce LH_2 for shipment to shore and conversion to electricity in fuel cells. The analysis is conducted for fuel saver with separation effect and without energy storage.

Assumed ocean parameters:

$\bar{T}$ = 8.5 sec

$\bar{P}$ = 100 KW/M

σ_T/T = .26

η_{cam} = .93

σ_P/P = 1.0

$\$_{electrolysis}$ = 89 \$/KW, η = .84

$\$_{liquefaction}$ = 234 \$/KW, η = .80

$\$_{fuel\ cell}$ = 179 \$/KW, η = .70

$\$_{transmission}$ = 114 \$/KW, η = .95

$\eta_0 = .13$

$P_{del} = 13$ KW/M

$\$_{structure} = \frac{1.139(9.5)^4}{13} = 714$ \$/KW

$\$_{CGT} = 1668$ (PR)

$MF_{CGT} = \frac{1668}{714}$ (PR), yields PR = .34

$\eta_{band} = .44$

CC = 714 + 1668 (.34) = 1281 \$/KW

$\overline{AV}_{fs} = .85\ \eta_{band} = .37$

FSV = 9.14 ¢/KWh

With this high cost occurring in such favorable ocean conditions it is unlikely that production of LH_2 will be feasible. Costs of electrolysis, liquefaction and fuel cells must be drastically reduced and efficiencies improved before LH_2 production will be feasible.

8.8 Value of Energy Storage

Using the calculations in the previous baseload credit analysis, the breakeven cost of energy storage may be computed.

$$\frac{CC + \$_{storage}}{CC} = \frac{\overline{AV}_{bl} \text{ (with storage)}}{\overline{AV}_{bl} \text{ (without storage)}}$$

$$\$_{storage} = \frac{.46}{.43} (908) - 908 = 63 \quad \$/KW$$

This is the breakeven cost for 5.16 hours of storage plus the cost of the I/O device. Assuming the I/O device represents 20% of total storage cost, the breakeven value of one unit of storage is,

$$\frac{63(.8)}{5.16} \cong 10 \quad \$/KWh$$

It is unlikely that any energy storage device will achieve this low cost of 10 \$/KWh. For this reason energy storage is considered infeasible for the WPG.

8.9 Structural Cost Reductions

The optimization methods for cam diameter in Chapter 6 were based on the cam being built entirely of steel. Calculations of costs in the fuel saver mode showed that structural

costs are about 70% of total cost even with the separation effect. Structural costs must be reduced.

It should be possible to build a cam having a small cylindrical steel strength member which houses machinery and a shroud of foam and plastic which forms the cam's shape to the design wavelength.

Figure 8-2 shows a proposed solution for structural cost reduction.

The size of the cylindrical steel core is governed by volume requirements of conversion and generation apparatus.

Let D_{core} = diameter of steel core

D_{skin} = diameter of water surface cylinder

The volume of the steel core per unit length = $\pi/4\ D_{core}^2$. Using the M.I.T. cam design, the volume of the shroud encompassing the steel core per unit length = $1.15 * D_{skin}^2 - \pi/4\ D_{core}^2$.

Let K_{conv} = conversion system volume density (M^3/KW)

K_{gen} = generation system volume density (M^3/KW)

K_{glass} = $\$/M^2$ of fiberglass coating

K_{poly} = $\$/M^3$ of polyurethane foam filler

P_{conv} = power to conversion system (KW/M)

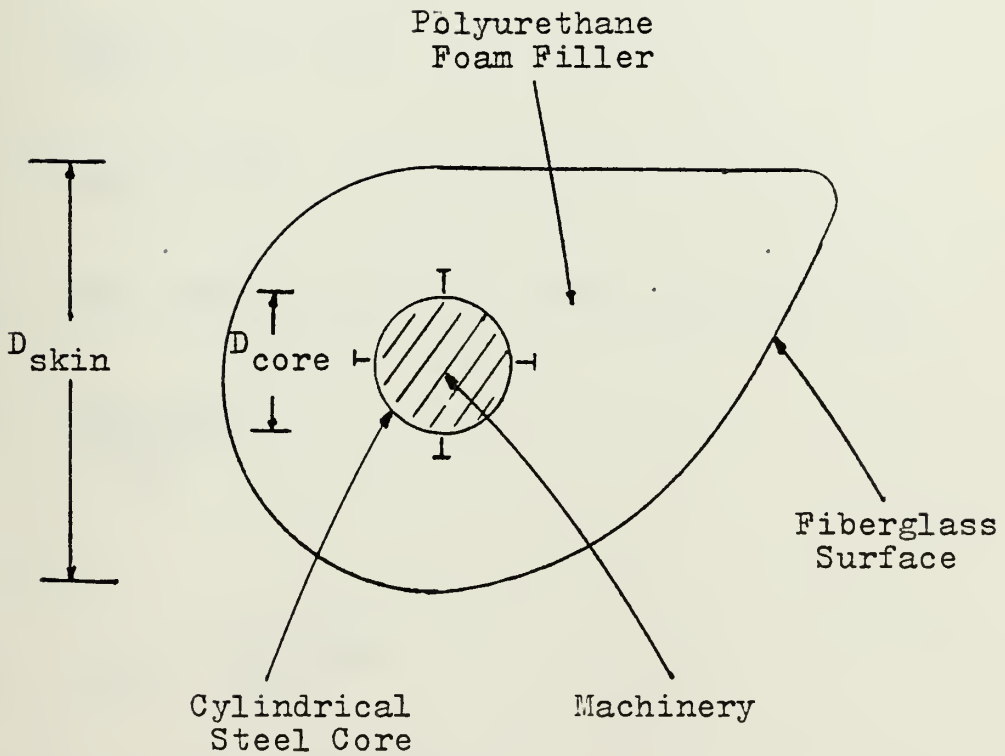

Figure 8-2: Proposed Reduced Cost Structural Design.

The required core diameter is

$$D_{core} = \left[\frac{4}{\pi} P_{conv} \left(K_{conv} + \eta_{conv} K_{gen}\right)\right]^{1/2}$$

Typical values of the above constants are,

$$K_{conv} = .23 \ M^3/KW$$

$$K_{gen} = .19 \ M^3/KW$$

$$\eta_{conv} = .65$$

It was shown that the cost of a steel structure is

$$\frac{199.71 \ D^2}{P_{del}}$$

Therefore,

$$\$_{core} = \frac{90 \ P_{conv}}{P_{del}}$$

The cost of the foam filler =

$$K_{poly} \left(1.15 \ D_{skin}^2 - \frac{\pi}{4} D_{core}^2\right)$$

The cost of the fiberglass surface =

$$K_{glass} \ (1.15 \ \pi \ D_{skin})$$

Typically,

$$K_{poly} = 28 \quad \$/M^3$$

$$K_{glass} = 4.3 \quad \$/M^2$$

The total material cost of the shroud =

$$32.2 \ D_{skin}^2 - 22 \ D_{core}^2 + 15.5 \ D_{skin}$$

Assuming that fabrication costs equal material costs (same as for all steel structure)

$$\$_{shroud} = 2(32.2 \ D_{skin}^2 - 22 \ D_{core}^2 + 15.5 \ D_{skin})$$

$$= 64.4 \ D_{skin}^2 + 31 \ D_{skin} - 20 \ P_{conv}$$

and the total cost of the structure is,

$$\$_{structure} = \frac{70 \ P_{conv} + 64.4 \ D_{skin}^2 + 31 \ D_{skin}}{P_{del}} \ \$/KW \qquad (9)$$

Revised versions of figures 6-5 and 6-15 may now be developed for optimizing structural costs using equation 9. Substituting parameters and non-dimensionalizing yields,

$$\frac{\$}{\$_{max}} = \frac{70\left(\frac{P}{P_{max}}\right) + 64.4\left(\frac{D}{D_{max}}\right)^2 + 31\left(\frac{D}{D_{max}}\right)}{165.4} \qquad (10)$$

Equation 10 is plotted in figure 8-4 for the case with separation and in figure 8-3 for the case without separation.

In figure 8-3 the minimum cost structure without separation occurs at $D/D_{max} = .66$ with $P/P_{max} = .79$.

In figure 8-4 the minimum cost structure with separation occurs at $D/D_{max} = .60$ with $P/P_{max} = .73$.

It was shown in section 8.4 that the maximum output diameter (D_{max}) occurs at $.2034\ T^2$ (without separation) and at $.1383\ T^2$ (with separation).

Total costs may now be expressed in terms of $\bar{T}$, with the added 10% mooring cost.

$$\$_{struct}\text{(without separation)} =$$

$$\frac{1.1[70\ P_{conv} + 64.4[(.66)(.2034)]^2 T^4 + 31(.66)(.2034)T^2]}{P_{del}}$$

$$= \frac{77\ P_{conv} + 1.28\ T^4 + 4.58\ T^2}{P_{del}} \ \$/KW \qquad (11)$$

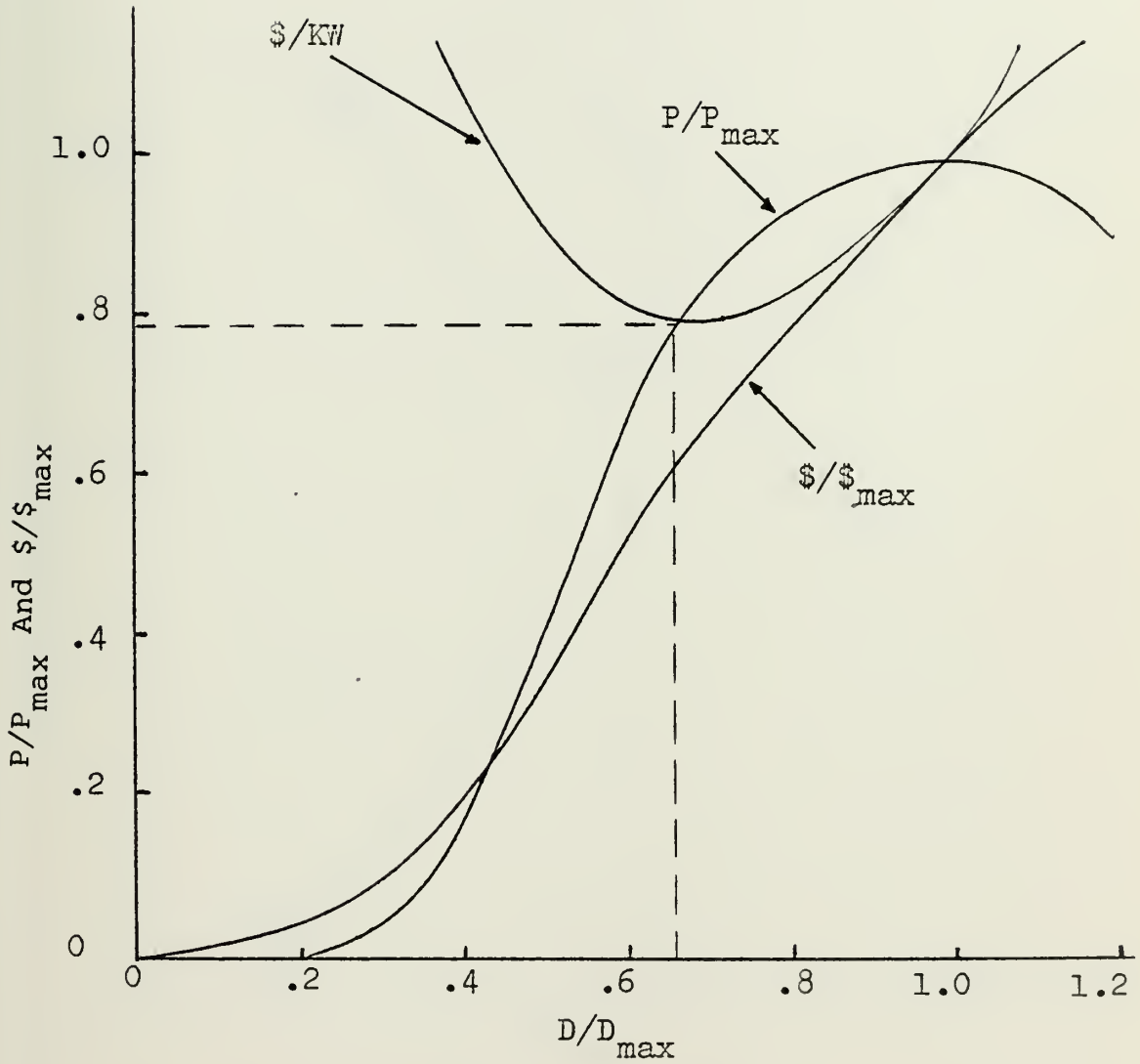

Figure 8-3: Minimum Cost Diameter Selection - No Separation.

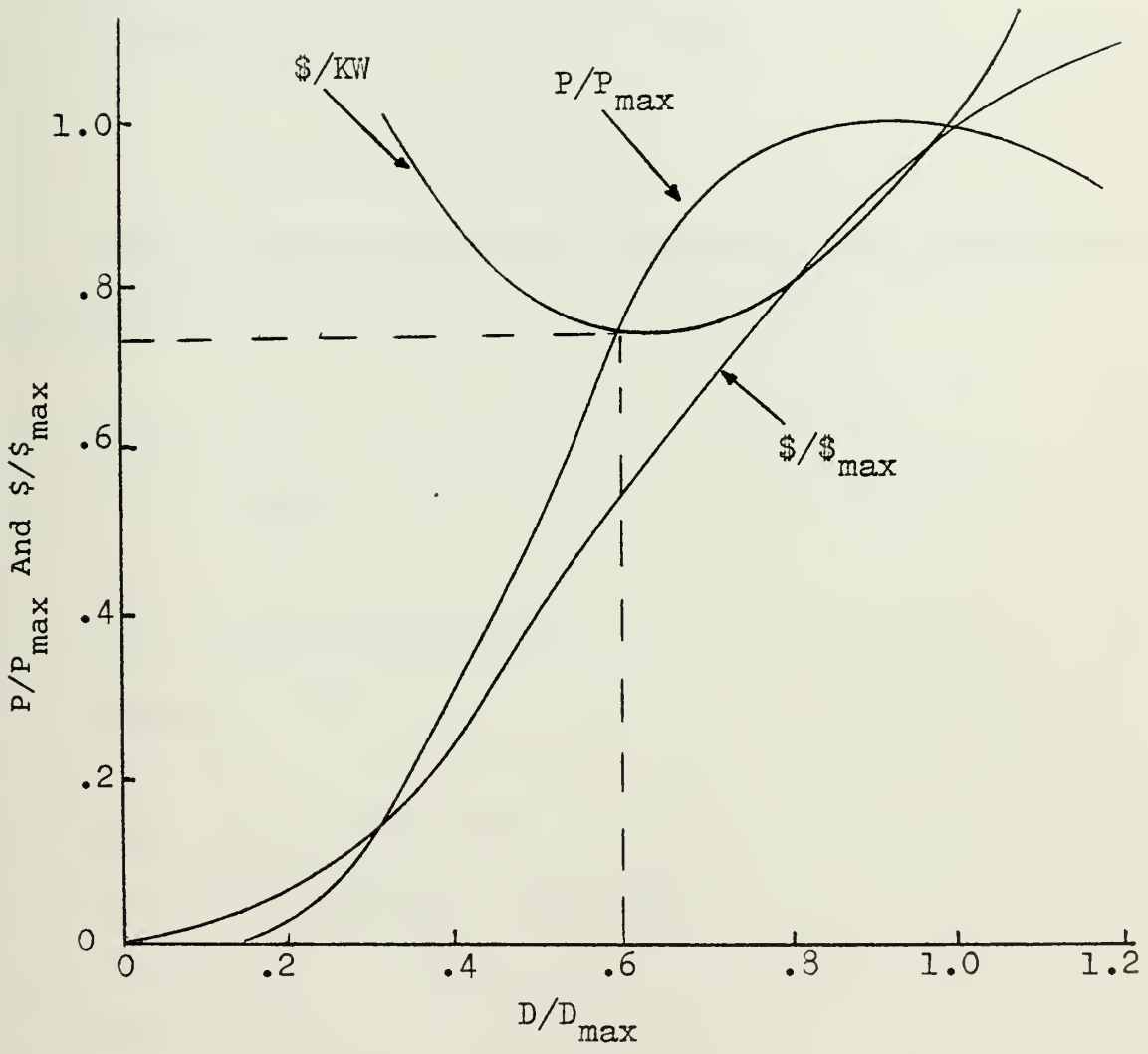

Figure 8-4: Minimum Cost Diameter Selection - With Separation.

$$\$_{struct}(\text{with separation}) =$$

$$\frac{1.1[70\ P_{conv} + 64.4[(.60)(.1383)]^2 T^4 + 31(.60)(.1383)T^2]}{P_{del}}$$

$$= \frac{77\ P_{conv} + .49\ T^4 + 2.83\ T^2}{P_{del}} \quad \$/KW \qquad (12)$$

8.9.1 Example fuel saver calculation with steel/foam construction. North Atlantic, with separation.

$\bar{T} = 8.5$ sec

$\bar{P} = 37.1$ KW/M

$\sigma_T/T = .31$

$\eta_{cam} = .83$ (figure 6-11)

$\eta_{design} = .73$

$\eta_0 = .32$

$P_{del} = \eta_o \bar{P} = 11.9$ KW/m

$P_{conv} = 1.883\ P_{del} = 22.4$ KW/m

Using equation 12,

$\$_{structure} = 377$ \$/KW

$MF_{CGT} = \frac{389}{377}$ (PR) yields, PR = .52

$\eta_{band} = .60$

$$CC = 377 + 389\ (.52) = 579 \quad \$/KW$$

$$\overline{AV}_{fs} = .85\ \eta_{band} = .51$$

$$FSV = \frac{579(.2337)}{87.6(.51)} = 3.03 \quad ¢/KWh$$

This compares with 4.49 ¢/KWh for the all-steel construction.

Fuel saver analysis calculations were performed for all six deep ocean locations around the U.S., for all-steel and steel-foam construction, with and without the separation effect. The results are displayed in table 8-1.

TABLE 8-1

BREAKEVEN FUEL SAVING VALUES FOR VARIOUS WPG CONFIGURATIONS

			Without Separation				With Separation			
			All-Steel		Steel-Foam		All-Steel		Steel-Foam	
	$\bar{T}$(sec)	$\bar{P}$(KW/M)	η_0	¢/KWh	η_0	¢/KWh	η_0	¢/KWh	η_0	¢/KWh
North Atlantic	8.5	37.1	.20	11.3	.25	5.5	.25	4.5	.32	3.0
Mid Atlantic	7.9	25.6	.18	13.1	.24	6.2	.24	4.8	.31	3.1
South Atlantic	6.7	22.1	.18	6.4	.24	4.4	.24	3.5	.31	2.5
North Pacific	11.0	81.0	.22	12.9	.29	6.1	.28	4.5	.36	3.1
Mid Pacific	10.3	52.0	.21	15.4	.28	7.2	.27	5.6	.35	3.5
South Pacific	13.2	25.0	.24	64.7	.32	27.2	.32	19.2	.41	10.5

8.10 Analysis of Costs

From table 8-1 the Middle Atlantic region and the North Pacific region yield comparable fuel saver values. The penalty for selecting high mean period ($\bar{T}$) sites is significant: for a constant fuel saver value, period increases from 7.9 to 11.0 seconds while power density increases from 22.1 to 81 KW/M.

The use of steel-foam instead of all-steel construction exhibits reduced costs, but a note of caution must be applied: Davis (ref. 7) showed that the cam's natural period of oscillation may be effectively raised by increasing the level of inertia of the cam. The steel-foam construction may be incapable of supporting the ballast at cam extremities for high levels of inertia.

The separation effect provides the most dramatic reduction in costs. For most ocean sites this reduction in cost is approximately a factor of two.

Using table 8-1 and figure 8-1 for IHR = 11000 BTU/KWh, the lowest breakeven price of oil is 14 $/BBL, corresponding to FSV = 2.5 ¢/KWh. It is unlikely that the WPG will ever achieve a breakeven cost lower than this. A median FSV = 5.5 ¢/KWh corresponds to a breakeven oil price of about 30 $/BBL.

The WPG is a resource competing not only with conventional plants but also with other fuel-less generation systems like Wind Power and Ocean Thermal Energy Conversion. Costs of these competing resources have been estimated (refs. 5, 6, 9, 13, 16, 21) to have FSV's ranging from 2.8 to 3.5 ¢/KWh. For the WPG to compete in this range it must be configured as follows:

1. Location in the open-ocean (approximately 100 miles off-shore) with seas characterized by short mean wave periods and/or very high power densities;
2. Separation between elements must be feasible; and
3. A construction less costly than all-steel must be utilized, or a means of reducing the effective required diameter must be found.

CHAPTER 9

CONCLUSIONS AND RECOMMENDATIONS

The following list summarizes the most notable conclusions reached in this report:

1. Ocean Waves

a. Wave heights and periods are independent;

b. Wave power distributions may be approximated by the exponential distribution;

c. East Coast waves are characterized by short wave periods and low power densities, while West Coast waves are characterized by long wave periods and high power densities;

d. The mean wave period remains essentially unchanged over the seasons;

e. A typical ocean site displays approximately mean annual power levels during the spring and fall, 60% of the mean in summer and 140% of the mean in winter.

2. Modelling

a. Simulation is a valuable tool for dealing with the complex WPG system;

b. For a given random ocean site there is one optimum cam diameter at a particular level of inertia;

c. Increasing the level of inertia reduces the

required cam diameter;

d. The most cost-effective diameter is rated at 68% of the mean power available without separation and at 56% with separation for the all-steel structure. For the steel-foam structure the most cost-effective diameter is rated at 79% of the mean power available without separation and at 73% with separation;

e. The parameter σ_T/T may be used in determining the cam's hydrodynamic efficiency in a random sea;

f. The separation effect results in higher efficiency, smaller maximum output diameter (D_{max}) and smaller minimum cost/KW diameter ratio (D/D_{max});

g. The most cost-effective level of energy storage for typical availabilities is 3 - 7 hours.

3. Feasibility Studies

a. Structural costs are proportional to $\bar{T}^4$;

b. Direct mechanical conversion systems are infeasible;

c. Hydrostatic conversion is well-suited to the WPG:

d. DC electrical generation/transmission yields best results;

e. The bandwidth of useable power may be optimized;

f. Flywheel energy storage is the most cost-effective storage medium.

4. Costs

a. The annual fixed charge rate is approximately 23%;

b. The concept of availability for the WPG is complicated by the variability of wave power;

c. Steel-foam construction produces lower costs than all-steel construction;

d. Breakeven costs with oil range from 14 to 30 $/BBL.

Recommendations

Accurate open ocean data needs to be collected, since power densities within 1 mile of the coast are too low to be economical. Data collection should concentrate on finding ocean areas characterized by high power densities and low mean annual wave periods.

Model tests of free-floating multi-cam units should be conducted to determine (1) the feasibility of utilizing the separation effect, (2) mooring forces, (3) direction-keeping problems and (4) the limiting increase in natural period of oscillation with increases in levels of inertia.

Low cost structural concepts may be necessary to achieve competitive costs. Such designs should be conducted with prior knowledge of optimum levels of inertia.

Inexpensive energy storage will increase the value of the WPG, but unit costs must be less than about 10 $/KWh to warrant storage use.

The WPG will not likely prove to be the panacea of world energy problems. Under the most favorable assumptions it is barely competitive on today's energy market having a minimum breakeven oil price of 14 $/BBL; under unfavorable assumptions it is infeasible with respect to today's energy costs. Before the WPG is eliminated from feasible contention as an efficient energy producer, further investigation is required.

REFERENCES

(1) Baumeister, T. (ed.), Mechanical Engineers Handbook, McGraw-Hill, N.Y., 1958.

(2) Budal, K., "Theory For Absorption of Wave Power by a System of Interacting Bodies," Journal of Ship Research, vol. 21, no. 4, December 1977, pp. 248-253.

(3) Clelland, R.C., J.S. deCani and F.E. Brown, Basic Statistics With Business Applications, John Wiley and Sons, N.Y., 1973.

(4) Comstock, J.P., Principles of Naval Architecture, SNAME, N.Y., 1967.

(5) Coste, W.H. and M. Lotker, "Evaluating a Combined Wind Power/Energy Storage System," Power Engineering, vol. 81, no. 5, May 1977, pp. 48-51.

(6) Considine, D.M. (ed.), Energy Technology Handbook, McGraw-Hill, N.Y., 1977.

(7) Davis, N.B., Performance of a "Salter" Rocking Cam Type Wave Energy Extractor - An Experimental Evaluation, S.M. Thesis, M.I.T., Cambridge, Ma., 1978.

(8) Dingwell, R.E., Predictions of Power Production by a Cam Type Wave Energy Converter For Various

Locations, S.M. Thesis, M.I.T., Cambridge, Ma., 1977.

(9) Dugger, G.L. and E.J. Francis, "Design of an Ocean Thermal Energy Plant Ship to Produce Ammonia Via Hydrogen," International Journal of Hydrogen Energy, vol. 2, 1977, pp. 231-249.

(10) Eagleson, P.S., R.G. Dean, C.L. Bretschneider, et al, Estuary and Coastline Hydrodynamics, McGraw-Hill, 1966.

(11) Fernandes, R.A. and H.D. Philipp, "Hydrogen Cycle Peak-Shaving on the New York State Grid Using Fuel Cells," IEEE Transactions on Power Apparatus and Systems, vol. PAS-96, no. 2, March/April 1977, pp. 467-477.

(12) Hogben, N. and F.E. Lumb, Ocean Wave Statistics, HMSO, London, 1967.

(13) Jorgensen, G.E., M. Lotker and R.C. Meier, "Design Economic and System Considerations of Large Wind-Driven Generators," IEEE Transactions on Power Apparatus and Systems, vol. Pas-95, no. 3, May/June 1976, pp. 870-878.

(14) Karassik, I.J., W.C. Krutzsch, W.H. Fraser and J.P. Messina (eds.), Pump Handbook, McGraw-Hill, N.Y., 1976.

(15) Kinsman, B., Wind Waves, Prentice-Hall, Englewood

Cliffs, N.J., 1965.

(16) Konopka, A., "Energy Transmission from Ocean Thermal Energy Conversion Plants," IECEC Record, 1976, pp. 940-948.

(17) Kyrkos, B., Shipbuilding Cost Estimation with Special Reference to Tankers, S.M. Thesis, M.I.T., Cambridge, Ma., 1978.

(18) Larew, W.B., Fluid Clutches and Torque Converters, Chilton Books, Phila., 1968.

(19) Merril, R., C. Missar, T. Gage and J. Bukey (eds.) Energy Primer, Portola Institute, Menlo Park, Ca., 1974.

(20) Nath, J.H. and R.M. Williams, "Preliminary Feasibility Study for Utilization of Water Wave Energy," Wave and Salinity Gradient Energy Conversion Workshop, ERDA, no. WA-76-3102, May 1976.

(21) Penner, S.S. and L. Icerman, Energy, Addison-Wesley, N.Y., 1975.

(22) Pierson, W.J. and R.E. Salfi, "The Temporal and Spatial Variability of Power from Ocean Waves Along the West Coast of America," Wave and Salinity Gradient Energy Conversion Workshop, ERDA, no. WA-76-3105, May 1976.

(23) Ramakumar, R., "Wind Driven Field Modulated Generating Systems," IECEC Record, 1976, pp. 1766-1769.

(24) Ramakumar, R., H.J. Allison and W.L. Hughes, "Solar Energy Conversion and Systems for the Future," IEEE Transactions on Power Apparatus and Systems, vol. Pas-94, no. 6, November/ December, 1975.

(25) Reed, M.R., Ship Synthesis Model for Naval Surface Ships, O.E. Thesis, M.I.T., Cambridge, Ma., 1976.

(26) Salter, S.H., "Wave Power," Nature, vol. 249, June 21, 1974, pp. 720-724.

(27) Salter, S.H., D.C. Jeffrey and J.R.M. Taylor, "The Architecture of Nodding Duck Wave Power Generators," The Naval Architect, January, 1976, pp. 21-24.

(28) Savina, J.M. (ed.), Wind Energy Conversion Systems, Workshop Proceedings, NSF/NASA, December, 1973.

(29) Simmons, D.M., Wind Power, Noyes Data Corp., Park Ridge, N.J., 1975.

(30) Smith, R.T. and T.S. Jayadev, "Electrical Generation by Wind Power," IECEC Record, 1975, pp. 1246-1250.

(31) Swift-Hook, D.T., B.M. Count, I. Glendenning and S.H. Salter, "Characteristics of a Rocking Cam Wave Power Device," Nature, vol. 254, April 10, 1975, pp. 504-506.

(32) Thompson, E.F., Wave Climate at Selected Locations Along U.S. Coasts, CERC, no. 77-1, January, 1977.

(33) Veziroglu, T.N., Hydrogen Energy, Plenum Press, N.Y., 1975.

(34) Weschler, L., C.E. Brown and T.R. Sundarm, "Engineering Analysis of Systems for Extracting Useful Energy from the Sea," Proceedings: National Needs and Ocean Solutions, M.T.S., September 25, 1974.

(35) Yeaple, F.D., Hydraulic and Pneumatic Power and Control, McGraw-Hill, N.Y., 1966.

(36) _____, Handbook of Power Drives, Trade and Technical Press, Morden, England, 1973.

(37) _____, "Wave Power Availability in the NE Atlantic," Nature, vol. 263, September 16, 1976, pp. 223-226.

(38) _____, Waves Recorded Off Station Papa, Marine Environmental Data Service, Canada, 1976.

APPENDIX A

MODEL DESCRIPTION

FUNCTIONS

1. NORML: Normal distribution for wave periods (argument = RN).
2. XPDIS: Exponential distribution for wave power (argument = RN).
3. CAMEF: Cam efficiency (argument = λ/D).
4. GENEF: Generator efficiency (argument = actual power rating seen by generator).
5. MULTI: Multiplier for increased power due to cam separation (argument = cam separation).

SAVEVALUES

1. DEMND: Demand (KW).
2. POWRT: Design generator power rating (KW).

3, 4, 5, 7, 11: Not used.

6. Pump efficiency (%).
8. Mean power level (KW).
9. Standard deviation of wave period (seconds).
10. Mean wave period (seconds).
12. Counter for assembling power from ten cams.
13. Remaining storage capacity (KW).

14. Total storage capacity (KW).
15. Accumulator of power for delivery to generator.
16. Counter for power sources.

VARIABLES

1. LAMDA: λ/D (wavelength/diameter)
2. POWER: Power available to each cam = power/length x length x MULTI.
3. POWLN: Power/length.
4. PERID: Wave period.
5. PRATE: Power rating actually seen by generator.
6. OUTGE: Power outage quantity
7. PMPLS: Power available after conversion losses.
8. CAMLS: Power available after cam losses.
9. GENLS: Final power delivered by system.
10. SUMPO: Power/length delivered by 10 cams.
11. POW: Demand counter.
12. TEMPC: Counter.
13. AVAIL: Power available in the storage.
14. KAYD: Kd (wavenumber x separation distance).

MATRIX SAVEVALUES

1. Array (1x10) of cam lengths (m).
2. Array (1x10) of cam diameters (m).

3. Array (1x10) of cam separations (m).

TABLES

1. PEROD: Period distribution.
2. POAVA: Power in wave distribution.
3. LMDAD: λ/D distribution.
4. EFFIC: Cam efficiency distribution.
5. PULOS: Power leaving the conversion system.
6. CALOS: Power leaving the cam.
7. GELOS: Power out of the system.
8. OUTAG: Outage distribution.
9. STOAR: Remaining capacity of storage.

MODEL CONFIGURATION AND FLEXIBILITY

The following model entities may be varied to test system response to different input configurations:

FUNCTIONS

1. Any empirical cam efficiency distribution may be read into the model with CAMEF.
2. Any empirical generator efficiency curve may be read into the model with GENEF.
3. Further model tests may yield different efficiency multipliers than those currently in the model and these may be input using the function MULTI.

MATRIX SAVEVALUES

The model is designed to accept 10 different cam configurations for each trial run. The design length of the total system was arbitrarily assigned to be 1 KM with each cam allotted 1/10 of the total system length. Cam diameters may be varied as desired.

SAVEVALUES

1. Demand: Power delivered and storage accumulation vary with changes in demand levels.
2. Power Rating: The ability of the system to deliver power depends on the generator power rating. This number divided into the actual power available to the generator determines the input value for the generator efficiency curve.
3. Conversion Efficiency: This is expressed as a constant and accounts for power losses after the cam but before the generator.
4. Mean Power Level: Power levels vary from one location to another. This number along with the Function XPDIS completely describe the power distribution.
5. Period: The mean and standard deviation of wave period vary from one location to another. These variables affect optimum cam diameter, storage and power

delivered.

6. Storage Capacity: The mean power delivered and the variability of this power are affected by changes in storage capacity.

TABLES

All significant model output is in the form of tables. Table means, standard deviations and cumulative percentages are all important identifiers of system output.

```
*
        SIMULATE
        JOB
*
*******************************************************************
*
 NORML FUNCTION   RN3,C22          NORMAL DISTRIBUTION FOR WAVE PERIODS
0,-2/.02275,-2
.06681,-1.5/.11507,-1.2/.15866,-1/.21186,-.8/.27425,-.6
.34458,-.4/.42074,-.2/.5,0/.57926,.2/.65542,.4
.72575,.6/.78814,.8/.84134,1/.88493,1.2/.93319,1.5
.97725,2/.99379,2.5/.99865,3/.99997,4/1,5
*
 XPDIS FUNCTION   RN3,C24          EXPON DISTRIBUTION FOR WAVE POWER
0,0/.1,.104/.2,.222/.3,.355/.4,.509/.5,.69/.6,.915/.7,1.2/.75,1.38
.8,1.6/.84,1.83/.88,2.12/.9,2.3/.92,2.52/.94,2.81/.95,2.99/.96,3.2
.97,3.5/.98,3.9/.99,4.6/.995,5.3/.998,6.2/.999,7/.9998,8
*
 CAMEF FUNCTION   P5,C17           CAM EFFICIENCY FOR WN=.9SECS.
0,0/4,48/5,79/6,89/7,93/9,94/10,93/11,90/12,84/13,77/14,68/15,57
16,44/17,35/18,31/23,22/33,0
*
 GENEF FUNCTION   V$PRATE,C6       GENERATOR EFFICIENCY
0,100/20,100/40,100/60,100/80,100/100,100
*
 MULTI FUNCTION   P7,C10           POWER MULTIPLIER FOR SEPARATION
0,100/25,100/30,130/45,193/50,150/60,81/70,70/80,90/90,115/100,130
*
```

```
********************************************************************************
        INITIAL     X$DEMND,9999
        INITIAL     X$POWRT,9999
        INITIAL     X6,85              PUMP EFFICIENCY
        INITIAL     X7,0               NOT USED
        INITIAL     X8,58              MEAN POWER LEVEL
        INITIAL     X9,1               STD DEV OF WAVE PERIOD
        INITIAL     X10,13             MEAN WAVE PERIOD
        INITIAL     X12,0              COUNTER
        INITIAL     X13,9999            REMAINING STORAGE CAPACITY
        INITIAL     X14,9999           TOTAL STORAGE CAPACITY
        INITIAL     X15,0              ACCUMULATOR OF POWER FOR GENERATOR
        INITIAL     X16,1              COUNTER FOR POWER SOURCES
*
 1      MATRIX      X,1,10             CAM LENGTH ARRAY
        INITIAL     MX1(1,1-10),100
 2      MATRIX      X,1,10             CAM DIAMETER ARRAY
        INITIAL     MX2(1,1-10),30
 3      MATRIX      X,1,10              CAM SEPARATION ARRAY
        INITIAL     MX3(1,1-10),190
********************************************************************************
 PEROD  TABLE       P6,0,1,25          PERIOD DISTRIBUTION
 POAVA  TABLE       P1,0,5,22          POWER AVAILABLE DISTRIBUTION
 LMDAD  TABLE       P5,0,2,19          WAVELENGTH TO DIAMETER RATIO
 EFFIC  TABLE       P3,0,5,22          CAM EFFICIENCY DISTRIBUTION
```

```
PULOS TABLE      P2,0,5,22          POWER LEAVING THE PUMP
CALOS TABLE      P2,0,5,22          POWER LEAVING THE CAM SYSTEM
GELOS TABLE      P9,0,2,28          POWER LEAVING THE TOTAL SYSTEM
OUTAG TABLE      V$OUTGE,-100,10,20  SHORTAGE OF POWER INCURRED
STOAR TABLE      X13,0,5,22         CAP OF STORAGE AFTER POWER DELIVERY
*******;*************************************************************
*******;*************************************************************
LAMDA FVARIABLE  P6*P6*156/MX2(1,P4)/100        WAVELENGTH/DIAMETER
POWER FVARIABLE  FN$MULTI*P8*P1/100
POWLN FVARIABLE  X8*FN$XPDIS                    POWER/UNIT LENGTH
PERID FVARIABLE  X9*FN$NORML+X10                WAVE PERIOD
PRATE FVARIABLE  P2*100/X$POWRT                 GENERATOR POWER RATING
OUTGE FVARIABLE  P9-X$DEMND                     OUTAGE
PMPLS FVARIABLE  X6*P2/100                      POWER OUT AT THE PUMP
CAMLS FVARIABLE  P3*P2/10000                    POWER OUT AT THE CAM
GENLS FVARIABLE  P2*FN$GENEF/100                POWER OUT OF SYSTEM
SUMPO FVARIABLE  X12/10                         POWER SUMMATION
POW   FVARIABLE  X$DEMND-X15                    DEMAND COUNTER
TEMPC FVARIABLE  P2-X13                         COUNTER
AVAIL FVARIABLE  X14-X13                        POWER IN STORAGE
KAYD  FVARIABLE  4028*MX3(1,P4)/(P6*P6*100)
*******;*************************************************************
*
*
*******;*************************************************************
* GENERATE A WAVE WITH FULLWORD PARAMETERS.  ASSIGN A RANDOM PERIOD   *
*  TO PARAMETER 6, AND ADVANCE THE CLOCK.  RESEED THE GENERATION      *
*  BLOCK FOR THE NEXT WAVE ARRIVAL.                                   *
*******;*************************************************************
```

```
        GENERATE    ,,,1,,,F
 AGAIN  ASSIGN      6,V$PERID
        ADVANCE     P6
*       TABULATE    PEROD
        SPLIT       1,AGAIN
********************************************************************************
*  ASSIGN QUANTITIES TO THE PARAMETERS OF EACH INDIVIDUAL CAM.  LOOP  *
*  TEN TIMES PRODUCING TEN DIFFERENT CAM CONFIGURATIONS.  SEND THE TEN*
*  TRANSACTIONS TO THE SYSTEM.                                        *
********************************************************************************
*       POWLN IS THE POWER PER UNIT LENGTH IN THE WAVE
        ASSIGN      1,V$POWLN
*       TABULATE    POAVA
*       P4 IS ASSIGNED A VALUE OF TEN FOR THE TEN CAMS
        ASSIGN      4,10
*       KAYD IS THE VARIABLE FOR ENTRY TO FN$MULTI
 BACK   ASSIGN      7,V$KAYD
*       P8 IS ASSIGNED THE CAM LENGTH
        ASSIGN      8,MX1(1,P4)
*       P2 IS ASSIGNED THE POWER TO THE CAM
        ASSIGN      2,V$POWER
*       P5 IS ASSIGNED THE WAVELENGTH TO DIAMETER RATIO
        ASSIGN      5,V$LAMDA
*       TABULATE    LMDAD
*       P3 IS ASSIGNED THE CAM EFFICIENCY FROM THE FUNCTION
        ASSIGN      3,FN$CAMEF
        TABULATE    EFFIC
*       THE SPLIT ELIMINATES THE CAM FROM FURTHER CALCULATIONS
        SPLIT       1,CAM
*       THE LOOP IS DONE 10 TIMES FOR THE 10 CAMS
        LOOP        4,BACK
        TERMINATE
```

```
********************************************************************
*  CALCULATE LOSSES DUE TO THE CAM AND PUMP INEFFICIENCIES.        *
********************************************************************
*       CAMLS CALCULATES LOSSES DUE TO CAM INEFFICIENCIES
 CAM    ASSIGN     2,V$CAMLS
*       TABULATE   CALOS
*       PMPLS CALCULATES LOSSES DUE TO PUMP INEFFICIENCIES
 PUMP   ASSIGN     2,V$PMPLS
*       TABULATE   PULOS
********************************************************************
*  ASSEMBLE THE TEN TRANSACTIONS INTO ONE WITH A POWER LEVEL EQUAL TO *
*  THE SUMMATION OF POWER FROM THE TEN CAMS.                       *
********************************************************************
*       SV12 IS USED AS A COUNTER FOR POWER ARRIVALS
 TEMP   SAVEVALUE  12+,P2
*       THE POWER FROM TEN CAMS IS ASSEMBLED
       ASSEMBLE   10
*       SUMPO CALCULATES THE MEAN POWER PER CAM FOR THE SYSTEM
       ASSIGN     2,V$SUMPO
       SAVEVALUE  12,0
********************************************************************
*  TEST TO SEE IF THE POWER IN THE WAVE EXCEEDS THE REMAINING STORAGE *
*  CAPACITY.  IF IT DOES, THEN FILL THE STORAGE TO ITS LIMITS AND    *
*  SEND ANY EXCESS POWER DIRECTLY TO THE GENERATOR.  IN THIS CASE    *
*  THERE MAY BE AN EXCESS OF POWER DELIVERED.  IF THE POWER AVAILABLE *
*  IS LESS THAN THE REMAINING CAPACITY OF THE STORAGE THEN SEND ALL   *
*  OF IT TO THE STORAGE WHERE A DETERMINATION WILL BE MADE AS TO HOW  *
*  MUCH POWER SHOULD BE SENT TO DEMAND AND HOW MUCH SHOULD REMAIN IN  *
*  THE STORAGE.  PARAMETER 9 SPECIFIES THE AMOUNT OF POWER SENT      *
*  DIRECTLY TO THE GENERATOR, WHILE PARAMETER 2 SPECIFIES POWER      *
*  RECEIVED FROM THE STORAGE.                                       *
********************************************************************
```

```
*       THE POWER LEVEL IS TESTED TO SEE IF IT IS GREATER THAN THE STORAGE
        TEST G      P2,X13,STOR
*       THE LOCK SYNCHRONIZES POWER DELIVERY FROM STORAGE AND DIRECT
        LOGIC S     LOCK
*       SV16 INDICATES THE NUMBER OF POWER SOURCES FOR A GIVEN WAVE
        SAVEVALUE   16,2
*       TEMPC IS THE EXCESS POWER OVER THAT AVAILABLE
        ASSIGN      9,V$TEMPC
*       THE SPLIT SENDS SOME OF THE WAVE POWER TO STORAGE
        SPLIT       1,GOSTO
        ASSIGN      2,0
*       THE TRANSFER IS A DIRECT POWER DELIVERY
        TRANSFER    ,GEN1
********************************************************************
*  THE LOCK IS USED TO ENSURE THAT THE STORAGE IS NOT PREMATURELY   *
*  EMPTIED.  SAVEVALUE 13 IS INCREMENTED AND DECREMENTED AS POWER   *
*  ENTERS AND LEAVES THE  THE  STORAGE.  PARAMETER 10 MUST NOT BE   *
*  ALLOWED TO GO LESS THAN ZERO, BECAUSE THIS TENDS TO ALLOW THE    *
*  SYSTEM TO CREATE POWER.                                          *
********************************************************************
*       AT GOSTO THERE IS AN EXCESS OF POWER, SO FILL THE STORAGE
 GOSTO  ASSIGN      2,X13
*       AGAIN THE LOCK IS USED TO SYNCHRONIZE POWER DELIVERY
 STOR   GATE LR     LOCK
*       THE STORAGE IS NOW FULL
        SAVEVALUE   13-,P2
*       POW IS THE POWER NEEDED TO FILL THE DEMAND
        ASSIGN      10,V$POW
*       P10 MUST BE GREATER THAN ZERO
```

```
        TEST GE     P10,0,CHNGE
 BACK1  TEST L      P10,V$AVAIL,GEN2
*       IF HERE, THEN SYSTEM IS ABLE TO COMPLETELY MEET DEMAND
        SAVEVALUE  13+,P10
*       P2 HOLDS THE AMOUNT DELIVERED FROM STORAGE
        ASSIGN     2,P10
        ASSIGN     9,0
*       THE TRANSFER DELIVERS THE POWER
        TRANSFER   ,GEN3
********************************************************************
*  SAVEVALUE 15 HOLDS THE AMOUNT OF POWER RECEIVED BOTH DIRECTLY AND  *
*  INDIRECTLY.  THE FINAL POWER OUT OF THE SYSTEM IS NOW CALCULATED   *
********************************************************************
*       IF HERE, THERE IS A SHORTAGE OF POWER SO DELIVER ALL AVAILABLE
 GEN2   SAVEVALUE  15+,V$AVAIL
        ASSIGN     9,0
        ASSIGN     2,0
*       THE STORAGE IS NOW EMPTY
        SAVEVALUE  13,X14
 GEN3   TABULATE   STOAR
        TRANSFER   ,COMP
*       TEST FOR AN EXCESS OF POWER ABOVE POWER RATING
 GEN1   TEST LE     P9,X$POWRT,EXCES
*       CALCULATE THE DIRECT POWER DELIVERED
 COMP   SAVEVALUE  15+,P9
        LOGIC R    LOCK
*       CALCULATE THE POWER DELIVERED FROM STORAGE
        SAVEVALUE  15+,P2
*       ASSEMBLE POWER DELIVERIES
        ASSEMBLE   X16
        SAVEVALUE  16,1
```

```
*       P2 HOLDS FINAL POWER DELIVERED
        ASSIGN      2,X15
*       GENLS CALCULATES LOSSES DUE TO GENERATOR INEFFICIENCIES
        ASSIGN      9,V$GENLS
        SAVEVALUE   15,0
*       GELOS IS THE TABLE DISTRIBUTION OF POWER OUT
        TABULATE    GELOS
*       TABULATE    OUTAG
        TERMINATE
*
*       DEMAND EXCEEDS POWER AVAILABLE
 CHNGE  ASSIGN      10,0
        TRANSFER    ,BACK1
*        EXCESS POWER IS DUMPED FROM THE SYSTEM
 EXCES  ASSIGN      9,X$POWRT
        TRANSFER    ,COMP
*
*              TIMER SEGMENT
        GENERATE    4000
        TERMINATE   1
        START       1
*
        RMULT       1,1,1,1,1,1,1,1
        INITIAL     X9,3              STD DEV OF WAVE PERIOD
        INITIAL     X13,9999           REMAINING STORAGE CAPACITY
        CLEAR       X$DEMND,X$POWRT,X6-X10,X12-X16
        INITIAL     MX1(1,1-10),100
        INITIAL     MX2(1,1-10),30
        INITIAL     MX3(1,1-10),190
        START       1
```

TABLE GELOS

ENTRIES IN TABLE	MEAN ARGUMENT	STANDARD DEVIATION	SUM OF ARGUMENTS	
320	39.740	43.562	12717.000	NON-WEIGHTED

UPPER LIMIT	OBSERVED FREQUENCY	PER CENT OF TOTAL	CUMULATIVE PERCENTAGE	CUMULATIVE REMAINDER	MULTIPLE OF MEAN	DEVIATION FROM MEAN
0	36	11.24	11.2	88.7	-.000	-.912
5	24	7.49	18.7	81.2	.125	-.797
10	28	8.74	27.4	72.5	.251	-.682
15	29	9.06	36.5	63.4	.377	-.567
20	26	8.12	44.6	55.3	.503	-.453
25	13	4.06	48.7	51.2	.629	-.338
30	15	4.68	53.4	46.5	.754	-.223
35	17	5.31	58.7	41.2	.880	-.108
40	13	4.06	62.8	37.1	1.006	.005
45	12	3.74	66.5	33.4	1.132	.120
50	13	4.06	70.6	29.3	1.258	.235
55	8	2.49	73.1	26.8	1.383	.350
60	10	3.12	76.2	23.7	1.509	.465
65	6	1.87	78.1	21.8	1.635	.579
70	13	4.06	82.1	17.8	1.761	.694
75	7	2.18	84.3	15.6	1.887	.809
80	4	1.24	85.6	14.3	2.013	.924
85	7	2.18	87.8	12.1	2.138	1.038
90	3	.93	88.7	11.2	2.264	1.153
95	6	1.87	90.6	9.3	2.390	1.268
100	4	1.24	91.8	8.1	2.516	1.383
OVERFLOW	26	8.12	100.0	.0		
AVERAGE VALUE OF OVERFLOW		147.00				

Sample Output Table